

**LAND USE AND LAND COVER CLASSIFICATION
USING SEMANTIC MODEL OF OBJECT-BASED
IMAGE ANALYSIS**

Phawinee Poojarit



**A Thesis Submitted in Partial Fulfillment of the Requirements for the
Degree of Master of Science in Geoinformatics**

Suranaree University of Technology

Academic Year 2015

การจำแนกการใช้ที่ดินและสิ่งปกคลุมดินโดยอาศัยแบบจำลองอรรถศาสตร์
ของการวิเคราะห์ภาพเชิงวัตถุ



วิทยานิพนธ์นี้เป็นส่วนหนึ่งของการศึกษาตามหลักสูตรปริญญาวิทยาศาสตรมหาบัณฑิต
สาขาวิชาภูมิสารสนเทศ
มหาวิทยาลัยเทคโนโลยีสุรนารี
ปีการศึกษา 255

LAND USE AND LAND COVER CLASSIFICATION USING SEMANTIC MODEL OF OBJECT-BASED IMAGE ANALYSIS

Suranaree University of Technology has approved this thesis submitted in partial fulfillment of the requirements for a Master's Degree.

Thesis Examining Committee

(Asst. Prof. Dr. Songkot Dasananda)

Chairperson

(Assoc. Prof. Dr. Suwit Ongsomwang)

Member (Thesis Advisor)

(Assoc. Prof. Dr. Sura Pattanakiat)

Member

(Asst. Prof. Dr. Sunya Sarapirome)

Member

(Prof. Dr. Sukit Limpijumnong)

Vice Rector for Academic Affairs
and Innovation

(Prof. Dr. Santi Maensiri)

Dean of Institute of Science

ภาวิณี ภูจรีต : การจำแนกการใช้ที่ดินและสิ่งปกคลุมดิน โดยอาศัยแบบจำลองอรรถศาสตร์ของการวิเคราะห์ภาพเชิงวัตถุ (LAND USE AND LAND COVER CLASSIFICATION USING SEMANTIC MODEL OF OBJECT-BASED IMAGE ANALYSIS) อาจารย์ที่ปรึกษา : รองศาสตราจารย์ ดร.สุวิทย์ อ่องสมหวัง 145 หน้า.

การวิเคราะห์ข้อมูลภาพเชิงวัตถุเป็นการวิเคราะห์ข้อมูลภาพรูปแบบหนึ่งที่มีศักยภาพสูง เนื่องจากการวิเคราะห์ข้อมูลภาพเชิงวัตถุสามารถนำรูปลักษณะของวัตถุที่มีหลากหลายมาใช้วิเคราะห์ร่วมกับข้อมูลอื่นๆ วัตถุประสงค์หลักของการศึกษาคือ (1) เพื่อพัฒนาแบบจำลองและการจำแนกเชิงอรรถศาสตร์ด้วยการวิเคราะห์ความสามารถการแยกจากกันและค่าขีดแบ่งและองค์ความรู้ของผู้เชี่ยวชาญเพื่อจำแนกการใช้ประโยชน์ที่ดินและสิ่งปกคลุมดินในพื้นที่ต้นแบบ (2) เพื่อประยุกต์แบบจำลองและการจำแนกเชิงอรรถศาสตร์ที่ได้พัฒนาขึ้นสำหรับการวิเคราะห์ความสามารถของการถ่ายโอนเชิงพื้นที่ และ (3) เพื่อดัดแปลงแบบจำลองและการจำแนกเชิงอรรถศาสตร์ที่ได้พัฒนาขึ้นในพื้นที่ต้นแบบสำหรับการวิเคราะห์ความสามารถของการถ่ายโอนเชิงเวลา พื้นที่ศึกษาครอบคลุม 3 อำเภอของจังหวัดนครราชสีมา ประกอบด้วย อำเภอปักธงชัยและวังน้ำเขียวซึ่งเป็นพื้นที่ต้นแบบ และอำเภอครบุรีซึ่งที่เป็นพื้นที่ทดสอบ องค์ประกอบหลักของวิธีการศึกษา ประกอบด้วย การสร้างแบบจำลองและการจำแนกเชิงอรรถศาสตร์ และการวิเคราะห์ความสามารถของการถ่ายโอนเชิงพื้นที่และเชิงเวลา

ผลการศึกษา พบว่า สามารถพัฒนาการสร้างแบบจำลองและการจำแนกเชิงอรรถศาสตร์ด้วยการวิเคราะห์ความสามารถการแยกจากกันและค่าขีดแบ่งได้เป็นผลสำเร็จ และนำไปใช้ในการจำแนกการใช้ประโยชน์ที่ดินและสิ่งปกคลุมดินจากข้อมูลภาพจากดาวเทียม Landsat 8 ในปี พ.ศ. 2556 ประกอบด้วย พื้นที่เมืองและสิ่งปลูกสร้าง นาข้าว มันสำปะหลัง ข้าวโพด อ้อย ไม้ยืนต้น และสวนผลไม้ พื้นที่ป่าไม้ และแหล่งน้ำ ความถูกต้องโดยรวมและสัมประสิทธิ์แคปปาของแผนที่ที่ได้รับมีค่าเท่ากับ ร้อยละ 84.24 และ 80.37 ตามลำดับ จากค่าสัมประสิทธิ์แคปปาที่ได้รับมากกว่า ร้อยละ 80 แสดงให้เห็นถึงความสอดคล้องความถูกต้องระหว่างแผนที่การจำแนกกับข้อมูลอ้างอิงทางภาคพื้นที่มีอยู่สูง ความถูกต้องที่ได้รับจากการศึกษาในครั้งนี้สามารถยอมรับได้อย่างชัดเจน เมื่อนำไปเปรียบเทียบกับผลการศึกษาค้นคว้าอื่น ซึ่งอาศัยตัวจำแนกโดยอาศัยกฎเกณฑ์ภายใต้การวิเคราะห์ข้อมูลภาพเชิงวัตถุ นอกจากนี้ พบว่า ความถูกต้องโดยรวมและสัมประสิทธิ์แคปปาของแผนที่การจำแนกการใช้ประโยชน์ที่ดินและสิ่งปกคลุมดินในปี พ.ศ. 2556 ภายใต้การวิเคราะห์ความสามารถของการถ่ายโอนเชิงพื้นที่ในพื้นที่ทดสอบ มีค่าเท่ากับ ร้อยละ 83.25 และ 79.17 ตามลำดับ จากผลลัพธ์ที่ได้รับอนุมานได้ว่า สามารถถ่ายโอนแบบจำลองการจำแนกการใช้ประโยชน์ที่ดินและสิ่งปกคลุมดินที่ได้พัฒนาขึ้นจากพื้นที่ต้นแบบไปยังพื้นที่ทดสอบเพื่อจำแนก

การใช้ประโยชน์ที่ดินและสิ่งปลูกคลุมดินได้ และผลจากการทดสอบค่าความแตกต่างของค่าสัมประสิทธิ์แคบปา พบว่า ไม่มีความแตกต่างกันอย่างมีนัยสำคัญ ในขณะเดียวกัน พบว่า ความถูกต้องโดยรวมและสัมประสิทธิ์แคบปาของแผนที่การจำแนกการใช้ประโยชน์ที่ดินและสิ่งปลูกคลุมดินในปี พ.ศ. 2557 จากข้อมูลภาพจากดาวเทียมในพื้นที่ต้นแบบ ภายใต้การวิเคราะห์ความสามารถของการถ่ายโอนเชิงเวลา มีค่าเท่ากับ ร้อยละ 66.00 และ 57.83 ตามลำดับ จากผลที่ได้รับนี้สามารถอนุมานได้ว่า แบบจำลองเชิงอรรถศาสตร์เพื่อการจำแนกการใช้ประโยชน์ที่ดินและสิ่งปลูกคลุมดินใน ปี พ.ศ. 2556 ในพื้นที่ต้นแบบที่พัฒนาขึ้น ไม่สามารถถ่ายโอนได้โดยตรงสำหรับการจำแนกการใช้ประโยชน์ที่ดินและสิ่งปลูกคลุมดินในปี พ.ศ. 2557 ในพื้นที่เดียวกัน โดยต้องทำการตัดแปลงแบบจำลองเชิงอรรถศาสตร์ด้วยวิธีการลองผิดลองถูกเพื่อเพิ่มความถูกต้องของแผนที่ให้สูงขึ้น ซึ่งการปรับแก้แบบจำลองต้องใช้เวลาและเป็นงานที่ค่อนข้างยุ่งยาก

จากผลการศึกษาที่ได้รับสามารถสรุปได้ว่า การสร้างแบบจำลองและการจำแนกเชิงอรรถศาสตร์โดยอาศัยการวิเคราะห์ความสามารถการแยกจากกันและค่าขีดแบ่ง สามารถนำมาใช้เป็นเครื่องมือใหม่ในการจำแนกการใช้ประโยชน์ที่ดินและสิ่งปลูกคลุมดินภายใต้การวิเคราะห์ข้อมูลภาพเชิงวัตถุ ได้อย่างมีประสิทธิภาพ



PHAWINEE POOJARIT : LAND USE AND LAND COVER
CLASSIFICATION USING SEMANTIC MODEL OF OBJECT-BASED
IMAGE ANALYSIS. THESIS ADVISOR : ASSOC. PROF. SUWIT
ONGSOMWANG, Dr. rer. Nat. 145 PP.

OBJECT-BASED IMAGE ANALYSIS / SEMANTIC MODEL AND
CLASSIFICATION / SEPARABILITY AND THRESHOLD ANALYSIS / LAND
USE AND LAND COVER CLASSIFICATION

Object-based image analysis (OBIA) is the one of digital image analysis offers great potential since it has a very large feature basis for classification and additional data from other data sources can be readily integrated and used for analysis. Main objectives of the study are (1) to develop semantic model and classification with SEaTH and expert's knowledge for LULC extraction in reference area; (2) to apply the developed semantic model and classification for spatial transferability analysis; and (3) to modify the developed semantic model and classification of reference area for temporal transferability analysis. Study area covers 3 districts of Nakhon Ratchasima Province include Pak Thong Chai and Wang Nam Khieo districts as reference area and Khon Buri district as testing area. Main components of the research methodology included semantic modelling and classification development, spatial transferability analysis and temporal transferability analysis.

As results, it was found that semantic modelling and classification with SEaTH analysis was successfully developed and applied to extract LULC data from Landsat image of 2013 which included urban and built-up area, paddy field, cassava, maize,

sugarcane, perennial trees and orchard, forest land, and water body. The obtained overall accuracy and Kappa hat coefficient of thematic LULC map were 84.24% and 80.37 %, respectively. Based on Kappa hat coefficient more than 80%, it represents strong agreement/accuracy between the classification map and the ground reference information. The achieved accuracy proved to be acceptable when it was compared with other studies that applied rule-based classifier under OBIA. In addition, overall accuracy and Kappa hat coefficient of the thematic LULC of 2013 in testing area under spatial transferability analysis were 83.25% and 79.17%, respectively. This finding infers that the developed semantic model for LULC classification in reference area can be transferred to testing area for LULC extraction and it can provide indifferent accuracy based on pairwise Z test. Meanwhile, overall accuracy and Kappa hat coefficient of the thematic LULC map of 2014 from Landsat 8 image in reference area under temporal transferability analysis were 66.00% and 57.83%, respectively. This finding deduces that the developed semantic model for LULC classification in 2013 in reference area cannot be directly transferred for LULC extraction in 2014 at the same area. The developed semantic model required to modify by mean of trial and error method for increasing the thematic accuracy. The modification of semantic model is time consumption and tedious works.

In conclusion, it appears that semantic modelling and classification with SEaTH analysis can be efficiently used as new tools for LULC extraction under OBIA.

School of Remote Sensing

Academic Year 2014

Student's Signature _____

Advisor's Signature _____

ACKNOWLEDGEMENTS

This thesis would not have been possible without the guidance and the help of several individuals who in one way or another contributed and extended their valuable assistance in the preparation and completion of this study.

First and foremost, I would like to express my thankfulness to my advisor, Assoc. Prof. Dr. Suwit Ongsomwang for his precious advice to complete this work. I also sincerely thank him for sparing his immensely valuable time to proof this thesis.

I am profoundly grateful to Asst. Prof. Dr. Songkot Dasananda, Asst. Prof. Dr. Sunya Sarapirome, and Assoc. Prof. Dr. Sura Pattanakit for serving as committee members and providing suggestions. Additionally, I am thankful to Dr. Pantip Piyatadsananon who provided me valuable comments and suggestions. I am also grateful to Suranaree University of Technology for providing scholarship. Special thanks to Dr. Patiwat Littidej, Ms. Pimpraphai Piphatnawakul, Ms. Warunee Aunphoklang and Ms. Salisa Saraisamrong, for kindness support in ground checking. I extend my thanks to staff in Remote Sensing laboratory, Mr. Tinn Thirakultomorn for supervision and preparation of field survey map. I also thank Ms. Parinda Pukongdueang and student of Remote Sensing for their help and support during my stay here. Finally, a note of thanks goes to my beloved parents, my sister and my brother whose love and persistent confidence on me. My graduation would not be achieved without their understanding and reassurance.

Phawinee Poojarit

CONTENTS

	Page
ABSTRACT IN THAI.....	I
ABSTRACT IN ENGLISH	III
ACKNOWLEDGEMENTS	V
CONTENTS.....	VI
LIST OF TABLES	IX
LIST OF FIGURES	XII
LIST OF ABBREVIATIONS.....	XVI
CHAPTER	
I INTRODUCTION.....	1
1.1 Background and significance of the study	1
1.2 Research objectives	4
1.3 Scope and limitations of the study and study area	4
1.3.1 Scope of the study	4
1.3.2 Limitation of the study	5
1.3.3 Study area	6
1.4 Benefit of the study	9
II BASIC CONCEPTS AND LITERATURE REVIEWS.....	10
2.1 Basic concept of object-based image analysis	10
2.1.1 Image Segmentation.....	14

CONTENTS (Continued)

	Page
2.1.2 Feature extraction.....	23
2.1.3 Semantic Modelling	28
2.1.4 Semantic Classification.....	32
2.2 Literature Reviews	33
III EQUIPMENT, DATA AND METHODOLOGY.....	44
3.1 Equipment	44
3.2 Research methodology	45
3.2.1 Data collection and preparation.....	46
3.2.2 Component I: Semantic model and classification development	52
3.2.3 Component II: Spatial transferability analysis	55
3.2.4 Component III: Temporal transferability analysis	57
IV RESULTS AND DISCUSSION.....	58
4.1 Preprocessing data product.....	58
4.1.1 Optimum pan-sharpening method of Landsat 8 imagery	58
4.1.2 Optimum four band combination dataset	63
4.2 Semantic modelling and classification development for LULC classification	65
4.2.1 Image segmentation by multiresolution segmentation.....	66
4.2.2 Feature extraction by SEaTH analysis	67
4.2.3 Semantic modeling	91
4.2.4 Semantic classification of LULC in 2013 in reference area	95

CONTENTS (Continued)

	Page
4.2.5 Accuracy assessment of thematic LULC map of 2013 in reference area.	100
4.3 Spatial transferability analysis.....	103
4.3.1 Semantic classification of LULC in 2013 in testing area.....	103
4.3.2 Accuracy assessment of thematic LULC map in 2013 in testing area..	107
4.4 Temporal transferability analysis	109
4.4.1 Semantic classification of LULC in 2014 in reference area	109
V CONCLUSION AND RECOMMENDATION	123
5.1 Conclusion.....	123
5.1.1 Optimum pan-sharpening method of Landsat 8.....	123
5.1.2 Optimum four band combination dataset of Landsat 8	124
5.1.3 Development of semantic model and classification for LULC extraction.	124
5.1.4 Application of semantic model and classification for spatial transferability analysis.....	124
5.1.5 Application of semantic model and classification for temporal transferability analysis.....	124
5.2 Recommendation.....	126
REFERENCES	128
APPENDIX	135
CURRICULUM VITAE.....	145

LIST OF TABLES

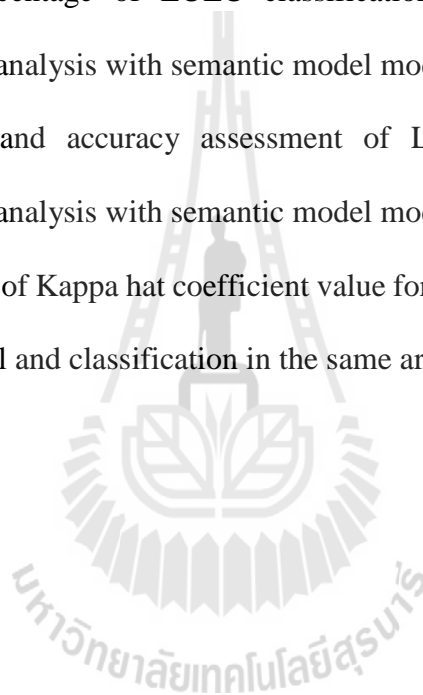
Table	Page
1.1 Major land use types in the study area based on LDD data in 2011.....	8
2.1 Summary of literature reviews for OBIA	42
3.1 List of hardware and software.....	44
3.2 Landsat 8 spectral sensor characteristics.	47
3.3 Characteristics of selected pan-sharpening algorithm.	50
4.1 Comparison of the image quality from different pan-sharpening methods for Landsat 8 of 2013 based on Q-average value.	62
4.2 Comparison of the image quality from different pan-sharpening methods for Landsat 8 of 2014 based on Q-average value.	62
4.3 OIF values of possible four band combination of pan-sharpened image from pan-sharpened Landsat 8 data of 2013 and 2014.	65
4.4 SI values of possible four band combination of pan-sharpened image from pan- sharpened Landsat 8 data of 2013 and 2014	65
4.5 Parameter setting of multiresolution segmentation and number of the derived image objects.....	67
4.6 List of selected 94 features for SEaTH analysis	70
4.7 Average mean value from 10 training areas of 94 features for 12 LULC classes	72
4.8 Average variance value from 10 training areas of 94 features for 12 LULC classes.....	76

LIST OF TABLES (Continued)

Table	Page
4.9 Candidate features may be used to classify forest land type I (FO1) from others LULC classes.	81
4.10 Semantic model for LULC extraction in reference area with Landsat 8 data in 2013 in table form.	93
4.11 Area and percentage of LULC classification for year 2013 in reference area ..	98
4.12 Comparison of LDD's land use data in 2011 and LULC data in 2013 by OBIA in reference area.	99
4.13 Error matrix and accuracy assessment of LULC in 2013 in reference area...	103
4.14 Area and percentage of final LULC classification of 2013 for spatial transferability analysis.	104
4.15 Comparison of LDD's land use data in 2011 and LULC data in 2013 by OBIA.	106
4.16 Error matrix and accuracy assessment of LULC of 2013 of spatial transferability analysis in testing area.	108
4.17 Pairwise Z test of Kappa hat coefficient value for LULC extraction by semantic model and classification between reference area and testing area.	109
4.18 Area and percentage of LULC classification of year 2014 of temporal transferability analysis without semantic model modification.....	111
4.19 Error matrix and accuracy assessment of LULC of 2014 of temporal transferability analysis without semantic modification.	112

LIST OF TABLES (Continued)

Table		Page
4.20	Modified semantic model for LULC extraction of temporal transferability analysis with Landsat 8 data in 2014.	117
4.21	Area and percentage of LULC classification of year 2014 of temporal transferability analysis with semantic model modification.	120
4.22	Error matrix and accuracy assessment of LULC of 2014 for temporal transferability analysis with semantic model modification.	121
4.23	Pairwise Z test of Kappa hat coefficient value for LULC extraction by modified semantic model and classification in the same area in different years.	122



LIST OF FIGURES

Figure	Page
1.1 Study site and its reference and testing area.	7
1.2 Topographic data of Nakhon Ratchasima province and study area.....	7
1.3 Distribution of main land use types in 2011 of study area.....	8
2.1 OBIA as an integrated approach	10
2.2 Structure of a hierarchical network. Braces indicate possible, fictitious semantics.	12
2.3 A hierarchical network of segmentation levels in eCognition Developer	12
2.4 Workflow of object-based image analysis in eCognition Developer.....	14
2.5 Weighted component of the homogeneity criteria.....	18
2.6 Multiresolution concept flow diagram.....	22
2.7 Example of multiresolution segmentation of THEOS data, Suranaree University of Technology. (a) Multi-resolution segmentation with scale 20, Color = 0.9, Shape = 0.1, Compactness and Smoothness = 0.5; (b) Color composite of THEOS data (Band 4, 3, 2).....	22
2.8 Examples of probability distributions	25
2.9 Threshold identification	28
2.10 Membership functions in eCognition 8.7.....	31
2.11 The general framework of building seismic vulnerability assessment	36
2.12 A flowchart demonstrating the overall procedure to generate final output	38
2.13 Overview of the method of gully feature extraction	39

LIST OF FIGURES (Continued)

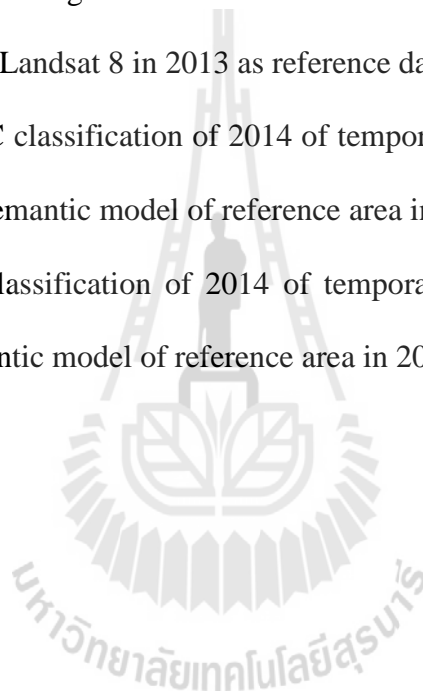
Figure	Page
2.14 The class hierarchy, and its associated features and rules used for land cover classification	40
3.1 Framework of research methodology.....	45
3.2 Composite image of Landsat 8 (Band 5, 4, 3): (a) Date 9 December 2013 and (b) Date 12 December 2014.....	46
3.3 Spatial and spectral subset of Landsat 8 acquired on 9 December 2013 (a) MS image (Band 5, 4, 3), (b) PAN image and Landsat 8 acquired on 12 December 2014 (c) MS image (Band 5, 4, 3), (d) PAN image.....	48
3.4 Workflow of Component I: Semantic modelling and classification development..	54
4.1 False color composite of original Landsat 8 data in 2013 and their pan-sharpened images, band 4, 5, and 3 (RGB): (a) original data (b) EF, (c), GS, (d) HPF, (e) MIHST and (f) WT.....	60
4.2 False color composite of original Landsat 8 data in 2014 and their pan-sharpened images, band 4, 5, and 3 (RGB): (a) original data (b) EF, (c), GS, (d) HPF, (e) MIHST and (f) WT	61
4.3 Image objects of pan-sharpened Landsat 8 data of 2013 by multiresolution segmentation.	66
4.4 Sample area selected image object for SEaTH analysis of 12 LULC types ...	68
4.5 Average mean and standard deviation of brightness feature of LULC classes ..	80

LIST OF FIGURES (Continued)

Figure	Page
4.7	Distribution of original LULC classification for year 2013 in reference area .. 95
4.8	Distribution of final LULC classification for year 2013 in reference area 96
4.9	Ground photograph of 8 LULC type.....97
4.10	Land use and LULC pattern comparison: (a) land use data in 2011 by LDD (b) LULC data in 2013 by OBIA 100
4.11	Distribution of sample points for accuracy assessment of thematic LULC map in 2013 102
4.12	Original LULC classification of 2013 for spatial transferability analysis 104
4.13	Final LULC classification of 2013 of spatial transferability analysis..... 105
4.14	Comparison of land use data 2011 by LDD and LULC in 2013 by OBIA: (a) by LDD (b) by OBIA 106
4.15	Sample points distribution for LULC data of 2013 accuracy assessment under spatial transferability analysis..... 108
4.16	Original LULC classification of 2014 for temporal transferability analysis without semantic model modification..... 111
4.17	Final LULC classification of 2014 of temporal transferability analysis without semantic model modification..... 112
4.18	Landsat 8 color composite image comparison between 2013 and 2014 due to phenological change of biological features of various LULC classes 114

LIST OF FIGURES (Continued)

Figure	Page
4.19 Landsat 8 color composite image comparison between 2013 and 2014 due to phenological change of physical features of reservoirs and dams.....	115
4.20 Comparison of histogram data of Landsat 8 in 2014 before and after histogram matching with Landsat 8 in 2013 as reference data.....	116
4.21 Original LULC classification of 2014 of temporal transferability analysis with the modified semantic model of reference area in 2013	119
4.22 Final LULC classification of 2014 of temporal transferability analysis with modified semantic model of reference area in 2013.....	120



LIST OF ABBREVIATIONS

EF	=	Ehlers Fusion Method GS
GLCM	=	Grey-Level Co-occurrence Matrix
GS	=	Gram-Schmidt Pan-Sharpening Method
HPF	=	High Pass Filtering Method
LDD	=	Land Development Department
LULC	=	Land Use and Land Cover
MIHST	=	Modified IHS Transformation Method
MS	=	Multispectral
NIR	=	Near Infrared
OBIA	=	Object- Based Image Analysis
OIF	=	Optimum Index Factor
PA	=	Producer's Accuracy
PAN	=	Panchromatic
Q	=	Quality indices
SEaTH	=	SEeparability And THresholds
SI	=	Sheffield Index
UA	=	User's Accuracy
WT	=	Wavelet Transformation

CHAPTER I

INTRODUCTION

1.1 Background problem and significance of the study

Image analysis of remotely sensed data is the science behind extracting information from the pixels within a scene or an image (Navulur, 2007). The advancement of feature recognition and advanced image analysis techniques facilitates the extraction of thematic information, for policy making support and informed decisions. The increased spectral variability among land covers in remotely sensed data demands classification algorithms based on the use of more spatial information that cannot be met with the conventional per-pixel image classification methods (Gao, 2009).

In the past, most digital image classification was based on processing the entire scene pixel by pixel. This is commonly referred to as per-pixel classification (Jensen, 2007). In summary, pixel-based classification methods can be considered under the term cluster analysis. In this case, the individual N-dimensional pixel vectors in an N-dimensional feature space are analyzed, for example, with the aid of statistical methods, with fuzzy-logic techniques or with neural networks and assigned to a class. The feature to be classified is generally the spectral signature of a pixel (Nussbaum and Menz, 2008). Until now pixel-based methods are still the most commonly used type of classification in remote sensing. Due to this fact, they are described in detail and

mathematically derived in the remote sensing textbook such as Thomas M. Lillesand, Ralph W. Kiefer and Jonathan W. Chipman (2004), Robert A. Schowengerdt (2007), James B. Campbell and Randolph H. Wynne (2011) and John A. Richards (2013).

In recent years, these purely pixel-based methods have increasingly reached their limits despite further developments. One reason is the fact that with increasing spatial resolution of the satellite data the (small) feature basis of spectral values often only provides insufficient results for classification. Furthermore, there is an increasing amount of additional data such as information from GIS systems or digital elevation models (DEMs). It appears meaningful for future investigations to integrate these additional data into satellite image analysis. Object-based image analysis offers great potential here, since it has a very large feature basis for classification and additional data from other data sources can be readily integrated and used for analysis (Nussbaum and Menz, 2008).

Blaschke (2010) reviewed OBIA for remote sensing, which aimed to delineate readily usable objects from imagery while at the same time combining image processing and GIS functionalities in order to utilize spectral and contextual information in an integrative way. The most common approach used for building objects is image segmentation, which dates back to the 1970s. Around the year 2000 GIS and image processing started to grow together rapidly through object based image analysis (OBIA - or GEOBIA for geospatial object based image analysis). The pixel paradigm is beginning to show cracks and the OBIA methods are making considerable progress towards a spatially explicit information extraction workflow. This is required for spatial planning as well as for many monitoring programs.

Horning, Robinson, Sterling, Turner, and Spector (2010) claimed that there are several advantages to this approach include:

- (1) It runs much faster since the number of segments is much less than the number of pixels in an image;
- (2) The relative scale of the segmentation output can be specified so different segmentation runs can be used to capture features of different sizes;
- (3) The classification algorithm can use the spectral characteristics (the pixel values) of an image as well as a host of other segment characteristics that describe the segment such as mean value, standard deviation, shape of the segments, and dimensions of the segment.
- (4) The resulting image does not suffer from the "salt and pepper" effect common to pixel-by-pixel classifiers.

In addition, in object-based image analysis, the “image object” is the central methodological element and as an object of investigation. To this end, image segmentation is conjoined with knowledge-based classification. Image segmentation decreases the level of detail, reduces image complexity. Segmentation produces image regions, and these regions, once they are considered “meaningful”, become image objects. A pixel as a technically defined unit can be interpreted in terms of its spectral behavior, in terms of the aggregation of spectral end-members, or in terms of its neighborhood. A pixel cannot be assigned a valid corresponding real-world object, but an image object can. Overcoming the pixel view and providing image objects that “make sense” opens a new dimension in rule-based automated image analysis; image objects can be labeled directly using a range of characteristics, including spatial ones,

or they can be used for modeling complex classes based on their spatial relationships, especially the use of rules based on expert knowledge explicit (Lang, 2008).

Therefore, semantic modelling and classification under object-based image analysis for land use and land cover (LULC) extraction is here developed in a reference area for spatial and temporal transferability analysis. The derived results are directly benefit to digital image analysts for extracting LULC information.

1.2 Research objectives

The specific objectives for LULC extraction using with semantic model and classification under OBIA are as follows:

- 1) To develop semantic model and classification with SEaTH and expert's knowledge for LULC extraction in reference area;
- 2) To apply the developed semantic model and classification of reference area for spatial transferability analysis;
- 3) To modify the developed semantic model and classification of reference area for temporal transferability analysis.

1.3 Scope and limitation of the study and study area

1.3.1 Scope of the study

- 1) Landsat 8 (LDCM) data acquiring in 2013 are used to develop semantic model and classification with SEaTH and/or expert's knowledge for LULC extraction in reference area.

2) The derived semantic model and classification in reference area is directly applied to Landsat 8 (LDCM) data acquiring in 2013 in different area for spatial transferability analysis.

3) The derived semantic model and classification in reference area is modified to Landsat 8 (LDCM) data acquiring in 2014 in reference area for temporal transferability analysis.

4) An optimum pan-sharpening technique, which include (1) Ehlers fusion (EF), (2) Gram-Schmidt pan-sharpening (GS), (3) High Pass Filtering (HPF) (4) Modified IHS transformation (MIHS), and (5) Wavelet fusion (WT), is firstly identified for Landsat 8 (LDCM) data in 2013 based on average of universal image quality index (Q-average). Then an optimum four band combination dataset is evaluated using Optimum Index Factor (OIF) and Sheffield Index (SI) to reduce number of bands. Later, an optimum four band combination dataset of Landsat 8 in 2013 are used to develop semantic model and classification. Finally the developed semantic model and classification is further applied for spatial and temporal transferability analysis.

5) Recent land use data and land use classification system in 2011 of Land Development Department (LDD) is used as a guideline for LULC extraction under reference area and test areas for spatial and temporal transferability analysis.

6) Classification rules of semantic model and classification under OBIA are based on the extracted feature's properties from SEaTH and/or an explicit expert's knowledge.

1.3.2 Limitation of the study

Due to limitation of the existing LULC data in 2013, field survey in 2015 and relevant very high spatial resolution image are used to assess accuracy for semantic

model and classification development in reference area and spatial and temporal transferability analysis.

1.3.3 Study area

The study area is a part of Nakhon Ratchasima province which consist of 32 districts. Herein two districts, namely Pak Thong Chai and Wang Nam Khieo districts are selected as reference area for semantic model and classification development for LULC in 2013 extraction and temporal transferability analysis for LULC in 2014 classification. In addition, Khon Buri district is chosen as testing area for spatial transferability analysis for LULC in 2013 extraction (Figure 1.1).

Nakhon Ratchasima province is located on the western end of the Khorat Plateau, separated from the Chao Phraya river valley by the Phetchabun and Dong Phaya Yen mountain ranges (Figure 1.2). It is 259 km from Bangkok and has an area of 20,494 sq. km, making it the biggest Thai province (Karnjanasin and Natthira, 2003). According to land use data of Land Development Department (LDD) in 2011, two main land use types in the study area are forest land (47.38%) and agricultural land (43.28%) as summary in Table 1.1 and Figure 1.3.

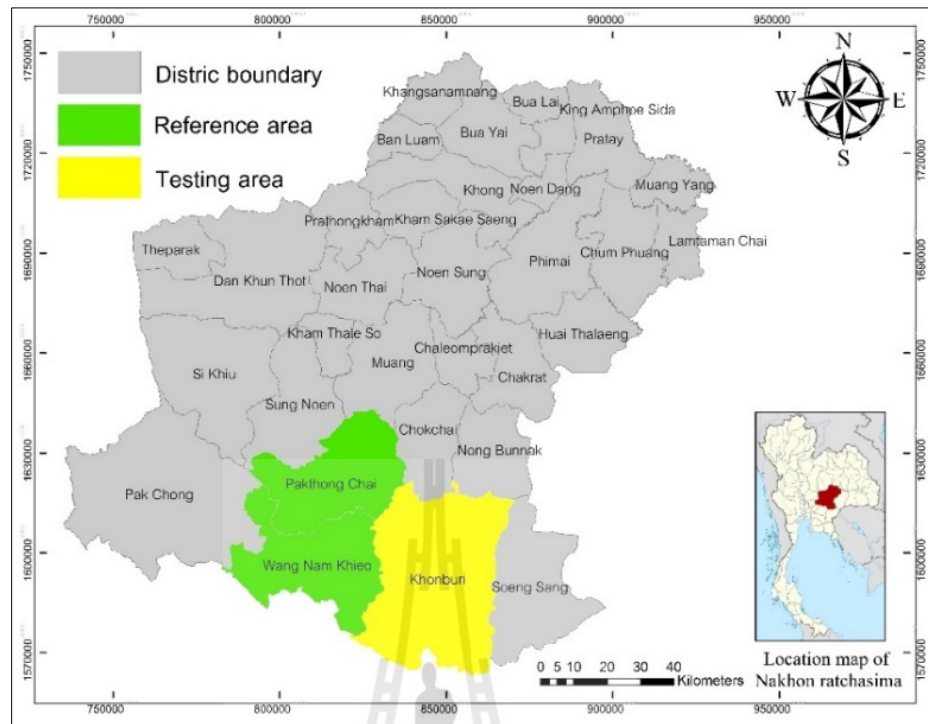


Figure 1.1 Study site and its reference and testing areas.

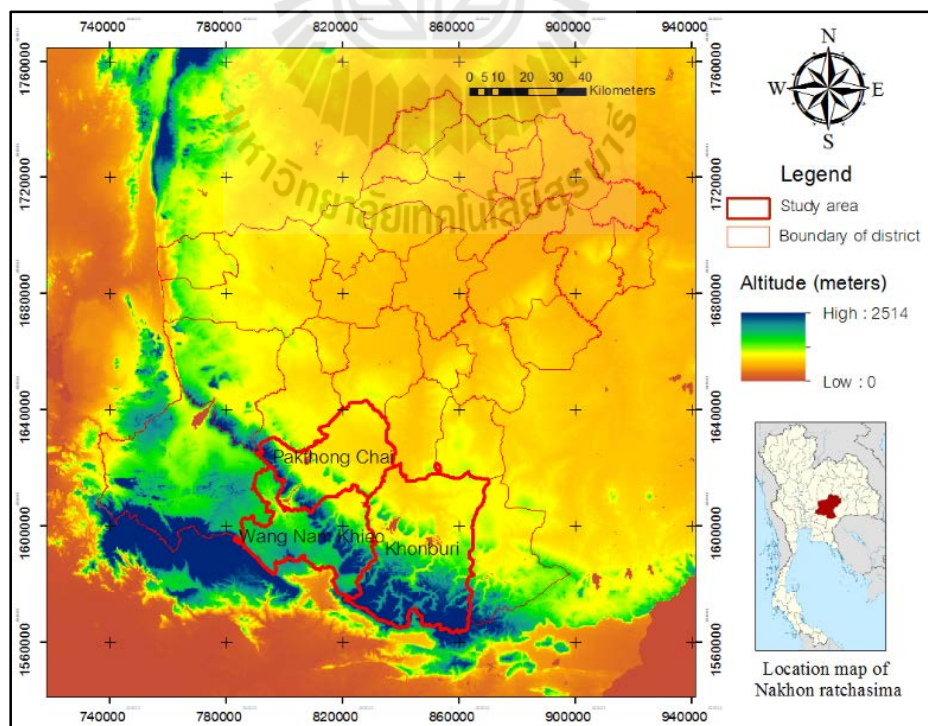
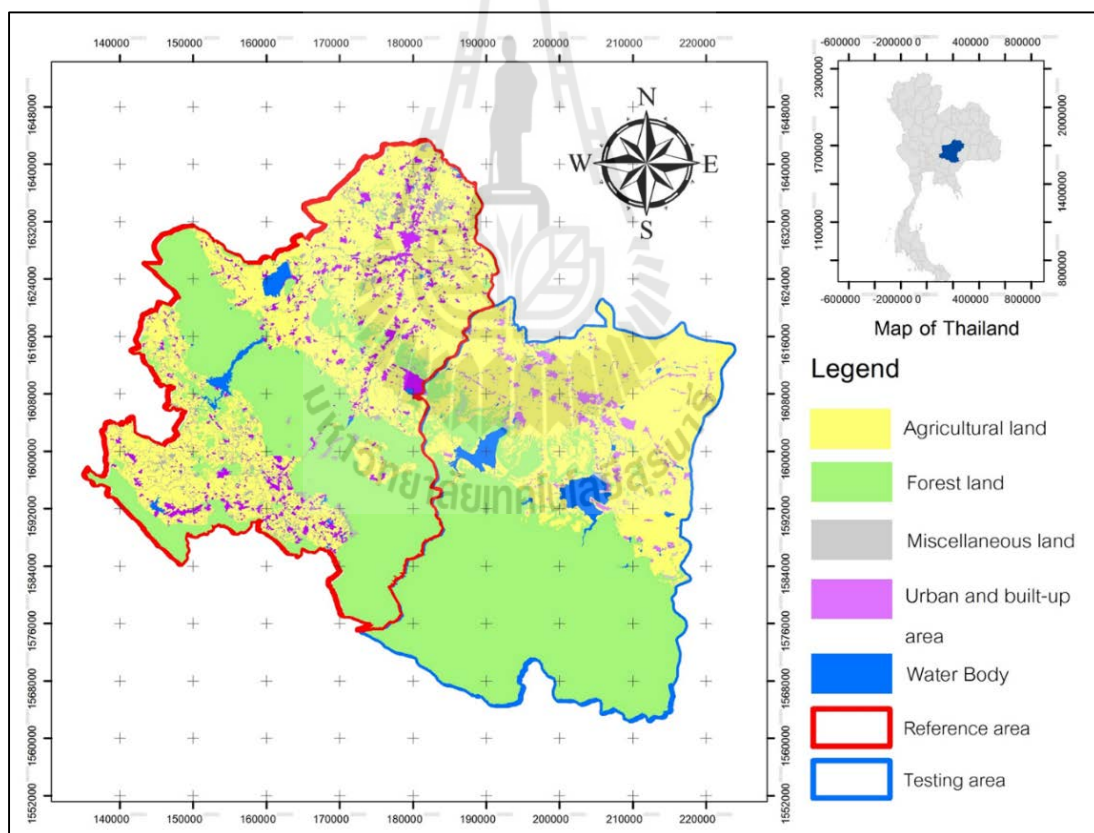


Figure 1.2 Topographic data of Nakhon Ratchasima province and study area.

Table 1.1 Major land use types in the study area based on LDD data in 2011.

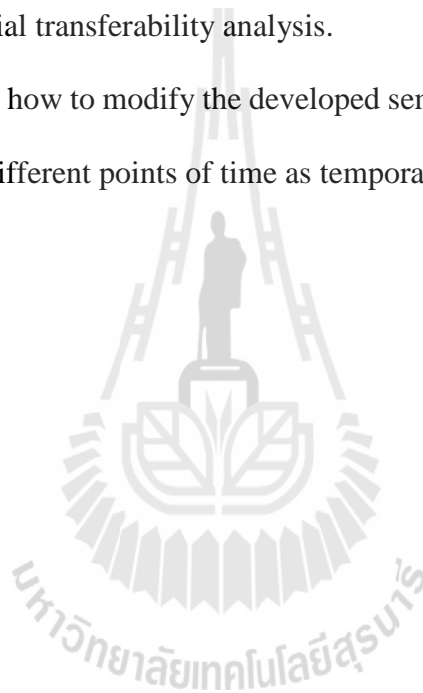
Land use type (sq. km)	Reference area		Testing area	Total	Percent
	Pak Thong chai	Wang Nam Khieo	Khon Buri		
Urban and built-up area	62.49	49.77	50.22	162.48	4.18
Agricultural land	584.82	371.53	726.44	1,682.79	43.28
Forest land	269.83	548.89	1,023.52	1,842.24	47.38
Water body	31.95	10.08	16.55	58.58	1.51
Miscellaneous land	36.92	51.17	53.82	141.91	3.65
Total	986.01	1,031.44	1,870.55	3,888.00	100.00

**Figure 1.3** Distribution of main land use types in 2011 of study area (LDD, 2011).

1.4 Benefit of the study

The benefits of the study have influenced with digital image analyst who are interested in OBIA as follows:

- (1) Obtaining semantic model and classification with rule-based classifier for LULC extraction from remotely sensed data under OBIA.
- (2) Knowing how to transfer the developed semantic model and classification in another area as spatial transferability analysis.
- (3) Knowing how to modify the developed semantic model and classification in in the same site at different points of time as temporal transferability analysis.



CHAPTER II

BASIC CONCEPTS AND LITERATURE REVIEWS

Under this chapter, object-based image analysis (OBIA) with key related concepts and literature reviews are here described.

2.1 Basic concepts of object-based image analysis

OBIA is one of alternative for extracting information. Every object is characterized by several features defined based on layer values, texture, shape and context of the object. Stefan Lang (2008) mentioned that OBIA applied an integration approach for information extraction including provision of units, regionalization, classification and interpretation (Figure 2.1).

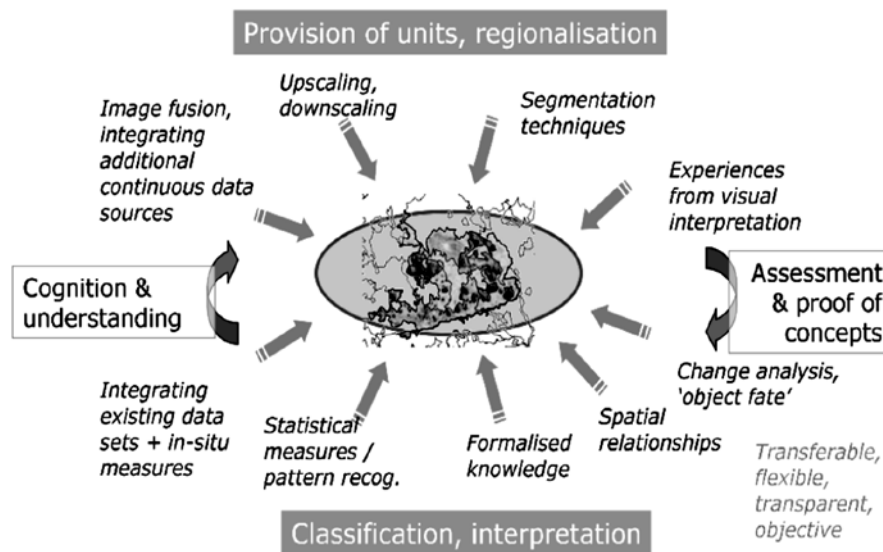


Figure 2.1 OBIA as an integrated approach (Lang, 2008).

OBIA can be compared in a first approximation with visual perception. A part from pure color information, patterns result from other features such as texture, shape, size or from the relations between individual objects. In general a procedure similar to visual interpretation is also aimed by OBIA and the eCognition software frequently used for image analysis in particular. Although the complexity and performance of human perception is by no means reached, there are certain parallels. OBIA methods rank among the so called computer-vision techniques (Wilkinson, 1999).

Under OBIA, an object can be defined as a grouping of pixels of similar spectral and spatial properties. Thus, applying the object-oriented paradigm to image analysis refers to analyzing the image in object space rather than in pixel space, and objects can be used as the primitives for image classification rather than pixels. Image segmentation is the primary technique that is used to convert a scene or image into multiple objects. The object-oriented paradigm allows us to exploit all aspects of remote sensing, including spectral, spatial, contextual, textural, and temporal properties for feature extraction (Navulur, 2007).

For the same scene, objects can also be created at different sizes and at multiple levels from the same image (Figures 2.2 and 2.3). The advantage of this approach is that you can mask out objects of no interest at larger scales, and focus on extraction of features of interest to the end user. Furthermore, by creating objects at different levels, parent-child relationships can be leveraged to improve/enhance feature extraction process in various applications such as change detection (Navulur, 2007).

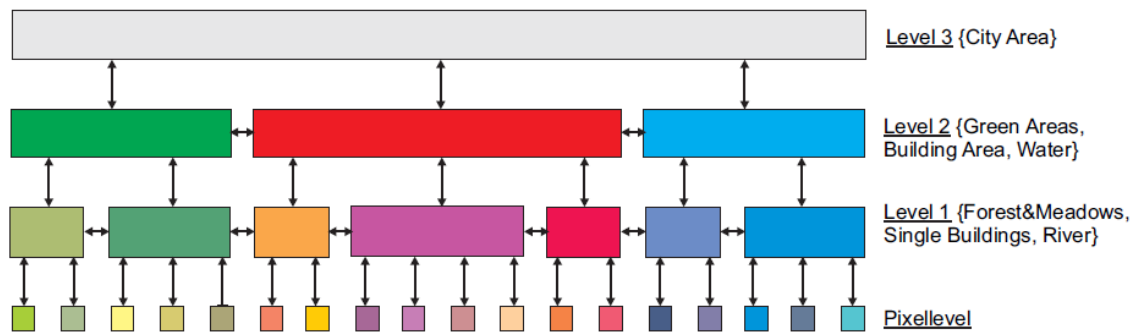


Figure 2.2 Structure of a hierarchical network. Braces indicate possible, fictitious semantics (Nussbaum and Menz, 2008).

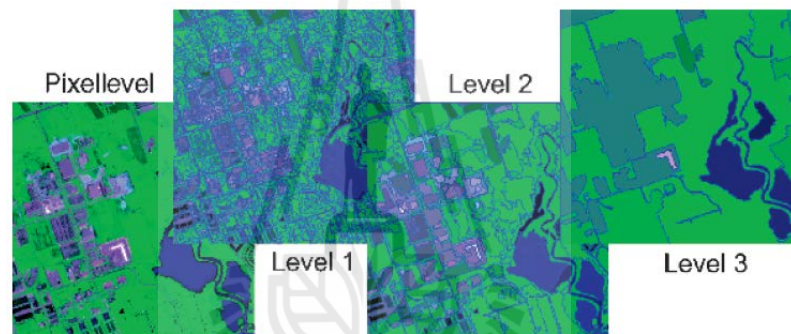


Figure 2.3 A hierarchical network of segmentation levels in eCognition Developer (Nussbaum and Menz, 2008).

For OBIA approach, an image to be analyzed is firstly segmented into individual image objects. The formed segments should well reflect the objects present in reality. Various methods can be used for segmenting. The objects can be then classified by heuristic methods or by knowledge-based techniques such as semantic networks. In knowledge-based systems, the rule base for classification is established via a feature combination. A part from the spectral signature, features such as shape, size, texture and neighborhood relations of the objects can additionally be used for object

description. A rating function is then used to allocate the objects to a number of classes according to their feature description.

OBIA integrates knowledge about the objects into the analysis. A differentiation is made here between declared knowledge (knowledge from various data sets), procedural knowledge (method for utilizing the data sets) and a priori knowledge (knowledge without relation to the analyzing data inventory). The investigations and analyses carried out in OBIA were performed against the background of a knowledge-based, object-based image analysis, where all types of knowledge available about the study region are integrated into the process (Nussbaum and Menz, 2008).

For an operational workflow for OBIA, the image analysis software copies the way in which human perception functions. The human brain constructs an overall image from individual objects. The objects are related on the basis of a large number of features with empirical values, existing knowledge and the surrounding objects. In the first step, the image pixels from the image are grouped to form objects with the aid of a multiscale segmentation. The simultaneous formation of several levels of segmentation on different scales is possible and indeed desirable. These levels are then hierarchically linked to each other. Since image objects, image information and processes are present simultaneously on several scales and the relation between these scales is known, important additional information can be obtained for interpretation purposes and real-world objects of different sizes can be classified. After multiscale segmentation, the features and relations of the individual object classes are defined within a hierarchical network. This step is also termed semantic modelling. The semantic classification of the objects into object classes is then performed on the basis of this semantic model (Nussbaum and Menz, 2008) as shown in Figure 2.4. Herewith

major tasks of OBIA which consist of (a) image segmentation, (b) feature extraction and (c) semantic modelling and classification are here separately described as below.

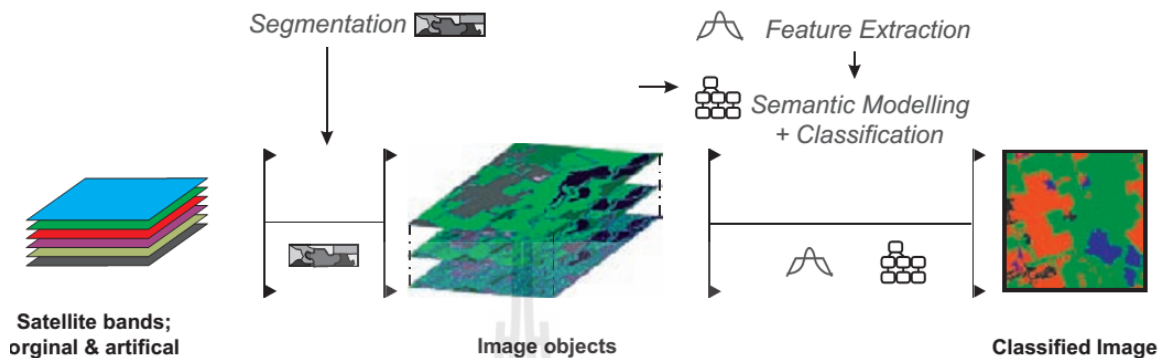


Figure 2.4 Workflow of object-based image analysis in eCognition Developer

(Nussbaum and Menz, 2008).

2.1.1 Image Segmentation

Image segmentation refers to the process of decomposing an input image into spatially discrete, contiguous, nonintersecting, and semantically meaningful segments or regions. These regions are patches comprising relatively homogeneous pixels. These pixels share a higher internal spectral homogeneity among themselves than external homogeneity with pixels in other regions (Ryherd and Woodcock, 1996). Herein, specific image segmentation methods for digital image classification include segmentation based on multiple criteria and multi-scale image segmentation are here introduced.

(1) Segmentation Based on Multiple Criteria Method

The pixel-, edge-, and region-based segmentation methods are limited in that the operation is based exclusively on one criterion, namely, pixel values in the multispectral domain. Thus, a huge amount of spatial information among pixels is wasted. This inability to make full use of the available spatial properties usually leads to poor segmentation outcomes, especially if the image has a fine spatial resolution. This deficiency may be overcome via three means:

First, by making use of more segmentation criteria. For instance, spatial relationship (e.g., contexture and shape) may be incorporated into segmentation by replacing the value of individual pixels that averaged in a neighborhood around each pixel.

Second, by making use of additional image characteristics other than pixel values (e.g., texture) as an extra criterion in the segmentation. The utility of texture in segmenting an image varies with the scene. Its use is the most beneficial for areas where the desired classes exhibit textural differences (Ryherd and Woodcock, 1996). The addition of texture into spectral image segmentation brings out stronger benefits in threshold-based segmentation than in minimum size-based segmentation.

Third, multiple criteria such as shape and texture combined in one image segmentation (Hu et al., 2005). Shape can be depicted by such geometric parameters as compactness (C) and smoothness (S). The compactness criterion is especially important to consider in segmenting urban scenes where building roofs and adjacent roads share similar spectral values but have a very dissimilar shape.

There are different ways of calculating compactness (C) and smoothness (S). One way for compactness is to divide the de facto border length (l) by

the square root of the number of pixels comprising this image object (n) (Eq. 2.1) and smoothness is defined as the ratio of the de facto border length (l) to the shortest possible border length (b), or the border length derived from the bounding box of an image object parallel to the raster provided by the bounding box for an image object corresponding to the raster (Eq. 2.2).

$$C = \frac{l}{\sqrt{n}} \quad (2.1)$$

$$S = \frac{l}{b} \quad (2.2)$$

Both smoothness and compactness are combined linearly to define the shape homogeneity criterion that is invaluable in preventing the formation of fractal objects in urban areas. Homogeneity of image objects may be defined by the spectral and contextual information determined from such parameters as shape. Shape heterogeneity describes the change in an object's configuration as measured by smoothness and compactness. The change in shape homogeneity accompanying a merge (Δh_{shape}) is calculated using the following formulae:

$$\Delta h_{shape} = \omega_{compt} \cdot \Delta h_{compt} + \omega_{smooth} \cdot \Delta h_{smooth} \quad (2.3)$$

where ω_{smooth} and ω_{compt} stand for the weight for smoothness and compactness, respectively, with values between 0 and 1. The proper allocation of these two weight parameters allows adaptation of the heterogeneity definition to an application and determines the success of multiple segmentation; Δh_{compt} and Δh_{smooth} represent compactness heterogeneity and smoothness heterogeneity, respectively, both of which are governed by the number of pixels in objects before and after the merge, or

$$\Delta h_{smooth} = n_{merge} \cdot S_{merge} - (n_{obj-1} \cdot S_{obj-1} + n_{obj-2} \cdot S_{obj-2}) \quad (2.4)$$

$$\Delta h_{compact} = n_{merge} \cdot C_{merge} - (n_{obj-1} \cdot C_{obj-1} + n_{obj-2} \cdot C_{obj-2}) \quad (2.5)$$

where subscript *merge* refers to the merged object; n_{merge} denotes the number of pixels within the merged object; subscripts *obj-1* and *obj-2* refer to the two objects prior to the merge; n_{obj-1} and n_{obj-2} represent the number of pixels in objects 1 and 2, respectively, before the merge. Multiple segmentation criteria calculated from different parameters are usually combined to derive a compound fusion value (f). For instance, the shape heterogeneity criterion derived in Eq. 2.5 may be fused with the spectral heterogeneity criterion Δh_{color} to calculate spatial heterogeneity. This combination minimizes the deviation derived from a compact or smooth shape (Benz, Hofmann, Willhauck, Lingenfelder, and Heynen, 2004). The fused value (f) is a weighted linear combination of spectral and shape heterogeneity. In fact, the similarity between any two regions j and k is calculated separately in each feature space used in the segmentation, or

$$\begin{aligned} Sim_{jk}(f_1, f_2, \dots, f_n) &= \sum_{i=1}^n W_i \rho_i = \omega_{color} \cdot \Delta h_{color} + \omega_{shape} \cdot \Delta h_{shape} \\ &= \omega \cdot \Delta h_{color} + (1 - \omega) \cdot \Delta h_{shape} \end{aligned} \quad (2.6)$$

where n denotes the total number of criteria used in segmentation; W_i refers to the weight assigned to the i^{th} criterion ρ_i (e.g., shape, color, size, texture, and so on); w_{color} and w_{shape} stand for the weights assigned to the spectral and geometrical parameters, respectively. Their sum equals 1. The determination of these weights is based on the significance of the criterion in defining the regions. Spectral heterogeneity Δh_{color} refers to the spectral variation induced by merging two image objects. Spectral or color heterogeneity is a weighted sum of standard deviation of pixel values within the

respective regions in a given spectral band, or the sum of the standard deviations of spectral values in each layer multiplied by its weight w_c (Eq. 2.7). The color heterogeneity criterion ensures the generation of meaningful objects.

$$\Delta h_{color} = \sum_b \omega_b [n_{merge} \cdot \sigma_{b,merge} - (n_{obj-1} \cdot \sigma_{b,obj-1} + n_{obj-2} \cdot \sigma_{b,obj-2})] \quad (2.7)$$

where σ_b stands for the standard deviation within an object in band (b); w_b denotes the weight assigned to band (Benz et al., 2004). This weight enables multi variant segmentation of an image based on spectral properties. The above calculation has many terms, the exact number being equal to the number of spectral bands of the image. The weight of shape and the image's bands on the homogeneity of an object can be flexibly modified (Figure 2.5). The segmentation results may be adjusted in accordance with the desired application by assigning different weights to spectral and shape heterogeneity (Benz et al., 2004).

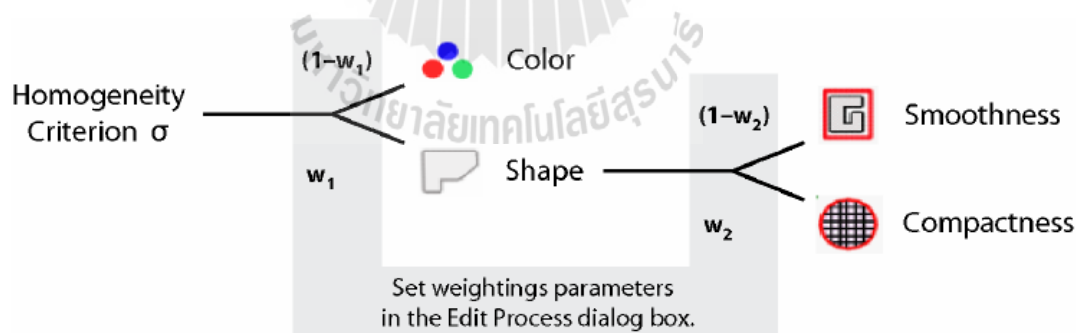


Figure 2.5 Weighted component of the homogeneity criteria (Trimble Germany GmbH, 2011).

(2) Multiscale (multiresolution) Image Segmentation

To successfully segment an image, it is imperative to take into account the scale at which the objects of interest occur in conjunction with the spatial resolution of the image. In most cases it is not possible to specify the exact scale level beforehand as there is no universally “ideal” scale for all features. This is especially true in urban areas where ground objects occur at a unique scale of their own. The appearance and characteristics of even the same type of objects vary with the scale of their rendition on satellite imagery. Segmentation of such objects must take place at multiscales. Scale is a unit less parameter related to image resolution. Thus, multiscale segmentation is synonymous with multiresolution segmentation. Analysis at multiresolution is necessitated by the fact that not all ground features occur at the same physical scale. The best segmentation result is achievable by segmenting an image at different scales (Burnett and Blaschke, 2003).

In multiresolution segmentation the input image is first segmented at a small scale by uniting the most similar objects, followed by a set of multiscale objects with their topological relationship fully obtained (Sun, Chen, and Li, 2006). During multiresolution segmentation the image is converted into object primitives that share a certain spectral behavior, shape, and context. These preliminary object features are then segmented at a higher level.

Multiresolution segmentation is a bottom-up region-merge starting with singular seed pixels, each of which is regarded as a potential region. In subsequent steps, these small regions are merged to form fewer big ones. A pair of neighboring image objects is evaluated to see if they meet the merging criteria. Whether adjoining objects should be merged is governed by the principle of homogeneity or lack

of it (i.e., heterogeneity). Namely, a merge should result in minimal growth in the selected heterogeneity criteria. Commonly used amalgamation criteria include area, perimeter, compactness, texture, and shape, all of which are derived from the segmented regions. Determination of their specific values is critical to achievement of segmentation results suitable for a particular type of application. Objects grow in size through successive iterations in which small objects are incrementally merged to form larger ones. This pairwise clustering is accompanied by an even and simultaneous growth of segments over a scene, and the calculation of the above indices for the newly formed objects. Such indices are applied to determining whether they should be amalgamated to form a large object after evaluation against a number of object properties. Expert knowledge may be involved in forming objects at different scales. As the merging process continues, the merged object becomes increasingly heterogeneous. Hence the heterogeneity criterion must be updated following every merge. It is imposed as a constraint on the merging process. The break-off criterion or the stop criterion is based on the relationship between these two objects and the comparison with the squared scale parameter. The merging process is terminated if all pixels have been assigned to regions or when the threshold derived from the user-defined parameters is reached (Batz and Schäpe, 2000).

The outcome of multiresolution image segmentation is affected by the scale parameter, the single layer weights, and the heterogeneity criteria. The scale parameter dictates the spatial extent within which pixel values are used to derive spectral heterogeneity in merging two regions. Its squared value internally determines the threshold for terminating the segmentation process. The extent of object growth also depends on the predefined break-off value. The broader this value, the bigger the

segmented object. Proper setting of the optimal breakoff value can overcome the limitation of pixel-based approaches in mapping large urban areas.

Multiresolution segmentation creates homogeneous image object primitives in a desired resolution, taking local contrasts into account without any prior knowledge (Blaschke and Hay, 2001). Multiresolution segmentation leads to a better understanding of the image content. A hierarchical network may be created to link image objects at different resolutions or scales. In this way the same image is represented at several resolutions (scales) simultaneously. The constructed hierarchy shows the horizontal neighbors (adjacent objects) of an image object at the same level, as well as their neighbors at other hierarchies. This multiscale representation enables differentiation of the same ground objects on several levels, hence increasing the reliability of their identification. If an image is segmented at multiresolution, it can be classified at different scales using the object-oriented method.

Summary of multiresolution concept by eCognition Developer software are presented in Figure 2.6 while an example of multiresolution image segmentation is displayed in Figure 2.7.

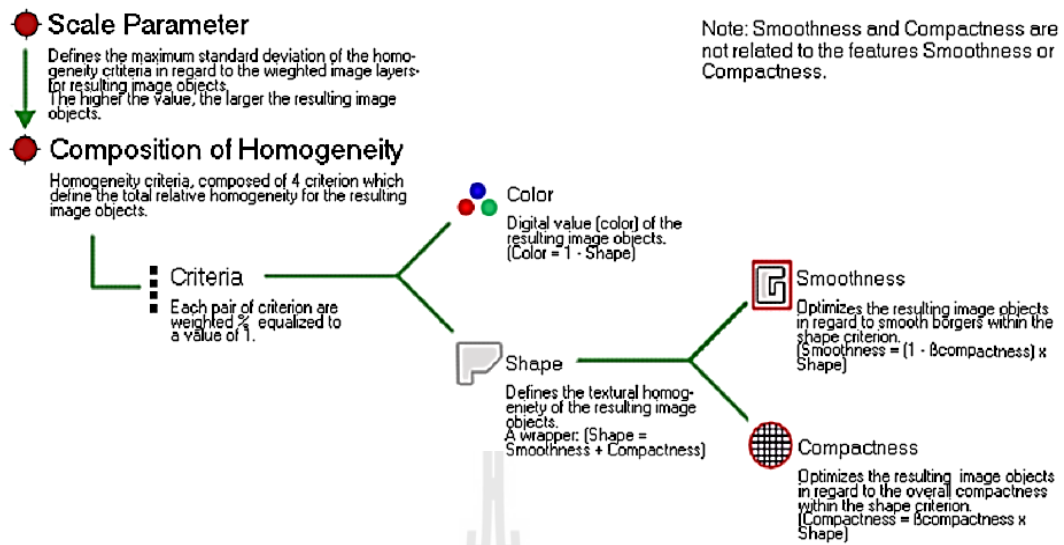


Figure 2.6 Multiresolution concept flow diagram (Trimble Germany GmbH, 2011).

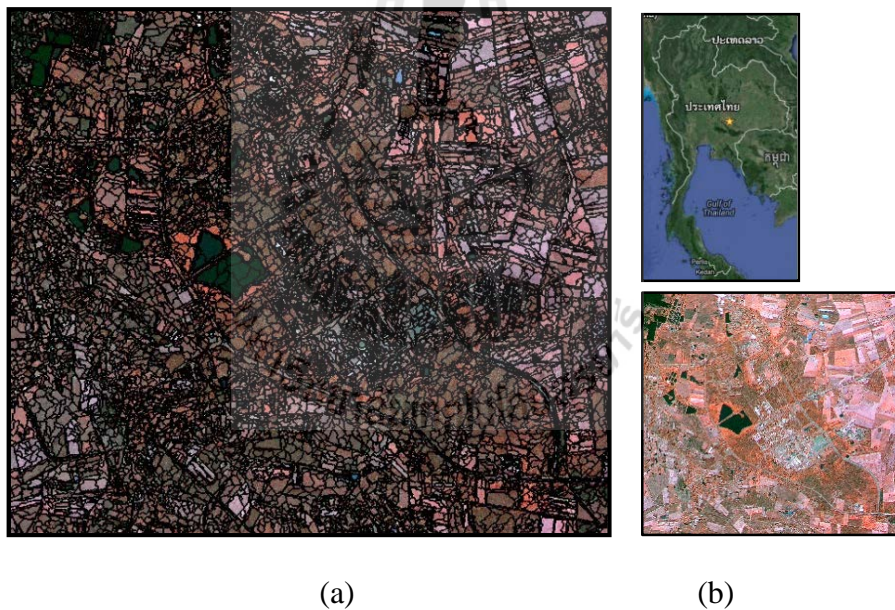


Figure 2.7 Example of multiresolution segmentation of THEOS data, Suranaree University of Technology. (a) Multi-resolution segmentation with scale of 20, Color=0.9, Shape=0.1, Compactness and Smoothness = 0.5; (b) Color composite of THEOS data (Band 4, 3, 2).

2.1.2 Feature extraction

As mentioned earlier, object-based image classification is a promising methodology as it is close to human perception. A typical object-based classification system starts with segmenting the image into smaller homogeneous regions (or image objects). These objects correspond to approximations of real-world objects. Every object is characterized by several features defined based on layer values, texture, shape and context of the object. This is where the possibility to automate the classification process becomes difficult. With a few input samples for every class and using the enormous object feature-space to our advantage, it is possible to automatically generate a rule base. However, the essential issue is to manage the huge information given by the color, shape, texture and context of the object. A good feature extraction is a basic prerequisite for successful work in OBIA. So SEaTH (SEparability and THresholds) which was introduced by Nussbaum and Menz (2008) for feature extraction are here summarized.

(1) SEaTH (SEparability and Thresholds)

The feature extraction tool of SEaTH identifies separability and thresholds characteristic features with a statistical approach based on training objects. These training objects represent a small subset out of the total amount of image objects and should be representative objects for each object class. The statistical measure for determining the representative features for each object class is the pairwise separability of the object classes among each other. Subsequently, SEaTH calculates the thresholds which allow the maximum separability in the chosen features.

The identification of the characteristic features is a problem of probability density estimation. On the basis of representative training data for each

object class, the probability distribution for each class can be estimated and used to calculate the separability between two object classes. Under the assumption of normal probability distributions, the Bhattacharyya distance (B) can be used as a suitable separability measure. Bhattacharyya distance is justified as a measure of separability from the Bayesian decision rule for misclassification probability as:

$$B = \frac{1}{8} (m_1 - m_2)^2 \frac{2}{\sigma_1^2 + \sigma_2^2} + \frac{1}{2} \ln \left[\frac{\sigma_1^2 + \sigma_2^2}{2\sigma_1\sigma_2} \right] \quad (2.8)$$

where m_i and σ_i , $i=1,2$, are the mean and the variance, respectively, for the two feature distributions. If the means coincide, the first term in vanishes, whereas the second term vanishes if the two feature distributions have equal variances

Figure 2.8 shows the probability distribution exemplified for two object classes (C_1 and C_2) and three notional feature (A, B and C). In feature A both object classes show a *partial separability*, this means that there is an area where the probability distributions of the object classes (C_1 and C_2) overlap in their feature characteristic. Given feature B this overlap is so large that its use for classification would result in a huge object misclassification rate. This feature therefore provides *poor separability* relative to object classes C_1 and C_2 . The ideal case is represented by feature C. Here the object classes have no overlap in the feature characteristic it is therefore well-suited for classification: the feature has *complete separability*.

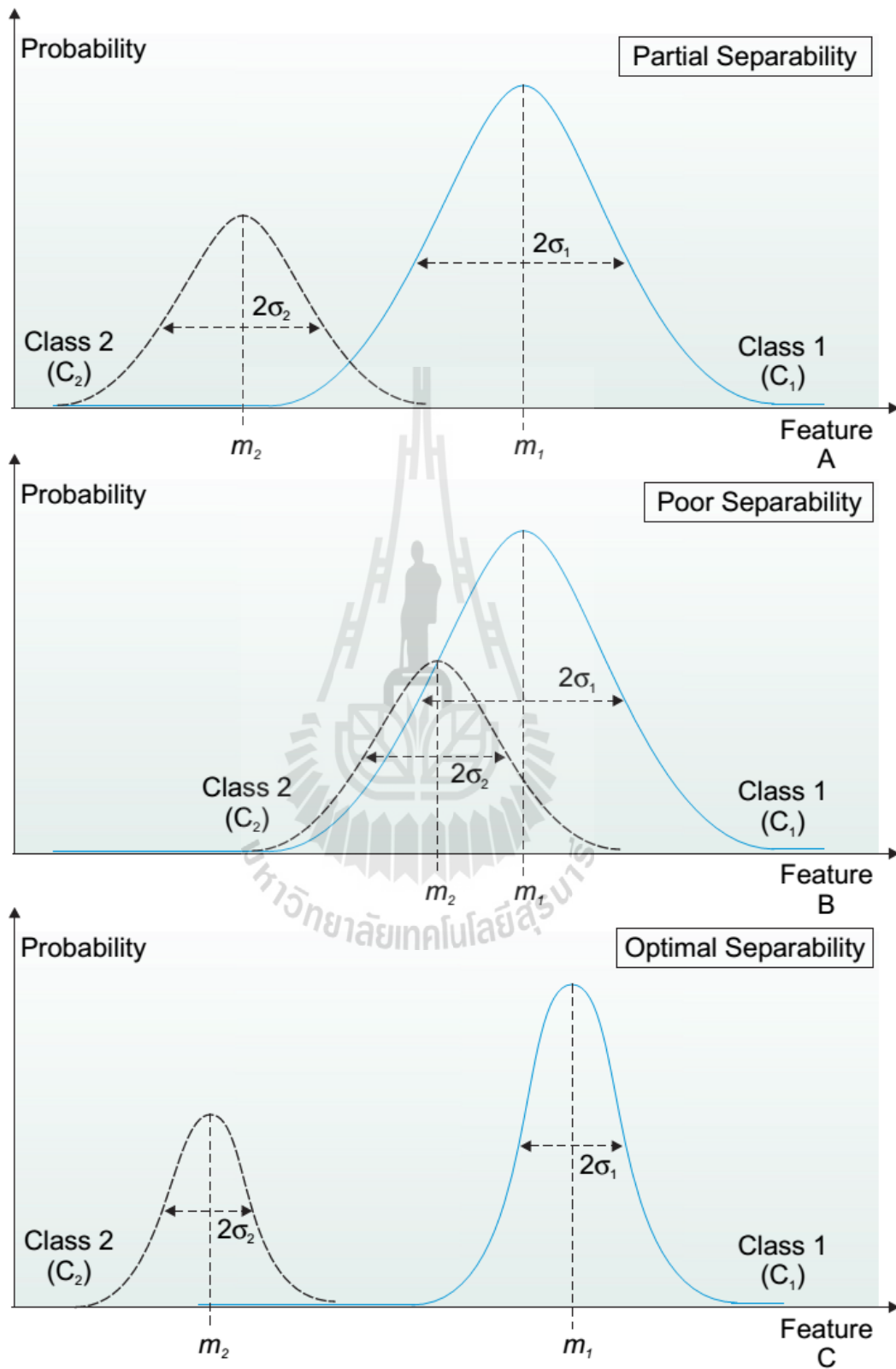


Figure 2.8 Examples of probability distributions (Nussbaum and Menz, 2008).

A more useful measure for separation in classification contexts is the Jeffries–Matusita distance (J) which has, unlike Bhattacharyya distance, a finite dynamic range. This allows a better comparison of the feature analysis results to identify that feature which has the best separability. The Jeffries–Matusita distance measures the separability of two classes on a scale [0–2] in terms of Bhattacharyya distance (B) as:

$$J = 2(1 - e^{-B}) \quad (2.9)$$

Complete separability of the two classes with respect to the analyzed feature is indicated by $J = 2$. On the basis of the training objects used, there will be no misclassifications if this feature is used for classification. The lower J is, the worse is the separability and the higher the number of misclassified objects. SEaTH calculates the separability for any number of given object classes and object class combinations.

Besides determining the features separating optimally the object classes among each other, it is essential to know also the decision threshold for the maximum separability. The knowledge of the optimum threshold is necessary for the assembly of a ruled-based classification model.

The optimum threshold is also calculated by SEaTH. A Gaussian probability mixture model of the form

$$p(x) = p(x|C_1)p(C_1) + p(x|C_2)p(C_2) \quad (2.10)$$

is fit to the frequency distribution of a feature for two object classes C_1 and C_2 where $p(x|C_1)$ is a normal distribution with mean, m_{C_1} and variance, $\sigma_{C_1}^2$ and similarly for

$p(x|C_2)$. The decision threshold which minimizes the error probability is obtained by solving

$$p(x|C_1)p(C_1) = p(x|C_2)p(C_2) \quad (2.11)$$

for x . Taking logarithms,

$$\frac{1}{2\sigma_{C_2}^2}(x - m_{C_2})^2 - \frac{1}{2\sigma_{C_1}^2}(x - m_{C_1})^2 = \log \left[\frac{\sigma_{C_1}}{\sigma_{C_2}} * \frac{p(C_2)}{p(C_1)} \right] = A \quad (2.12)$$

$$x_{1(2)} = \frac{1}{\sigma_{C_1}^2 - \sigma_{C_2}^2} \left[m_{C_2}\sigma_{C_1}^2 - m_{C_1}\sigma_{C_2}^2 \pm \sigma_{C_1}\sigma_{C_2} \sqrt{(m_{C_1} - m_{C_2})^2 + 2A(\sigma_{C_1}^2 - \sigma_{C_2}^2)} \right] \quad (2.13)$$

The relevant solution of the two can be determined by requiring that it lies between the two means m_1, m_2 of the probability distributions. Thus, for the example in Figure 2.9, x_1 is the correct choice. Since the distributions are only partially separated, there will be some misclassifications when using this feature for classification of unknown object classes. Given the validity of the normal approximation assumption, SEaTH will minimize their number. If the probabilities are not normally distributed, the calculated separability for this feature is low, i.e. it will not be used for classification purposes. This thus ensures that only very good features are taken into consideration.

In practice, to identify the best features for the classification SEaTH calculates the separability and the corresponding threshold for every object class combination and for every feature. Any number of object classes and features can be analyzed. An interpretation of the results allows a fast preparation of a classification model, with statistically optimized features and thresholds. SEaTH makes it possible to analyze a large number of features for object description in a short time.

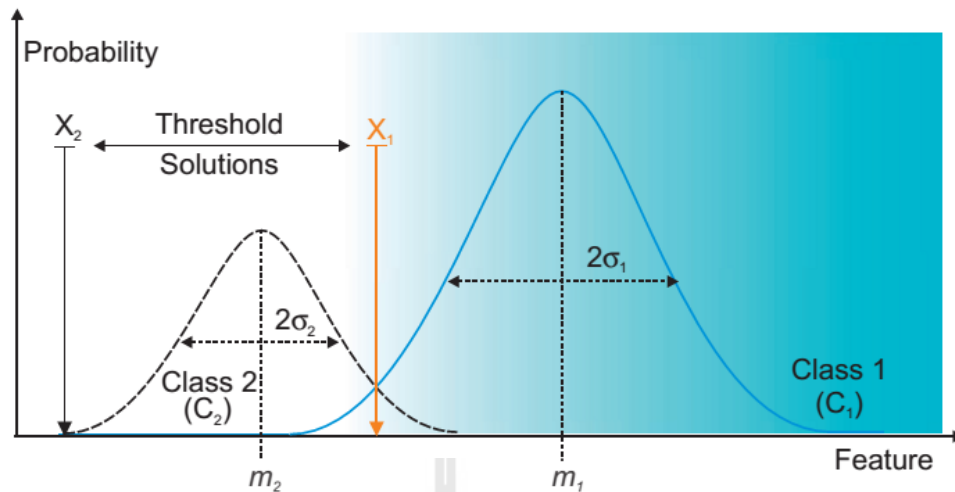


Figure 2.9 Threshold identification (Nussbaum and Menz, 2008)

2.1.3 Semantic Modelling

The major function of semantic modelling is to maintain the domain knowledge for representing spatial semantics associated with image databases. Queries at this level are generally descriptive in nature, and focus mostly on semantics and concepts present in image databases. For most of the applications, semantics at this level are based on “spatial events” describing the relative locations of multiple objects. Such semantics are used for high-level indexing and content-based retrieval of images. An example involving such semantics is a range query which involves spatial concepts such as close by, in the vicinity, larger than, etc. The most common applications employing spatial semantics and content-based retrieval based on range queries are map databases and geographic information systems (GIS). This type of systems is extensively used in urban planning and resource management scenarios. In clinical radiology applications, relative sizes and positions of objects are critical for medical diagnosis and treatment (Al-Khatib et al., 1999).

Under OBIA, an object can be described by characteristic features such as its spectral signature, shape, size, texture and neighborhood relations to other objects. These representative features enable a later classification into object classes. For semantic modelling, these typical features of the object classes must first be determined and combined in a semantic model (Nussbaum and Menz, 2008).

Nussbaum and Menz (2008) mentioned that the model is constructed as a rule-based semantic network, which constitutes a form of knowledge presentation. The advantage of a network is the possibility of a hierarchical arrangement and the inter-linkage of all information on the objects. The individual object class in the model is termed node. Concepts provide the generic description of the object classes. The implementation of this concept in the satellite scene under consideration is called instances.

The nodes of the network are linked to each other by edges. These edges describe the relations between neighboring, lower or upper objects. In technical terms, these relations can be broken down into hierarchical, topological, optional and obligatory relations. Hierarchical and topological relations result from the structural relations between the objects, whereas optional and obligatory relations are determined via the minimum and maximum number in the relations of the network.

The features of an object class are described by attributes. They have a measured value and a value range to which methods for calculation are allocated. The knowledge inherent in a semantic network can be separated into declared and procedural knowledge. Declared knowledge contains the concepts and relations, whereas procedural knowledge comprises the methods for calculating the concept

attributes and for evaluating the concepts and relations. The procedural knowledge thus determines the order of the analysis, which can be presented by a set of rules.

This rule base contains a condition and an action part. The condition verifies whether there is a new interpretation state for the neighboring node in the semantic network and the action part adapts this state accordingly. If there are several conditions characterizing an object class, they are linked by (logical) operators [e.g. and, or, not]. (Nussbaum and Menz, 2008)

The semantic modelling in eCognition consists of a feature analysis for the image objects obtained in the multiscale segmentation with the subsequent formation of a network of rule-based semantic features. In eCognition there are a large number of predefined features for describing object properties. Furthermore, user-defined features, so-called customized features can be set up. The membership of image objects in object classes is defined via so-called membership functions of the features (see Figure 2.10). This means that it is a member of a certain object class depending on the feature intensity of an image object. The dynamic range of these functions is $[0, 1]$ in eCognition and is plotted on their axes. The x-axis indicates the respective feature intensity. Membership can either be defined as a fixed threshold value or as a fuzzy logic threshold value. In the case of fixed threshold values, an image object either belongs to object class [1] or it does not [0]. The membership functions 3, 4, 9 and 12 from Figure 2.10 can be used here. In the case of a fuzzy logic threshold value, membership of a class varies depending on the feature intensity so that an object may belong to two object classes. The object is then assigned to that object class to which it has the highest membership value. Typical membership functions based on fuzzy logic are the shapes 1, 2, 5 and 6 in Figure 2.10. Twelve membership functions

are already predefined in eCognition. Furthermore, any functions required can be interactively set up and modified.

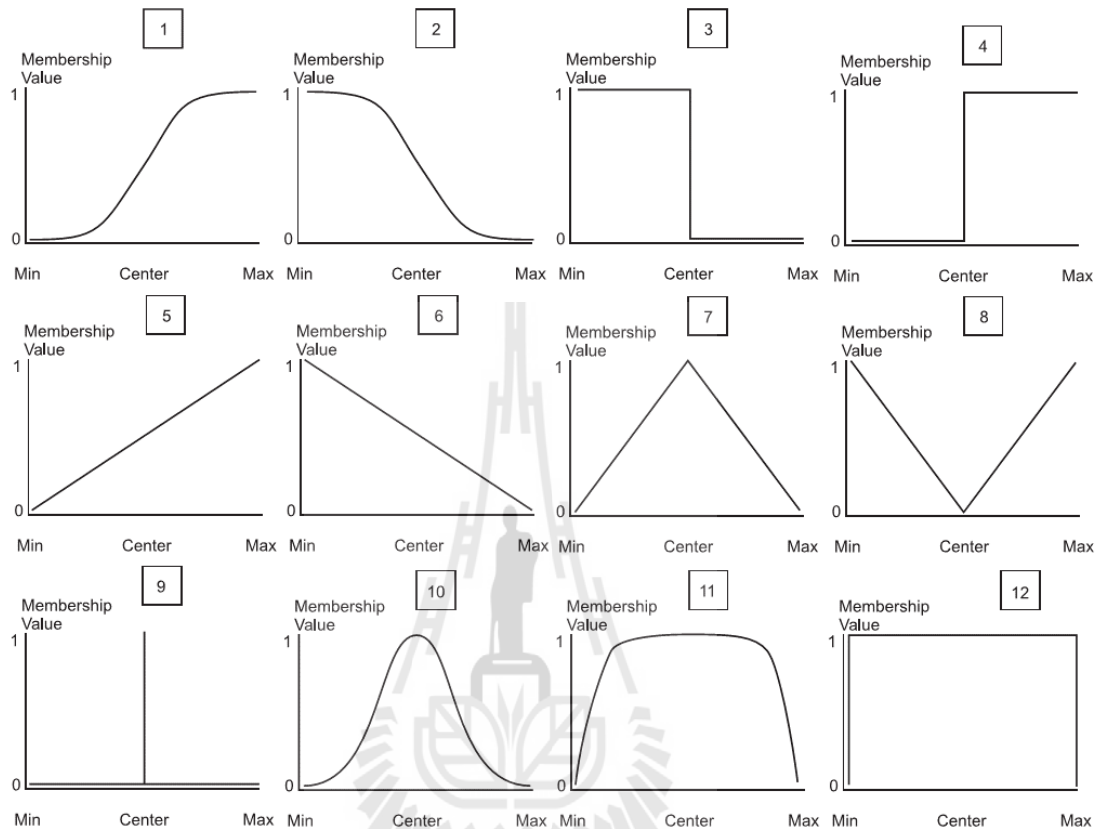


Figure 2.10 Membership functions in eCognition 8.7 (Nussbaum and Menz, 2008).

The feature analysis has the task of identifying characteristic features for the individual object classes. Once these typical features have been determined classification rules are drawn up for each object class. The object classes defined via classification rules by means of feature intensity are combined to form a hierarchical network, the class hierarchy the class hierarchy has the following possible relations.

Inheritance: It permits the formation of parent classes and child classes. The parent class passes on its feature descriptions to the children (1st

generation) who can themselves also have child classes (2nd generation). The 2nd generation inherits the features of the parents and the first generation of children.

Groups: Classes which have a semantic relation can be combined to form groups.

Structure: Object classes can be combined to form structural groups as a basis for the classification-based segmentation.

2.1.4 Semantic Classification

After multiscale segmentation with subsequent semantic modelling, the semantic classification is performed, dividing the image objects into object classes. The semantic classification determines whether or not an object belongs to a certain object class on the basis of its significance. A rating function determines a level of confidence by comparing the individual features of the object to be classified with the attributes. This confidence level provides information about whether the object belongs a class, so that the rating various approaches (Nussbaum and Menz, 2008).

As mentioned above in semantic modelling, the representative features of the object classes are determined with the associated threshold value and implemented in a semantic model. This is then the basis for the classification. Membership of objects in certain classes is then regulated via classification rules with fixed threshold values. In general, fixed threshold values can determine class membership or else threshold values based on fuzzy logic. A fuzzy set A is characterized by its membership function μ_A , which assigns to every element in the reference set X a real number in a closed interval $(0,1)$ (Tizhoosh, 1998) as:

$$A = \{x, \mu_A(x) \mid x \in X\} \quad (2.14)$$

This contrasts with the classical logical sets in which only elements with the membership value of 0 or 1 can be given, i.e. whether the object belongs to the class described (value=1) or not (value=0). In fuzzy set theory, on the other hand, the object may be a member of various classes. It is finally assigned to the object class with which it has the greatest membership.

In practice, a classification model with fixed threshold values is used for the classification. For example, if an object exceeds a certain boundary in the feature under consideration then it no longer belongs to the described object class. The modelled features and threshold values are statistically optimal due to the analysis with SEaTH for feature extraction.

2.2 Literature Reviews

OBIA have been applied to classify LULC since delivery of very high spatial remotely sensed image and release of eCognition software. Relevant application of OBIA to this study are here reviewed and summarized as below.

Khamphilung, Strobl, and Tiede (2013) used object-based image analysis for rural land use/land cover classification based on village forms and shapes in Northeastern, Thailand. QuickBird pan-sharpened imagery with spatial resolution of 0.6 meter was used in this study. A multiresolution segmentation algorithm was firstly used for creating image objects from heterogeneous pixel values. Then, land use was classified into 8 classes based on the classification system of LDD, Thailand (e.g. urban/built-up land, agricultural area, forest land, water and rangeland). A rule-based classifier with membership function was used for the classification. The final results consisted of 2 classes: non-village and residential. This study demonstrates that OBIA

with topographic variables produces better classification results than OBIA with spectral information only. The overall accuracy was about 70% and Kappa index of agreement was 0.64.

Ceccarelli et al. (2013) proposed an approach for generating land cover information from single-date Landsat 7 images integrating pixel-based and object-based classifiers in two study areas: Oristano Province and region of Campania. The process consisted of (a) pre-processing; (b) segmentation; (c) classification based on radiometric properties and integration with textural properties and vegetation indices. The rule-set of OBIA was developed in Oristano area and used for the classification of the whole Region of Campania with minor changes. The obtained overall accuracy was 87% in Oristano and 88% in Campania region.

Wu, Cheng, Shi, Miao and Xu (2013) presented OBIA for building seismic vulnerability assessment using high-resolution remote sensing imagery. The main objective is to investigate how to extract building attributes from high resolution remote sensing imagery using OBIA to accurately and conveniently assess building seismic vulnerability by the combination of in situ field data. A general framework for the assessment of building seismic vulnerability is presented in Figure 2.11 included (1) the extraction of building information using OBIA, (2) building height estimation, and (3) the support vector machine based building seismic vulnerability assessment. The results show that all 48 buildings among the study area have been well detected with an overall accuracy of 80.67 % and the mean error of heights estimated from building shadow is less than 2 m.

Campbell and Congalton (2012) applied OBIA by using rule set to extraction land cover change. They provided a generalized framework for land cover change

analysis through the creation of atmospheric correction and topographic normalization models and the development of an object-based land cover change rule set. They also explored the accuracy of a range of segmentation parameters and a new principal component analysis (PCA) change detection method. Herein two selected Landsat 5 TM data in 2006 and 2011 were used to perform image differencing and resulted as input data. The result suggested that segmentation with relatively small scale parameter and complete influence of color over shape produced the most accurate classification. This method resulted in an overall accuracy of 80.32%.

Laiberte, Browning and Rango (2012) compared three feature selection methods for object-based classification of sub-decimeter resolution UltraCam-L imagery. In this study they evaluated three feature selection methods, (1) Jeffries–Matusita distance (J), (2) classification tree analysis (CTA), and (3) feature space optimization (FSO) for object-based vegetation classifications with sub-decimeter digital aerial imagery in arid rangelands of the southwestern U.S. They assessed strengths, weaknesses, and best uses for each method using the criteria of ease of use, ability to rank and/or reduce input features, and classification accuracies. For the five sites tested, J resulted in the highest overall classification accuracies for three sites, while CTA yielded highest accuracies for two sites. FSO resulted in the lowest accuracies. CTA offered ease of use and ability to rank and reduce features, while J had the advantage of assessing class separation distances.

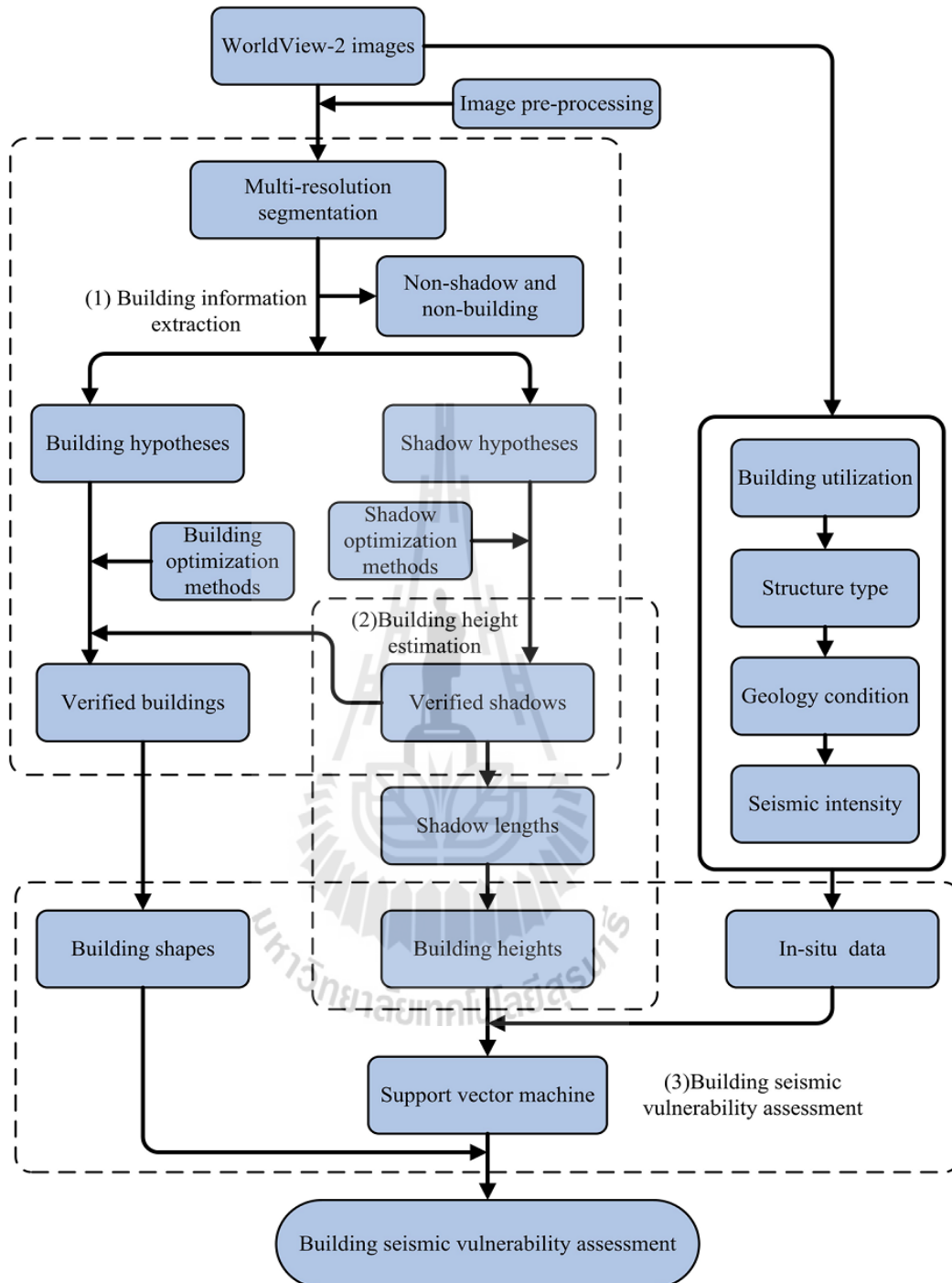


Figure 2.11 The general framework of building seismic vulnerability assessment (Wu, Cheng, Shi, Miao and Xu, 2013).

Myint, Gober, Brazel, Grossman-Clarke, and Weng (2011) compared pixel-based versus object-based classification of urban land cover extraction using high spatial resolution imagery. They employed five different classification procedures with the object-based paradigm that separates spatially and spectrally similar pixels at different scales. The classifiers to assign land covers to segmented objects were used in the study included membership functions and the nearest neighbor classifier (Figure 2.12). The object-based classifier achieved a highest overall accuracy (90.40%), whereas the most commonly used decision rule, namely maximum likelihood classifier, produced a lower overall accuracy (67.60%). This study demonstrated that the object-based classifier was better than the classical per-pixel classifiers. Furthermore, this study examined application of different parameters for segmentation and classification.

Shruthi, Kerle, and Jetten (2011) applied OBIA to extract gully erosion features from satellite imagery, using a combination of topographic, spectral, shape (geometric) and contextual information obtained from IKONOS and GEOEYE-1 data. A rule-set was developed and tested for a semi-arid to sub-humid region in Morocco. Figure 2.13 demonstrated overview of the method for gully feature extraction. The percentage of gully feature area indicated negligible overestimations between the reference area and the OBIA area in two sub-watersheds (0.03% and 1.77%). They also observed that finer gully related edges within the complex gully systems were better identified semi-automatically than was possible by manual digitization, suggesting higher detection accuracy. OBIA gully mapping is quicker and more objective than traditional methods, and is thus better suited to provide essential information for land managers to support their decision making processes, and for the erosion research community.

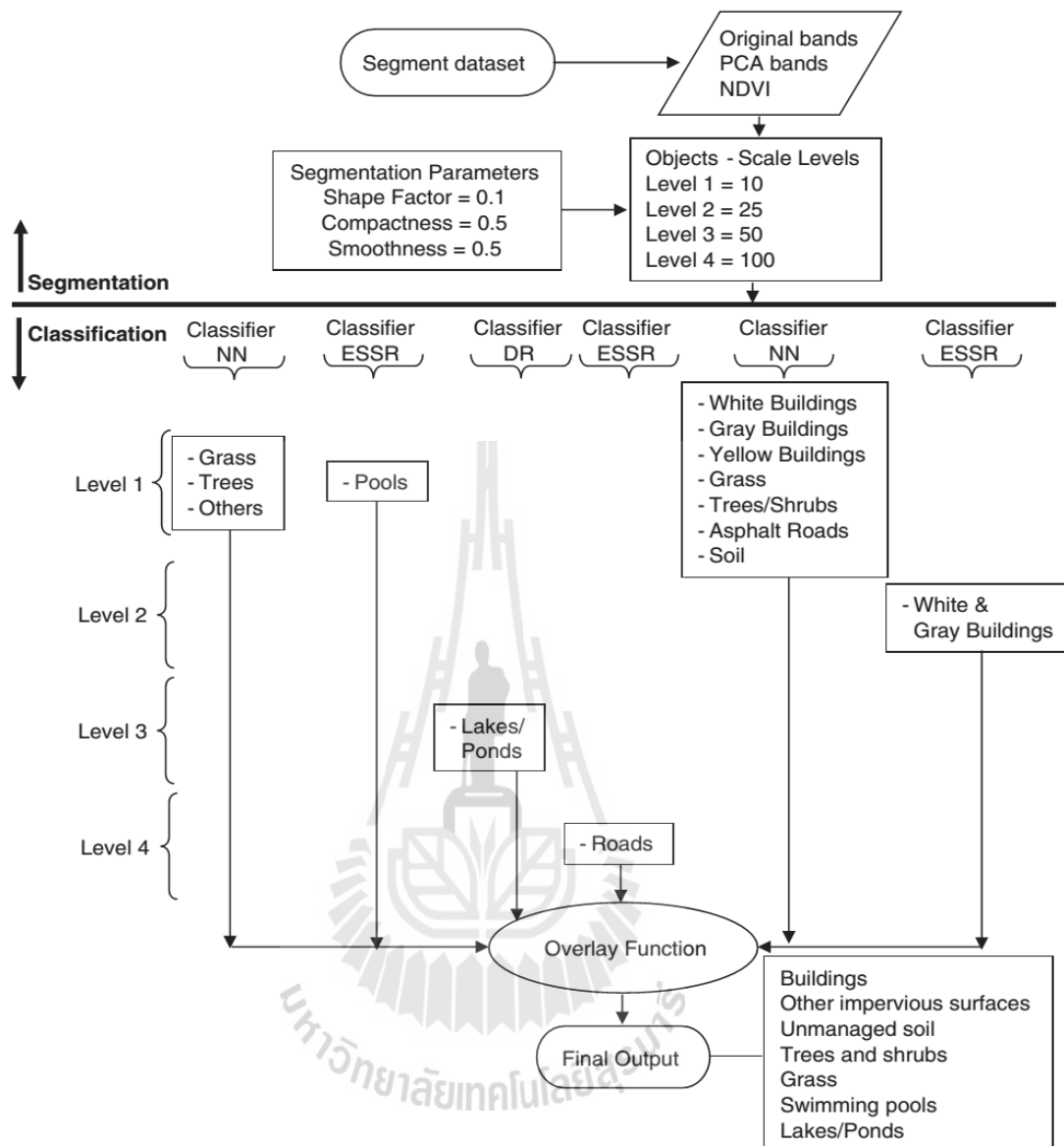


Figure 2.12 A flowchart demonstrating the overall procedure to generate final output (Myint, Gober, Brazel, Grossman-Clarke, and Weng, 2010).

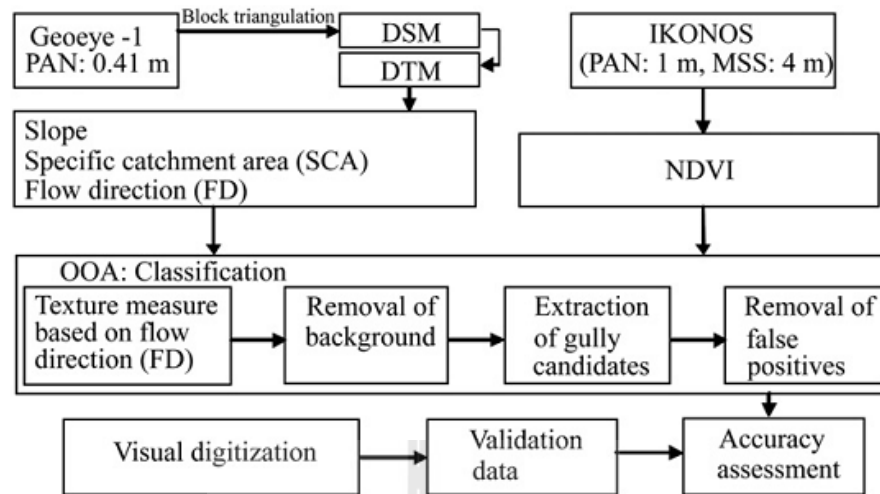


Figure 2.13 Overview of the method of gully feature extraction (Shruthi, Kerle, and Jetten, 2010).

Zhou, Huang, Troy and Cadenasso (2009) presented object-based land cover classification of shaded areas by comparison study of three methods for land cover classification from high spatial resolution imagery in an urban environment. Method 1 combined spectral information in shaded areas with spatial information for shadow classification. Method 2 applied a shadow restoration technique, the linear-correlation method, to create a “shadow-free” image before the classification. Method 3 used multisource data fusion to aid in classification of shadow. Decision rule for land cover classification of three methods presented in Figure 2.14. The results indicated that Method 3 achieved the best accuracy, with overall accuracy of 88 %.

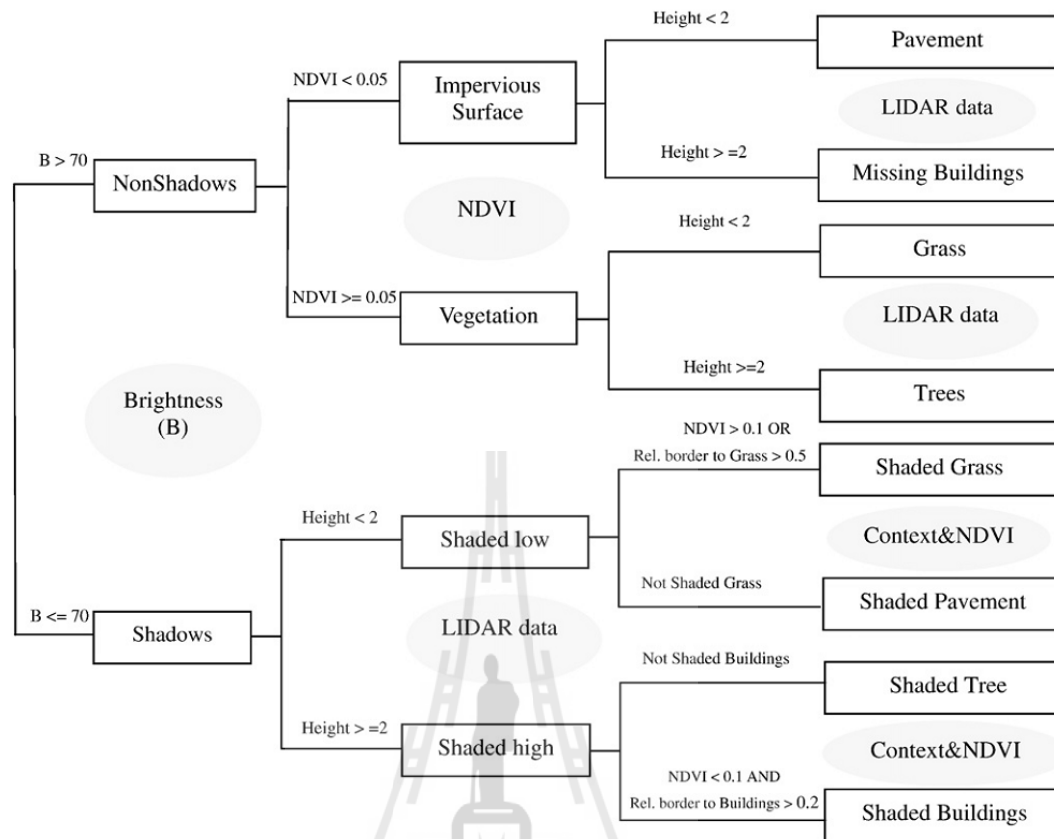


Figure 2.14 The class hierarchy, and its associated features and rules used for land cover classification (Zhou, Huang, Troy and Cadenasso, 2009).

Eddy et al. (2008) used hybrid segmentation technique for the modified chlorophyll absorption in reflectance index (MCARI) designed to be responsive to both chlorophyll variation and resistant to non-photosynthetic material effects. This segmentation was used to separate vegetation from background. They used a new hybrid segmentation with Artificial Neural Network (HS-ANN) method and compared to standard maximum likelihood classification for improving crop/weed species discrimination in Site-Specific Herbicide Management (SSHM) in Precision Agriculture. Herewith, very high spatial resolution (1.25 mm) ground-based hyperspectral image data required development of a simple efficient vegetation index

(MCARI) threshold segmentation to separate vegetation from soil for classification. The HS-ANN consistently outperformed MLC in both single date and multi-temporal classifications. Higher class accuracies were obtained with multi-temporally trained ANNs (84 to 92 percent overall), with improvements up to 31 percent over MLC.

Liu, Pattey, and Nolin (2008) applied OBIA with high resolution SAR images for homogeneous zone delineation within field. The fuzzy k-mean classifier be applied for classification approach. Image segmentation procedure were classified as basic processing units using SAR data by eCognition software. Results were evaluated using analysis of variance and variance reduction of soil electrical conductivity (EC), leaf area index (LAI), and crop yield. The object-based approach provided better results than a pixel-based approach. The variance reduction in LAI, and soil EC varied with SAR acquisition time and incidence angle. Although the variance reduction of yield was not as significant as that of LAI and EC, average yield among the delineated zones were different in most cases. The SAR data classification produced interpretable patterns of soil and crop spatial variability, which can be used to infer within field management zones.

Zhou and Wang (2008) used OBIA for extraction of impervious surface areas from high spatial resolution imagery. They developed an algorithm of multiple agent segmentation and classification (MASC) that includes sub-models of segmentation, shadow-efface, MANOVA (Multivariate Analysis of Variance) -based classification, and post-classification. The segmentation sub-model replaced the spectral difference with heterogeneity change for regions merging. Shape information was introduced to enhance the performance of impervious surface areas (ISA) extraction. The shadow-effect sub-model used a split-and-merge process to separate shadows and the objects

that cause the shadows. The MANOVA-based classification sub-model took into account the relationship between spectral bands and the variability in the training objects and the objects to be classified. Existing GIS data were used in the classification and post-classification process. The MASC successfully extracted ISA from high spatial resolution airborne true-color digital orthophoto and space-borne QuickBird-2 imagery in the testing areas, and then was extended for extraction of high spatial resolution ISA in the State of Rhode Island.

In addition, an identified data and classification algorithm for OBIA from literature reviews are here synthesized as summary in Table 2.1.

Table 2.1 Summary of literature reviews for OBIA.

Title	Authors	Used data	Classification algorithm
Village forms classification by object-based image analysis	Khamphilung, Strobl, and Tiede (2013)	QuickBird pan-sharpened	A rule-based classifier with membership function used for the classification.
Land cover data from Landsat single-date imagery: an approach integrating pixel-based and object-based classifiers	Ceccarelli et al., (2013)	Landsat 7 (ETM+)	The rule-set of OBIA applied for generating land cover information from single-date by images integrating pixel-based and object-based classifiers in two study areas
An object-based image analysis for building seismic vulnerability assessment using high-resolution remote sensing imagery	Wu, Cheng, Shi, Miao and Xu (2013)	WorldView-2	The thresholding from expert knowledge applied for rule-based creation using for classification.
Landsat-based land cover change analysis in Northerastern Oregons's Timeber-resource-dependent communities	Campbell and Congalton (2012)	Landsat 5 (TM)	Topographic normalization models, and the development of an object-based land cover change applied rule set to extraction land cover change with using PCA change detection method based on image differencing of two Landsat images
A comparison of three feature selection methods for object-based classification of sub-decimeter resolution UltraCam-L imagery	Laiberte, Browning and Rango. (2012)	UltraCam-L digital mapping imagery	They evaluated three feature selection methods, (1) Jeffreys–Matusita distance (JM), (2) classification tree analysis (CTA), and (3) feature space optimization (FSO). Classification separate by vegetation class using nearest neighbor classifier which be applied for three method.
Per-pixel vs. object-based classification of urban land cover extraction using high spatial resolution imagery	Myint, Gober, Brazel, Grossman-Clarke, and Weng (2011)	QuickBird image	Pixel-based used statistics for selected land-cover classes namely maximum likelihood, object-based classifier with nearest neighbor algorithm, expert knowledge and decision rule for classification.

Table 2.1 (Continued)

Title	Authors	Used data	Classification algorithm
Object-based gully feature extraction using high spatial resolution imagery	Shruthi, Kerle, and Jetten (2011).	IKONOS and GEOEYE-1 data.	Segmented by chessboard segmentation. A rule-set was developed for gully feature extraction
Object-based land cover classification of shaded areas in high spatial resolution: a comparison study	Zhou, Huang, Troy and Cadenasso (2009)	Color-infrared digital aerial image data from Emerge Inc.	Method 1 combined spectral information in shaded areas with spatial information for shadow classification. Method 2 applied a shadow restoration technique Method 3 used multisource data fusion to aid in classification of shadow. Final classify shaded objects using rule-based classification with 3 method.
Hybrid segmentation artificial neural network classification of high resolution hyperspectral imagery for site-specific herbicide management in agriculture	Eddy, Smith, Hill, Peddle, Coburn, and Blackshaw (2008)	The hyperspectral camera system was situated on a boom arm, mounted on a flat-bed truck and centered at 1 m target distance	Applied new hybrid segmentation artificial neural network (HS-ANN) method and compare the results with standard maximum likelihood classification (MLC)
Object-based classification of high resolution SAR images for within field homogeneous zone delineation	Liu, Pattey, and Nolin (2008)	CV-580 SAR Data	A bottom up region merging procedure used for segmentation. Unsupervised fuzzy k-mean applied for classification
Extraction of impervious surface areas from high spatial resolution imagery by multiple agent segmentation and classification	Zhou and Wang (2008)	QuickBird-2 satellite	The MANOVA-based classification took into account the relationship between spectral bands and the variability in the training objects and the objects to be classified. GIS data were used in the classification and post-classification process.



CHAPTER III

EQUIPMENT AND RESRACH METHODOLOGY

Equipment and details of research methodology including (1) data collection and preparation; (2) semantic modelling and classification development; (3) spatial transferability analysis and (4) Temporal transferability analysis are here explained in this chapter.

3.1 Equipment

Equipment include hardware and software which are used in this study is summarized in Table 3.1 as below:

Table 3.1 List of hardware and software.

Equipment	Application	Source	
Hardware	GPS	Ground surveying	
	Tablet, notebook, desktop computer	Data analysis and documentation	Personnel
	Digital camera	Ground surveying	
	Laser printer	Document and map printing	
Software	ERDAS Imagine	Digital image processing	
	RSI ENVI	Digital image processing	
	ESRI ArcMap	Spatial analysis and map production	
	Definiens eCognition Developer	Object-based image analysis	
	MS Excel	SEaTH analysis	
	MS Word	Documentation	
	Google Earth	Accuracy assessment	Google Inc.

3.2 Research methodology

Framework of research methodology consists of one common task, data collection and preparation and three components: (1) semantic modelling and classification development (2) spatial transferability analysis and (3) temporal transferability analysis as shown in Figure 3.1. Details of common task and research components are separately described in the following sections.

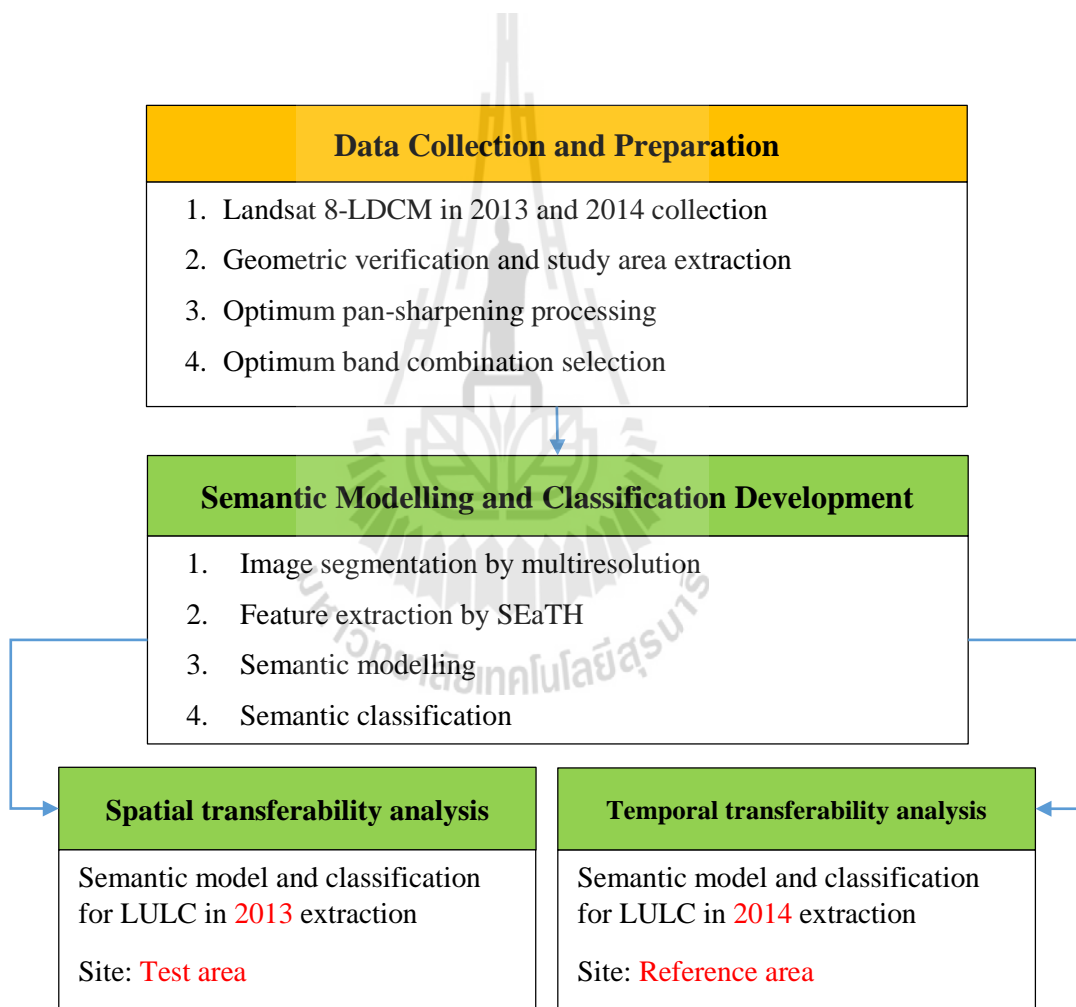


Figure 3.1 Framework of research methodology.

3.2.1 Data collection and preparation

Landsat 8 LDCM data at Level 1 (path 128, row 50) in 2013 and 2014 are firstly downloaded from USGS website (www.glovis.usgs.gov) and then converted from zip format to be image format for geometric data verification as shown Figure 3.2. Spectral sensor characteristics of Landsat 8 LDCM is summarized in Table 3.2. After that, the verified Landsat 8 data are extracted spectral subset for MS band 2-7 and PAN band 8 and spatial subset covering study area as result shown in Figure 3.3. The main task for data preparation includes optimum pan-sharpening processing and optimum band combination selection are briefly described as below.

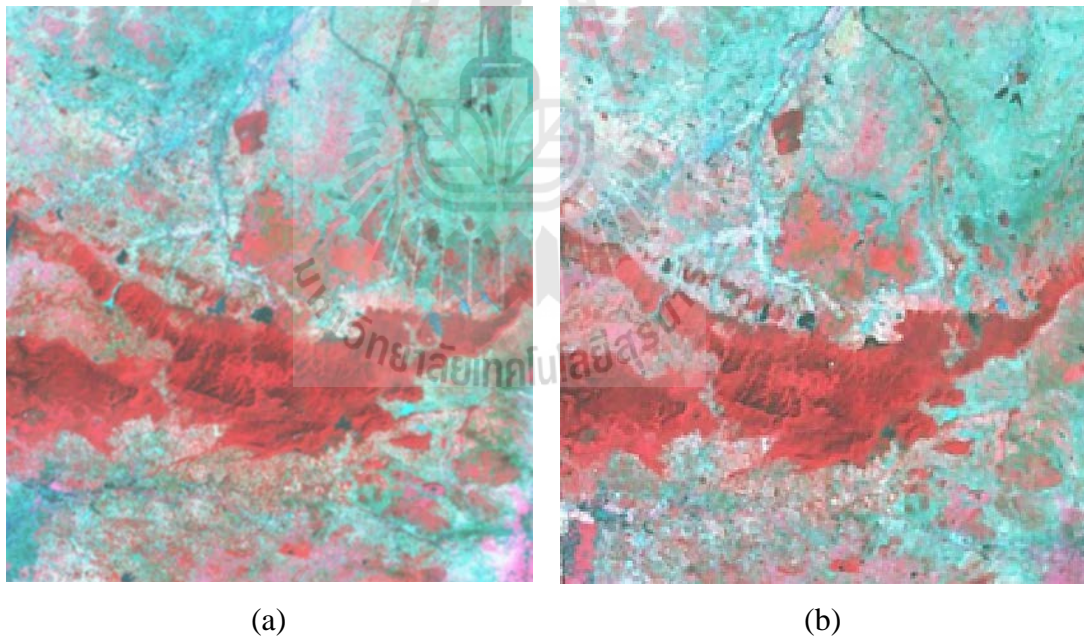
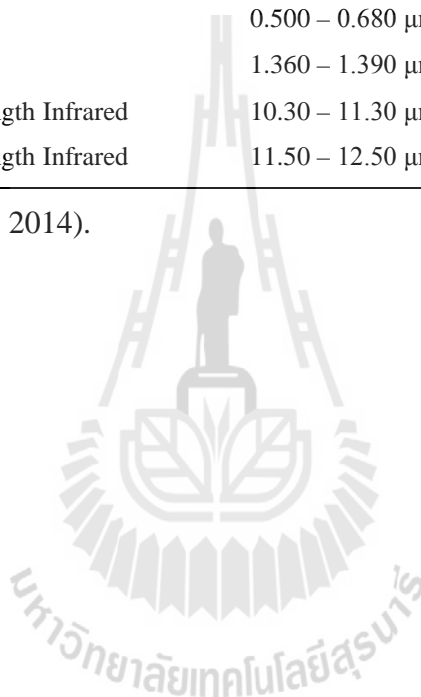


Figure 3.2 Composite image of Landsat 8 (Band 5, 4, 3): (a) Date 9 December 2013 and (b) Date 12 December 2014.

Table 3.2 Landsat 8 spectral sensor characteristics.

Spectral Band	Wavelength	Resolution
Band 1 – Coastal / Aerosol	0.433 – 0.453 μm	30 m.
Band 2 – Blue	0.450 – 0.515 μm	30 m.
Band 3 – Green	0.525 – 0.600 μm	30 m.
Band 4 – Red	0.630 – 0.680 μm	30 m.
Band 5 – Near Infrared	0.845 – 0.885 μm	30 m.
Band 6 – Short Wavelength Infrared	1.560 – 1.660 μm	30 m.
Band 7 – Short Wavelength Infrared	2.100 – 2.300 μm	30 m.
Band 8 – Panchromatic	0.500 – 0.680 μm	15 m.
Band 9 – Cirrus	1.360 – 1.390 μm	30 m.
Band 10 – Long Wavelength Infrared	10.30 – 11.30 μm	100 m.
Band 11 – Long Wavelength Infrared	11.50 – 12.50 μm	100 m.

(Source: USGS, [www](http://www.usgs.gov), 2014).



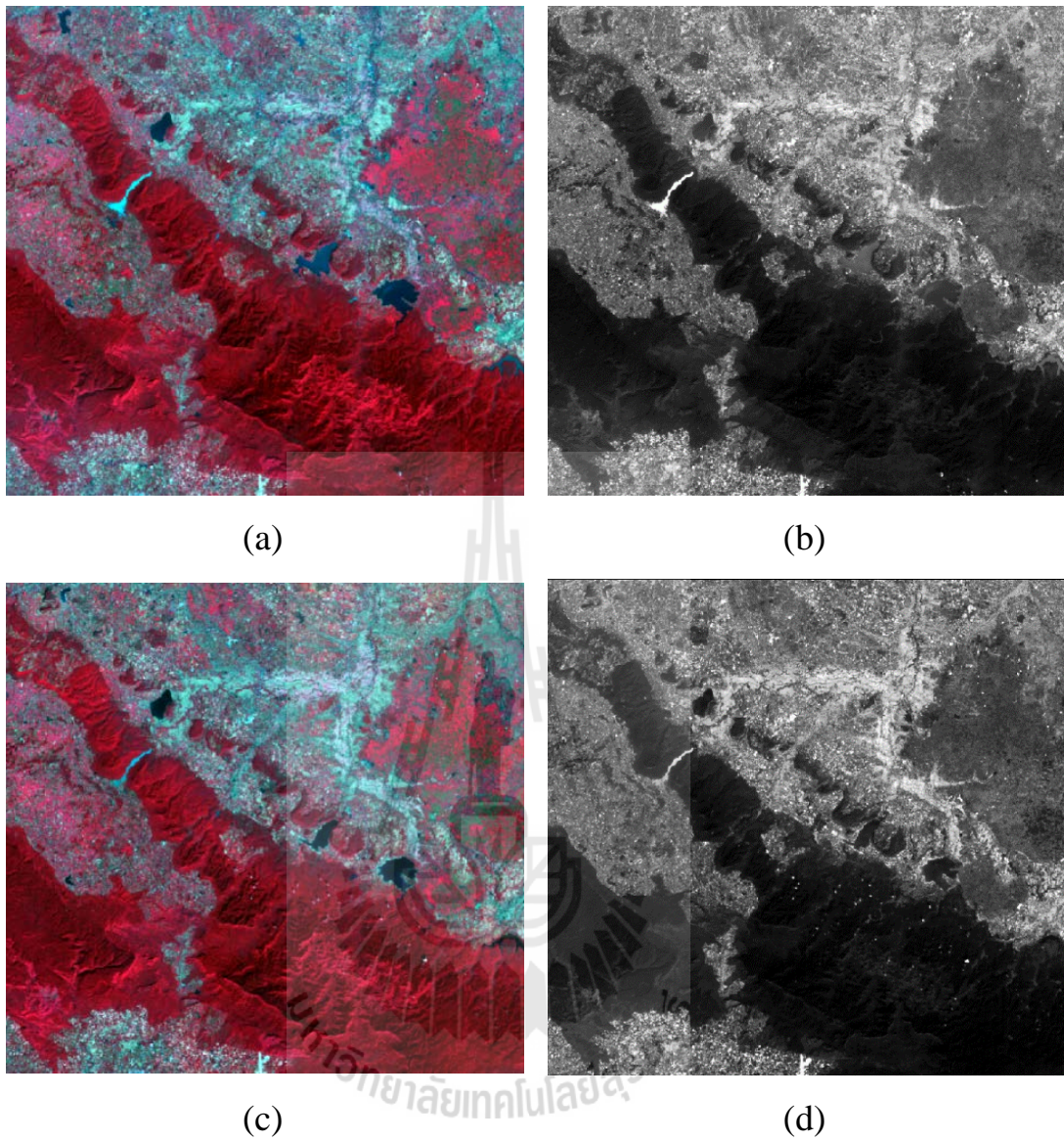


Figure 3.3 Spatial and spectral subset of Landsat 8 acquired on 9 December 2013 (a) MS image (Band 5, 4, 3), (b) PAN image and Landsat 8 acquired on 12 December 2014 (c) MS image (Band 5, 4, 3), (d) PAN image.

(1) Optimum pan-sharpening processing

Pan-sharpening processing for Landsat 8 data in 2013 and 2014 are firstly separately conducted using the selected methods which can provide more than 3 bands of pan-sharpened image included EF, GS, HPF, MIHS, and WT. Herein, multispectral bands of Landsat-8 included band 2 (B), 3 (G), 4 (R), 5 (NIR), 6 (SWIR), and 7 (SWIR) and 8 (PAN) are used in pan-sharpening process. The characteristic of the selected pan-sharpening methods is summarized in Table 3.3. After that the derived pan-sharpened image of Landsat 8 data in 2013 and 2014 are separately evaluated image quality using the Universal Image Quality Index (Q) developed by Wang and Bovik (2002) as:

$$Q = \frac{\sigma_{xy}}{\sigma_x \sigma_y} * \frac{2\bar{x}\bar{y}}{(\bar{x}^2) + (\bar{y}^2)} * \frac{2\sigma_x \sigma_y}{\sigma_x^2 + \sigma_y^2} \quad (3.1)$$

Herewith x is pixel value of original image and y is test image, where

$$\bar{x} = \frac{1}{N} \sum_{i=1}^N x_i,$$

$$\bar{y} = \frac{1}{N} \sum_{i=1}^N y_i,$$

$$\sigma_x^2 = \frac{1}{N-1} \sum_{i=1}^N (x_i - \bar{x})^2,$$

$$\sigma_y^2 = \frac{1}{N-1} \sum_{i=1}^N (y_i - \bar{y})^2,$$

$$\sigma_{xy} = \frac{1}{N-1} \sum_{i=1}^N (x_i - \bar{x})(y_i - \bar{y})$$

The dynamic range of Q is [-1 to 1]. The best achievable value is consequently 1 whenever $y_i = x_i$, i.e. the original image and the test image are identical.

Q can be rewritten as a combination of three factors:

$$Q = \frac{\sigma_{xy}}{\sigma_x \sigma_y} * \frac{2\bar{x}\bar{y}}{(\bar{x}^2) + (\bar{y}^2)} * \frac{2\sigma_x \sigma_y}{\sigma_x^2 + \sigma_y^2} \quad (3.2)$$

The first factor in the Eq. 3.2 gives the correlation coefficient of x and y . This factor measures the degree of linear agreement and in the ideal case (two images are identical) is thus = 1 and if there is no correlation then = 0. The second factor compares the means of the two images. The range of values is between 0 and 1. The third factor finally examines the variance of the two images. In this case the dynamic range is also [0, 1]. In conformity with the correlation, mean value and variance, these three factors provide a value of 1 and thus Q is also equal to 1 (Wang and Bovik, 2002). Therefore, method which provides the highest average Q values is considered as an optimum pan-sharpening process to apply for Landsat 8 data.

Table 3.3 Characteristics of selected pan-sharpening algorithm.

Method	Basic characteristics	Reference
Ehlers fusion (EF)	This method is based on IHS transformation coupled with Fourier domain filtering.	Klonus and Ehlers (2009)
Gram-Schmidt pan-sharpening (GS)	This method is firstly simulated a panchromatic band from lower spatial resolution spectral bands. Then Gram-Schmidt transformation is performed on the simulated panchromatic band and the spectral bands and replaced the high spatial resolution panchromatic band with the first Gram-Schmidt band. Finally, inverse Gram-Schmidt transformation is performed to generate a pan-sharpened image.	Laben and Brower (2000)
High pass filtering (HPF)	This method involves a convolution using high pass filter on PAN image and merging the result with MS image.	Gangkofner et al. (2008)

Table 3.3 (Continued).

Modified intensity hue saturation transform (MIHST)	This method was firstly proposed by Siddiqui (2003). It allows combining multispectral image with panchromatic image more than three bands at a time. The method works best when there is significant overlap of wavelengths of combining images (Nikolakopoulos, 2008).	Nikolakopoulos (2008) Siddiqui (2003)
Wavelet transform (WT)	This method is a modification of the work of King and Wang (2001). The process involves separating original image into different image components by wavelet decomposition and substituting their components between MS and PAN image components to produce a pan-sharpened image.	Klonus and Ehlers (2009) King and Wang (2001)

(2) Optimum band combination selection

The derived pan-sharpened data which produced using an optimum pan-sharpening method is further used to identify an optimum four band selection by the Optimum Index Factor (OIF) developed by Chavez et al., (1982) and Sheffield Index (SI) developed by Sheffield (1985). Both OIF and SI, which are based on the amount of total variance and correlation and covariance, respectively within and between various band combinations, can be easily applied to any multispectral remote sensing dataset.

The algorithm used to compose OIF for any subset of four band combination is

$$OIF = \frac{\sum_{k=1}^4 s_k}{\sum_{j=1}^4 Abs(r_j)} \quad (3.3)$$

where s_k is the standard deviation for band k , and r_j is the absolute value of the correlation coefficient between any two of the four bands being evaluated. Standard

deviation represents the discrete degree. The more value, it will be the more radiation intensity difference and the less of the absolute value of the correlation coefficient, the less of repeated degree (Debdip and Girls, 2013).

While, algorithm uses to compute SI for any subset of four band combination is:

$$SI = |Cov_{p \times p}| \quad (3.4)$$

where, $|Cov_{p \times p}|$ is the determinant of the covariance matrix of subset size $p \times p$. The band combination that results in the largest determinant is selected for the optimum four band combination.

3.2.2 Component I: Semantic modelling and classification development

The semantic model which creates a form of knowledge to present and determine features of classes with associate to threshold value in the model. The workflow of Component I: Semantic modelling and classification development is shown in Figure 3.4. Herewith, three major tasks after preprocessing include (1) multiresolution segmentation, (2) feature extraction, and (3) semantic modelling and classification development are implemented.

(1) Multiresolution segmentation: The optimized pan-sharpening data of Landsat 8 in 2013 are segmented using multiresolution algorithm under eCognition software. Herewith multilevel scale and optimum weighting for color and shape is applied. The multilevel scale is examined between 25 and 100 meanwhile weight of color are varied between 0.5- 0.7 and weight for smoothness and compactness of shape is 0.5.

(2) Feature Extraction. In this study SEaTH (Separability and Thresholds) technique is used for feature extraction. For separability, all pairwise of two object classes are firstly computed spectral distance using J distance (Eq. 2.9) based on selected feature characteristics such as spectral value, geometry, and texture. After that threshold value based on Gaussian probability mixture model are then calculated to identify the optimum value for the maximum separability in the chosen features (Eq. 2.12).

(3) Semantic modelling and classification development. Under this step major tasks are processed as following

- Semantic Modelling: The model is constructed as a rule-based semantic network, which constitutes a form of knowledge presentation. The statistical measure for determining the representative features for each object class is the pairwise separability of the object classes among each other. Most outstanding features from SEaTH analysis are used to draw up for each object class.

- Semantic Classification: The representative features of the object classes which determined with the associated threshold value from semantic modelling is implemented in a semantic classification. Membership of objects in certain classes is then regulated via classification rules with fixed threshold values. In this study, fixed threshold values are used to determine continuous class membership. The final product is LULC map.

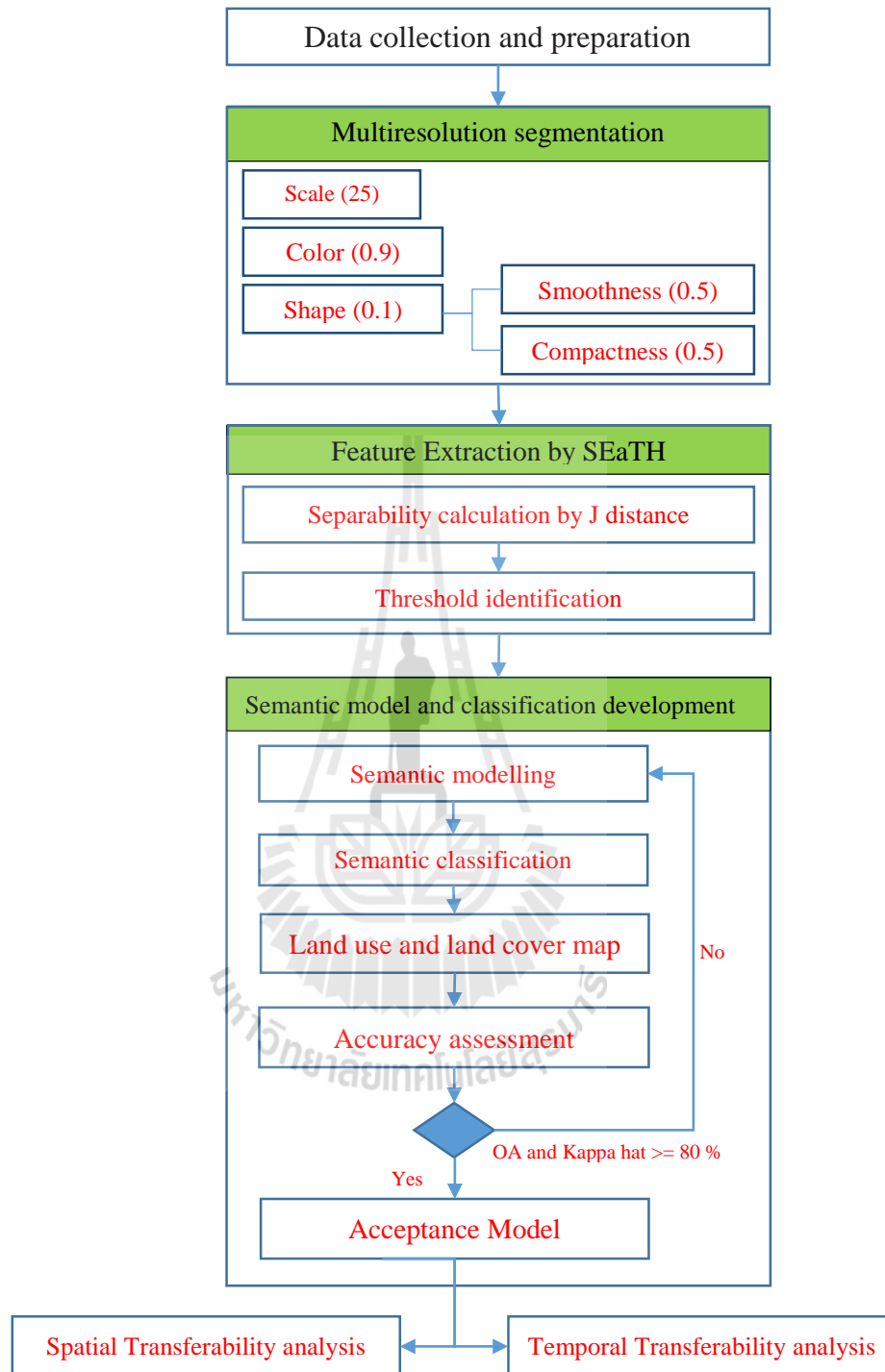


Figure 3.4 Workflow of Component I: Semantic modelling and classification development.

- Accuracy assessment. Standard measurement for accuracy assessment includes overall accuracy and Kappa hat coefficient of agreement is evaluated for the classified LULC map in reference. Herewith overall accuracy and Kappa hat coefficient for acceptance the semantic modelling and classification is equal or greater than 80 percent before applying the developed semantic model in spatial and temporal transferability analysis.

For accuracy assessment, number of sample points, in general, is firstly estimated and sampling scheme is then selected for sample point allocation. In this study, number of sample point for accuracy assessment is calculated based on binomial probability distribution theory suggested by Fitzpatrick-Lins (1981) as:

$$N = \frac{Z^2(p)(q)}{E^2} \quad (3.5)$$

where P is the expected percent accuracy of the entire map,

q is $100 - p$

E is the allowable error

Z is 2 from the standard normal deviate of 1.96 for the 95% two side confidence level.

Meanwhile stratified random sampling is chosen to allocate sample points.

3.2.3 Component II: Spatial transferability analysis

Spatial transferability analysis is used to determine whether the developed semantic model and classification can be transferred to other site. Basically, spatial transferability should be easily applied when characteristic of test area is similar to reference area. In this study, a developed semantic model in Component I is directly

applied for spatial transferability analysis in testing area. Herewith accuracy assessment are also conducted to confirm the accuracy of the spatial transferability. Fundamentally, the accuracy values from Component I and II should no significant difference if the biophysical characteristics of two test sites are similar. In this study, significant different of accuracy between Component I and II is tested using standard normal distribution or Z statistics (Pairwise Z test) as:

$$Z = \frac{|\widehat{K}_1 - \widehat{K}_2|}{\sqrt{\widehat{var}(K_1) + \widehat{var}(K_2)}} \quad (3.6)$$

where Z is normalized and standard normal distribution

\widehat{K}_1 is KHAT for Component I

\widehat{K}_2 is KHAT for Component II

$\widehat{var}(K_1)$ is variance of KHAT for Component I

$\widehat{var}(K_2)$ is variance of KHAT for Component II

Meanwhile, variance of KHAT is calculated by:

$$\widehat{var}(K) = \frac{1}{n} \left\{ \frac{\theta_1(1-\theta_1)}{(1-\theta_2)^2} + \frac{2(1-\theta_1)(2\theta_1\theta_2-\theta_3)}{(1-\theta_2)^3} + \frac{(1-\theta_1)^2(\theta_4-4\theta_2^2)}{(1-\theta_2)^4} \right\} \quad (3.7)$$

where

$$\theta_1 = \frac{1}{n} \sum_{i=1}^k n_{ii}$$

$$\theta_2 = \frac{1}{n^2} \sum_{i=1}^k n_{i+} n_{+i}$$

$$\theta_3 = \frac{1}{n^2} \sum_{i=1}^k n_{ii} (n_{i+} + n_{+i})$$

$$\theta_4 = \frac{1}{n^3} \sum_{i=1}^k \sum_{j=1}^k n_{ij} (n_{j+} + n_{+i})^2$$

Under pairwise Z test, given the null hypothesis $H_0: (\widehat{K}_1 - \widehat{K}_2) = 0$, and the alternative

$H_1: (\widehat{K}_1 - \widehat{K}_2) \neq 0$, H_0 is accepted if $Z < Z_{\alpha/2}$, where $\alpha/2$ is the confidence level of the

two-tailed Z test and the degrees of freedom are assumed to be infinity (Congalton and Green, 2009).

3.2.4 Component III: Temporal transferability analysis

Temporal transferability analysis is a process to verify consistency of the developed semantic model with features and threshold values on satellite data in the same site at different points of time. It has been shown that the features identified by SEaTH are characteristic of the individual object classes and can also be transferred over considerable periods of time. In practice, some features can be taken over completely and the threshold values might be used with minor modification, especially phonological change of vegetation (Nussbaum and Menz, 2008). Similarly to spatial transferability analysis, a developed semantic model in Component I is examined and modified for temporal transferability analysis in reference area in different year. In addition, significant different of accuracy between Component I and III is also tested using pairwise Z test to confirm the accuracy of temporal transferability.

CHAPTER IV

RESULTS AND DISCUSSION

Major results of three main components of the research methodology included (1) preprocessing data product, (2) semantic modelling and classification development, (3) spatial transferability analysis and (4) temporal transferability analysis are described and discussed in this chapter.

4.1 Preprocessing data product

Major preprocessing data products included optimum pan-sharpening method of Landsat 8 imagery and optimum four band combination dataset are summarized and discussed as below.

4.1.1 Optimum pan-sharpening method of Landsat 8 imagery

The products of pan-sharpening of two Landsat 8 data of 2013 and 2014 are separately displayed in Figures 4.1 and 4.2, respectively. It was found that four pan-sharpening methods except MIHST can provide good brightness and contrast image in both dataset and they visualized similar to an original MS image and their spatial resolution are better than the original one. In case of MIHST, its pan-sharpened image is quite different from other methods. The false color composite of the vegetated areas displayed as dark purple.

The Q average values for the pan-sharpened image of Landsat 8 data in 2013 and 2014 are presented in Tables 4.1 and 4.2, respectively. It revealed that WT displayed the best result for Landsat 8 data of 2013 with value of 0.97 and followed by EF, HPF, GS and MIHST with value of 0.96, 0.96, 0.90 and 0.85, respectively. At the same time, WT also displayed the best result for Landsat 8 data of 2014 with value of 0.96 and followed by HPF, EF, GS and MIHST with value of 0.95, 0.95, 0.90 and 0.83, respectively.



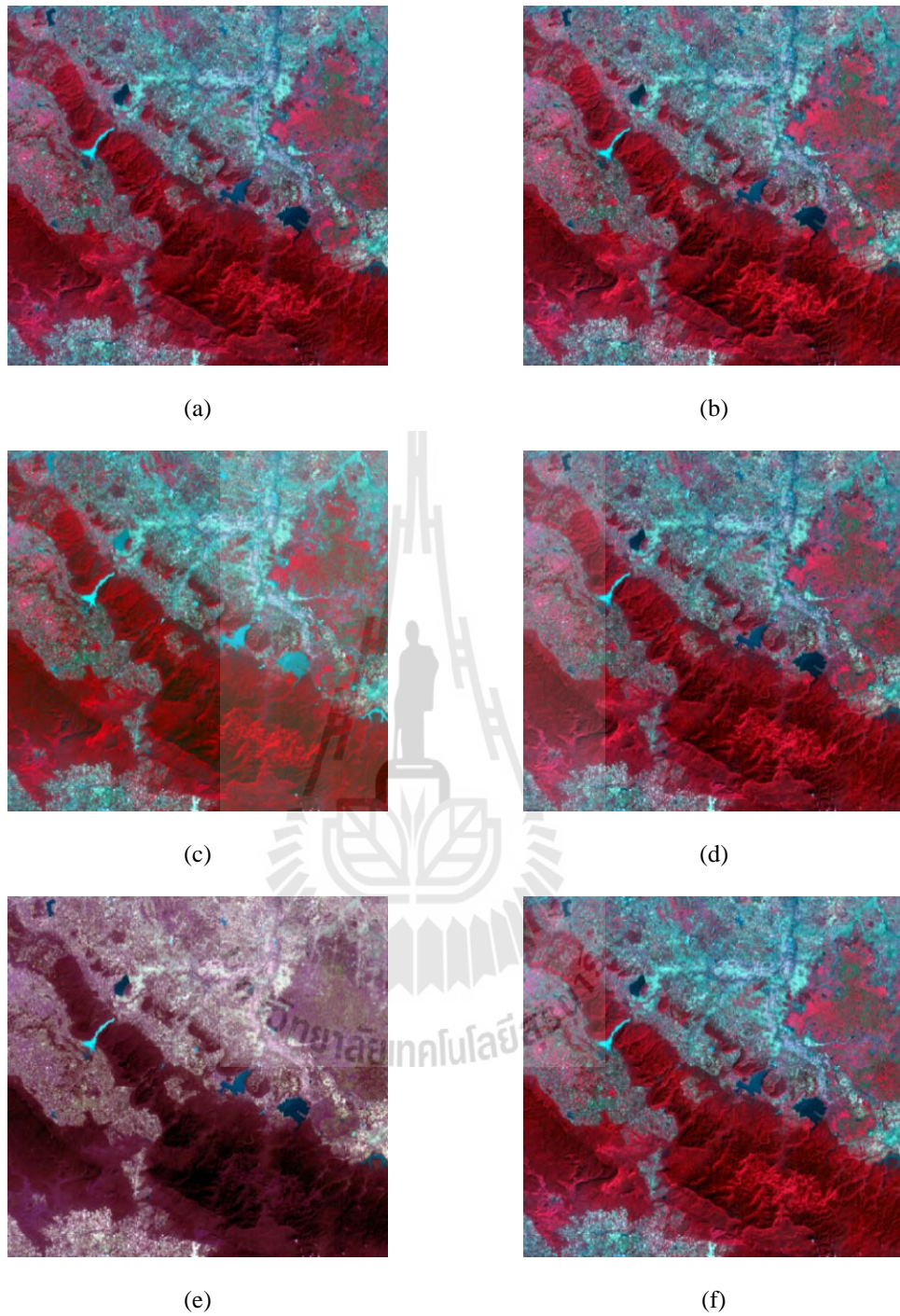


Figure 4.1 False color composite of original Landsat 8 data in 2013 and their pan-sharpened images, band 4, 5 and 3 (RGB): (a) original data (b) EF, (c), GS, (d) HPF, (e) MIHST and (f) WT.

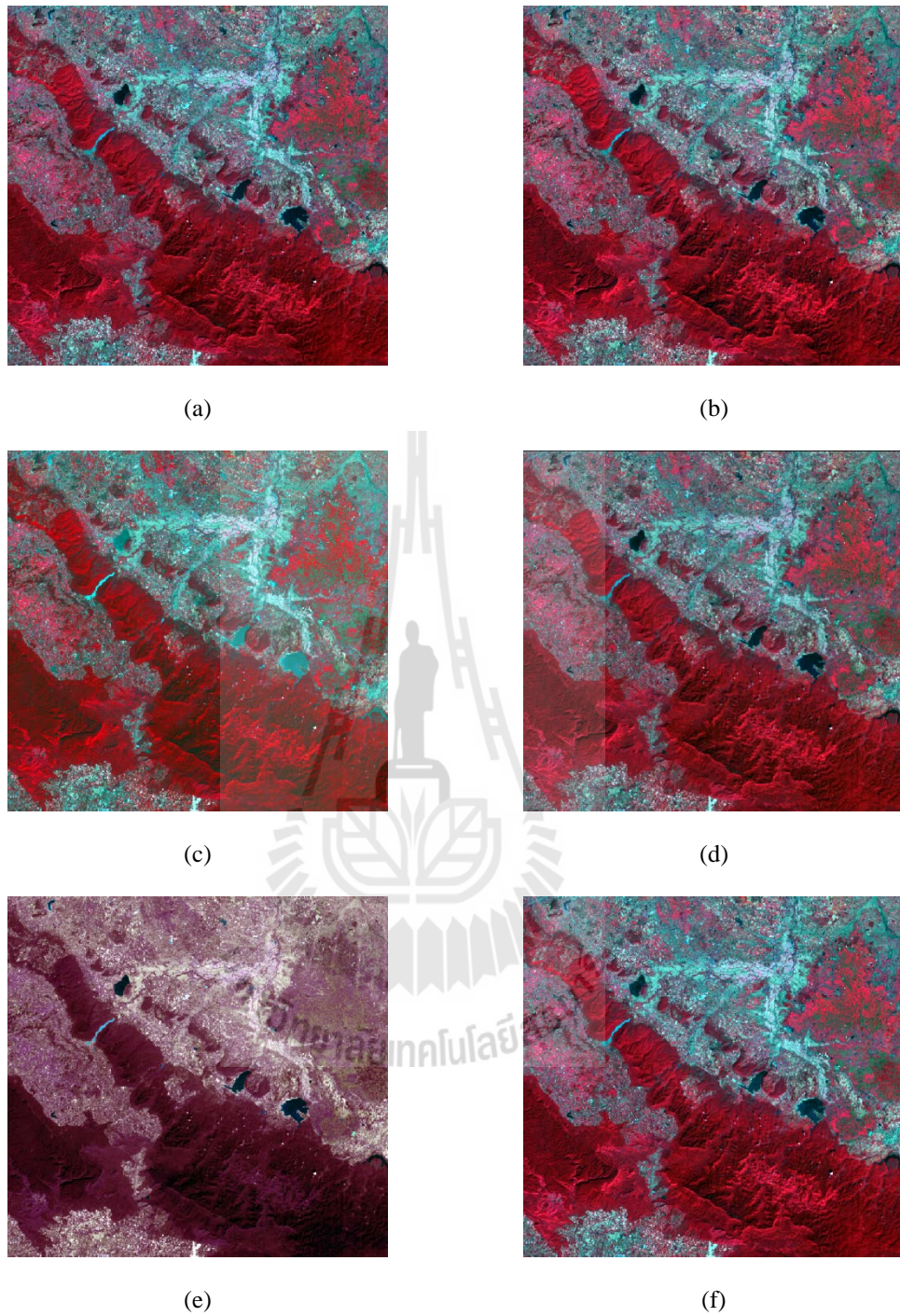


Figure 4.2 False color composite of original Landsat 8 data in 2014 and their pan-sharpened images, band 4, 5 and 3 (RGB): (a) original data (b) EF, (c), GS, (d) HPF, (e) MIHST and (f) WT.

Table 4.1 Comparison of the image quality from different pan-sharpening methods for Landsat 8 data of 2013 based on Q-average value.

Landsat 8 data in 2013					
Band	Q and Q-average of various pan-sharpening methods				
	EF	GS	HPF	MIHST	WT
2	0.979113093	0.926665028	0.965599674	0.974766308	0.967333112
3	0.975474832	0.916928814	0.96314923	0.969882	0.965402081
4	0.985886392	0.916492895	0.961095247	0.982436987	0.964434155
5	0.893648333	0.89570461	0.935498599	0.256437685	0.999480745
6	0.965246499	0.879480797	0.954033955	0.921912278	0.966184355
7	0.964259823	0.890923556	0.954702699	0.979397667	0.96435536
Sum	5.763628973	5.426195701	5.734079403	5.084832921	5.827189809
Q-average	0.960604829	0.90436595	0.955679901	0.847472153	0.971198301
Ranking	2	4	3	5	1

Table 4.2 Comparison of the image quality from different pan-sharpening methods for Landsat 8 data of 2014 based on Q-average value.

Landsat 8 data in 2014					
Band	Q and Q-average of various pan-sharpening methods				
	EF	GS	HPF	MIHST	WT
2	0.962327303	0.914067036	0.961363078	0.96565798	0.95844202
3	0.950411819	0.90406116	0.959765429	0.959314374	0.95655615
4	0.976433924	0.909337998	0.958655979	0.978554287	0.955951358
5	0.896365233	0.886733067	0.933863549	0.172631192	0.998828408
6	0.966972553	0.875525052	0.95441916	0.902345738	0.954582022
7	0.954143398	0.889063419	0.95537031	0.972864788	0.953944634
Sum	5.706654231	5.378787731	5.723437504	4.951368359	5.778304592
Q-average	0.951109038	0.896464622	0.953906251	0.82522806	0.963050765
Ranking	3	4	2	5	1

As results, the most appropriate method for pan-sharpening Landsat 8 data is WT and the possibly appropriate methods may include HPF, EF, and GS. This possibility is useful when software availability is considered. On contrary, the least appropriate method for pan-sharpening producing from Landsat 8 data is MIHST. Q value of band 5 (SWIR) from MIHST for year 2013 and 2014 was rather low (with value of 0.25 and 0.17, respectively) when it was compared with other bands. This result directly effects to Q average value of MIHST method.

The major cause for identifying the most and least pan-sharpening method (WT and MIHST) based on spectral authenticity may be possible due to algorithm and data. Nikolakopoulos (2008) claimed the MIHST method works best when there is significant overlap of wavelengths of combining images.

4.1.2 Optimum four band combination dataset

The OIF and SI values of four band combination for two derived pan-sharpened image from WT method are separately summarized in Tables 4.3 and 4.4, respectively. It demonstrated that the combination of band 3 (G), 4 (R), 5 (NIR) and 6 (SWIR) from pan-sharpened Landsat 8 data in 2013 provided the highest OIF and SI value with value of 32.38 and 989,934,354.93, respectively while the combination of band 2 (B), 3 (G), 4 (R) and 7 (SWIR) provided the lowest OIF and SI values with value of 12.35 and 4,059,983.93, respectively. These results show that the best band combination from pan-sharpened Landsat 8 data of 2013 should be band 3 (G), 4 (R), 5 (NIR) and 6 (SWIR).

On contrary, it revealed that the combination of band 4 (R), 5 (NIR), 6 (SWIR) and 7 (SWIR) from pan-sharpened Landsat 8 data of 2014 provided the highest

OIF value with value of 21.95 but the combination of band 3 (G), 4 (R), 5 (NIR) and 6 (SWIR) provided the highest SI value with value of 44,036,757.71 and the combination of band 2 (B), 3 (G), 4 (R) and 7 (SWIR) provided the lowest OIF and SI values with value of 8.31 and 185,153.04, respectively.

Though, these results show a common best band combination from both pan-sharpened Landsat 8 data when it was justified based on SI is band 3 (G), 4 (R), 5 (NIR) and 6 (SWIR). Nevertheless, this common best band combination does not agree with OIF value. However, the first rank: band 4 (R), 5 (NIR), 6 (SWIR) and 7 (SWIR) and second rank: band 3 (G), 4 (R), 5 (NIR) and 6 (SWIR) based on OIF value have no significant difference with value of 0.30067. This cannot be compared with the significant difference of SI with value of 25,212,713.72 between the first rank: band 3 (G), 4 (R), 5 (NIR) and 6 (SWIR) and second rank: band 4 (R), 5 (NIR), 6 (SWIR) and 7 (SWIR) based on SI value (see Tables 4.4 and 4.5).

As results, the most optimum four band combination from Landsat 8 pan-sharpened data is band 3 (G), 4 (R), 5 (NIR) and 6 (SWIR) and the least optimum four band combination is band 2 (B), 3 (G), 4 (R) and 7 (SWIR). This finding is similar to the previous work of Debdip and Girls (2013) who applied OIF for three band combination of Landsat 5 data. They found the best three band combination of Landsat 5 data was band 1 (B), 4 (NIR) and 5 (SWIR) and the least three band combination was band 1 (B), 2 (G), and 3 (R).

Table 4.3 OIF values of possible four band combination of pan-sharpened image from pan-sharpened Landsat 8 data of 2013 and 2014.

Band combination	Pan-sharpened Landsat 8 data of 2013		Pan-sharpened Landsat 8 data of 2014	
	OIF value	Ranking	OIF value	Ranking
2,3,4,5	29.62363	2	19.550498	4
2,3,4,6	15.18227	5	9.32851469	5
2,3,4,7	12.34569	6	8.30909777	6
3,4,5,6	32.38322	1	21.6874493	2
3,4,5,7	28.76582	4	20.9533679	3
4,5,6,7	29.02805	3	21.9504101	1

Table 4.4 SI values of possible four band combination of pan-sharpened image from pan-sharpened Landsat 8 data of 2013 and 2014

Band combination	Pan-sharpened Landsat 8 data of 2013		Pan-sharpened Landsat 8 data of 2014	
	SI value	Ranking	SI value	Ranking
2,3,4,5	53,198,355.79	4	2,630,416.14	4
2,3,4,6	28,673,107.18	5	544,662.33	5
2,3,4,7	4,059,983.93	6	185,153.04	6
3,4,5,6	989,934,354.93	1	44,036,757.71	1
3,4,5,7	140,150,013.33	3	14,483,014.73	3
4,5,6,7	180,547,654.20	2	18,824,043.99	2

4.2 Semantic modelling and classification development for LULC classification

Major results and findings of semantic modelling and classification development for LULC extraction in reference area included (1) image segmentation

by multiresolution segmentation; (2) feature extraction by SEaTH analysis; (3) semantic model, (4) semantic classification, and (5) accuracy assessment are described and discussed as below.

4.2.1 Image segmentation by multiresolution segmentation

The derived pan-sharpened imagery of Landsat 8 in 2013 were partitioned for image objects using multiresolution segmentation under eCognition software with the scale factor of 25 and color parameter of 0.9 and compactness of 0.5 as result shown in Figure 4.3 and Table 4.5. The minimum image object size as minimum mapping unit (MMU) is about 21 x 21 sq. m. The extracted image object with their feature properties are further used as input data for training samples selection and their feature properties identification for feature extraction by SEaTH analysis.

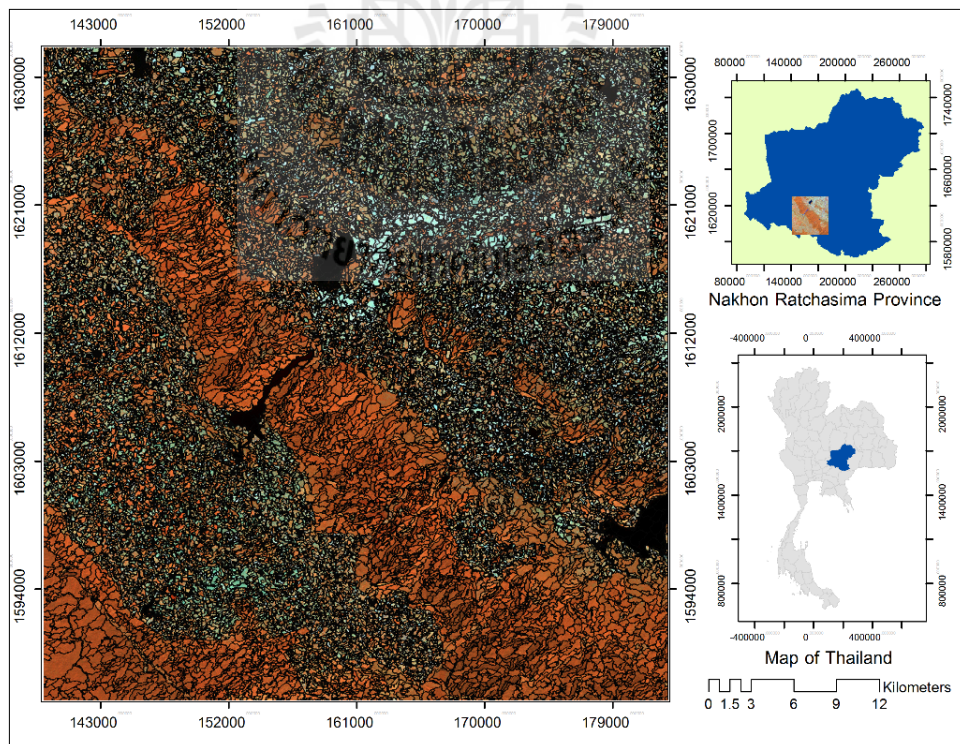


Figure 4.3 Image objects of pan-sharpened Landsat 8 data of 2013 by multiresolution segmentation.

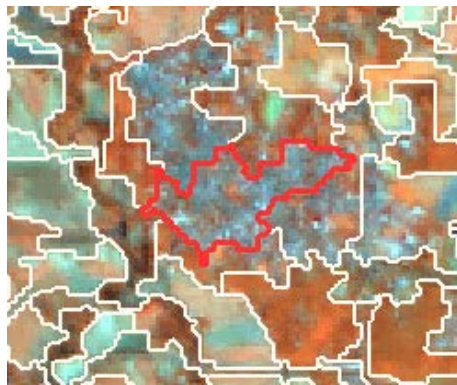
Table 4.5 Parameter setting of multiresolution segmentation and number of the derived image objects.

Scale	Color weight	Shape weight = 0.1		Number of image objects
		Compactness	Smoothness	
25	0.9	0.5	0.5	39,038

4.2.2 Feature extraction by SEaTH analysis

SEaTH analysis, which are used to extract separability value and to identify an optimum threshold value, was here applied on all possibly pairwises between two identified LULC classes based on the selected 94 features of image objects as summary in Table 4.6. Herewith, basic features included brightness value and its standard deviation, ratio and texture characteristics of image objects were selected to characterize LULC classes.

Under SEaTH analysis, basic statistical values include mean, standard deviation and variance are firstly extracted from 10 sample areas (image objects) for 10 LULC classes, which include 1) urban and built-up area (UR), 2) paddy field type I (PD1), 3) paddy field type II (PD2), 4) cassava type I (CA1), 5) cassava type II (CA2), 6) maize (MA), 7) sugarcane (SU), 8) perennial trees and orchard (PO), 9) forest type I (FO1), 10) forest type II (FO2), 11) forest type III (FO3), and (12) water body (WA). (See example of sample area in Figure 4.4) Average mean and variance values of all selected features for 12 LULC classes is presented in Tables 4.7 and 4.8, respectively. Figure 4.5 shows an example of average mean and variance of brightness feature of LULC classes.



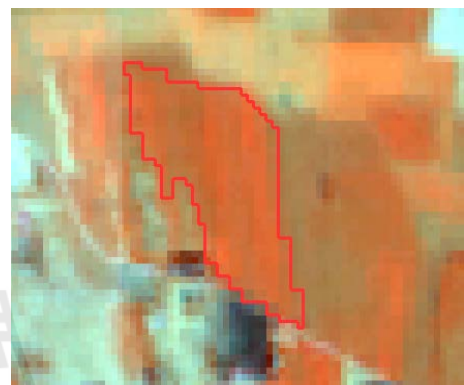
Urban and built-up area (UR)



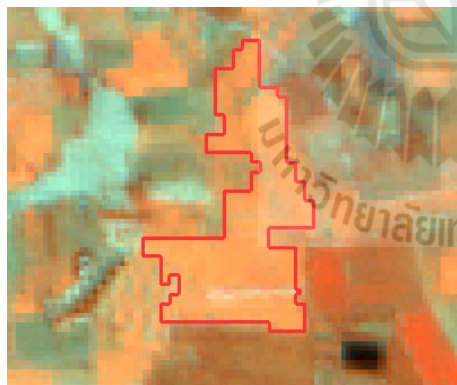
Paddy field type I (PD1)



Paddy field type II (PD2)



Cassava type I (CA1)



Cassava type II (CA2)



Maize (MA)

Figure 4.4 Sample area selected image object for SEaTH analysis of 12 LULC types.



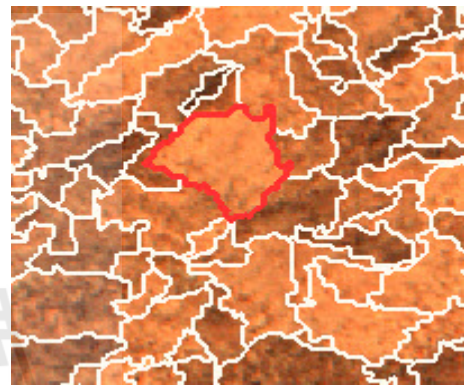
Sugarcane (SU)



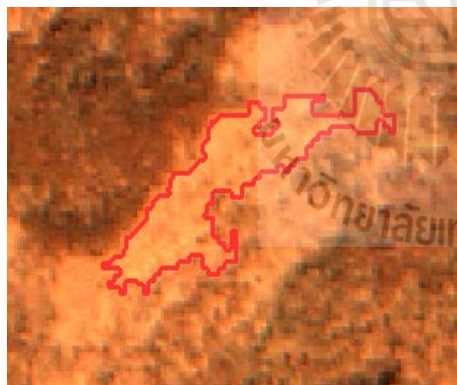
Perennial trees and Orchard (PO)



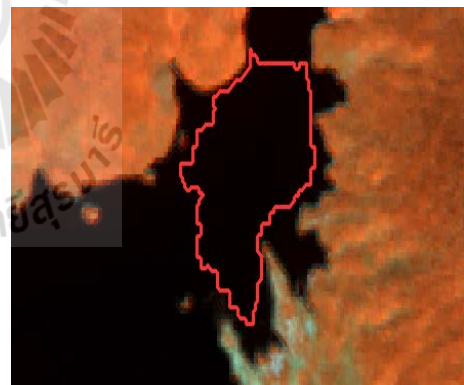
Forest type I (FO1)



Forest type II (FO2)



Forest type III (FO3)



Water body (WA)

Figure 4.4 (Continued)

Table 4.6 List of selected 94 features for SEaTH analysis.

No	Features
1	Brightness
2	Layer 1
3	Layer 2
4	Layer 3
5	Layer 4
6	Max. diff.
7	Std Layer 1
8	Std Layer 2
9	Std Layer 3
10	Std Layer 4
11	Pixel-based Layer 1 (Ratio layer 1)
12	Pixel-based Layer 2 (Ratio layer 2)
13	Pixel-based Layer 3 (Ratio layer 3)
14	Pixel-based Layer 4 (Ratio layer 4)
15	GLCM Homogeneity (all dir.)
16	GLCM Homogeneity (all dir.) Layer 1
17	GLCM Homogeneity (all dir.) Layer 2
18	GLCM Homogeneity (all dir.) Layer 3
19	GLCM Homogeneity (all dir.) Layer 4
20	GLCM Mean (quick 8/11) (all dir.)
21	GLCM Mean (quick 8/11) (all dir.) Layer 1
22	GLCM Mean (quick 8/11) (all dir.) Layer 2
23	GLCM Mean (quick 8/11) (all dir.) Layer 3
24	GLCM Mean (quick 8/11) (all dir.) Layer 4
25	GLCM Dissimilarity (all dir.)
26	GLCM Dissimilarity (all dir.) Layer 1
27	GLCM Dissimilarity (all dir.) Layer 2
28	GLCM Dissimilarity (all dir.) Layer 3
29	GLCM Dissimilarity (all dir.) Layer 4
30	GLCM Entropy (all dir.)
31	GLCM Entropy (all dir.) Layer 1
32	GLCM Entropy (all dir.) Layer 2
33	GLCM Entropy (all dir.) Layer 3
34	GLCM Entropy (all dir.) Layer 4
35	GLCM Ang. 2nd moment (all dir.)
36	GLCM Ang. 2nd moment (all dir.) Layer 1
37	GLCM Ang. 2nd moment (all dir.) Layer 2
38	GLCM Ang. 2nd moment (all dir.) Layer 3
39	GLCM Ang. 2nd moment (all dir.) Layer 4
40	GLCM StdDev (all dir.)
41	GLCM StdDev (all dir.) Layer 1
42	GLCM StdDev (all dir.) Layer 2
43	GLCM StdDev (all dir.) Layer 3
44	GLCM StdDev (all dir.) Layer 4
45	GLCM Contrast (all dir.)
46	GLCM Contrast (all dir.) Layer 1
47	GLCM Contrast (all dir.) Layer 2
48	GLCM Contrast (all dir.) Layer 3
49	GLCM Contrast (all dir.) Layer 4
50	GLCM Mean (all dir.)
51	GLCM Mean (all dir.) Layer 1

Table 4.6 (Continued).

No	Features
52	GLCM Mean (all dir.)Layer 2
53	GLCM Mean (all dir.)Layer 3
54	GLCM Mean (all dir.)Layer 4
55	GLCM Correlation (all dir.)
56	GLCM Correlation (all dir.) Layer 1
57	GLCM Correlation (all dir.) Layer 2
58	GLCM Correlation (all dir.) Layer 3
59	GLCM Correlation (all dir.) Layer 4
60	GLCM Homogeneity (quick 8/11) (all dir.)
61	GLCM Homogeneity (quick 8/11) (all dir.) Layer 1
62	GLCM Homogeneity (quick 8/11) (all dir.) Layer 2
63	GLCM Homogeneity (quick 8/11) (all dir.) Layer 3
64	GLCM Homogeneity (quick 8/11) (all dir.) Layer 4
65	GLCM Contrast (quick 8/11) (all dir.)
66	GLCM StdDev (quick 8/11) (all dir.) Layer 1
67	GLCM StdDev (quick 8/11) (all dir.) Layer 2
68	GLCM StdDev (quick 8/11) (all dir.) Layer 3
69	GLCM StdDev (quick 8/11) (all dir.) Layer 4
70	GLCM Dissimilarity (quick 8/11) (all dir.)
71	GLCM Dissimilarity (quick 8/11) (all dir.) Layer 1
72	GLCM Dissimilarity (quick 8/11) (all dir.) Layer 2
73	GLCM Dissimilarity (quick 8/11) (all dir.) Layer 3
74	GLCM Dissimilarity (quick 8/11) (all dir.) Layer 4
75	GLCM Entropy (quick 8/11) (all dir.)
76	GLCM Entropy (quick 8/11) (all dir.) Layer 1
77	GLCM Entropy (quick 8/11) (all dir.) Layer 2
78	GLCM Entropy (quick 8/11) (all dir.) Layer 3
79	GLCM Entropy (quick 8/11) (all dir.) Layer 4
80	GLCM Ang. 2nd moment (quick 8/11) (all dir.)
81	GLCM Ang. 2nd moment (quick 8/11) (all dir.) Layer 1
82	GLCM Ang. 2nd moment (quick 8/11) (all dir.) Layer 2
83	GLCM Ang. 2nd moment (quick 8/11) (all dir.) Layer 3
84	GLCM Ang. 2nd moment (quick 8/11) (all dir.) Layer 4
85	GLCM Contrast (quick 8/11) (all dir.) Layer 1
86	GLCM Contrast (quick 8/11) (all dir.) Layer 2
87	GLCM Contrast (quick 8/11) (all dir.) Layer 3
88	GLCM Contrast (quick 8/11) (all dir.) Layer 4
89	GLCM Contrast (quick 8/11) (all dir.) Layer 1
90	GLCM Correlation (quick 8/11) (all dir.)
91	GLCM Correlation (quick 8/11) (all dir.) Layer 1
92	GLCM Correlation (quick 8/11) (all dir.) Layer 2
93	GLCM Correlation (quick 8/11) (all dir.) Layer 3
94	GLCM Correlation (quick 8/11) (all dir.) Layer 4

Table 4.7 Average mean value from 10 training areas of 94 features for 12 LULC classes.

No	Features	UR	PD1	PD2	CA1	CA2	MA	SU	PO	FO1	FO2	FO3	WA
1	Brightness	62.2390	91.1600	74.8200	72.3200	58.6630	61.2810	66.5540	53.5650	42.2820	50.0920	65.5660	11.7337
2	Layer 1	52.1650	88.1340	65.6600	24.6000	42.7690	43.6730	32.8600	25.6650	9.3432	11.4363	13.5292	36.8360
3	Layer 2	98.9760	115.6260	134.0560	163.8910	94.6290	83.0180	163.6020	119.7870	110.7570	133.0870	165.5690	7.0998
4	Layer 3	71.6400	119.2220	76.2700	80.4990	72.0050	89.0620	57.0580	55.9070	41.1360	47.0020	68.6530	2.5905
5	Layer 4	26.1720	41.6550	23.2900	20.2880	25.2510	29.3720	12.7020	12.8980	7.8954	8.8432	14.5110	0.4044
6	Max. diff.	1.1720	0.8587	1.4825	1.9823	1.1665	0.9857	2.2694	1.9963	2.4352	2.4807	2.3330	3.0450
7	Std Layer 1	13.3600	6.8731	8.1803	3.5590	5.8203	4.6740	4.8978	3.6122	2.5627	1.9017	3.9232	1.4111
8	Std Layer 2	13.0640	6.6970	9.8896	16.9046	12.7386	8.7649	12.5979	5.7207	9.7303	7.3421	14.1760	1.8367
9	Std Layer 3	12.7840	7.5198	7.4839	3.9745	6.0711	6.7510	6.5824	4.1774	4.2288	3.1007	7.0606	1.2756
10	Std Layer 4	6.9144	3.1684	3.3258	1.6310	2.4276	3.0576	2.7408	2.1489	1.4971	1.1392	2.3887	0.4694
11	Pixel-based Layer 1	0.2093	0.2416	0.2187	0.0853	0.1851	0.1780	0.1232	0.1194	0.0551	0.0569	0.0513	0.7713
12	Pixel-based Layer 2	0.3980	0.3173	0.4485	0.5659	0.4000	0.3391	0.6150	0.5593	0.6552	0.6643	0.6315	0.1523
13	Pixel-based Layer 3	0.2877	0.3269	0.2550	0.2785	0.3066	0.3631	0.2142	0.2611	0.2431	0.2347	0.2619	0.0664
14	Pixel-based Layer 4	0.1050	0.1142	0.0778	0.0703	0.1083	0.1197	0.0476	0.0602	0.0466	0.0442	0.0553	0.0100
15	GLCM Homogeneity (all dir.)	0.1472	0.2815	0.2888	0.3377	0.3368	0.3442	0.3850	0.3939	0.3103	0.3827	0.2216	0.6675
16	GLCM Homogeneity (all dir.) Layer 1	0.1023	0.2157	0.2230	0.3001	0.2404	0.2942	0.3373	0.3329	0.2990	0.3745	0.2252	0.5926
17	GLCM Homogeneity (all dir.) Layer 2	0.2368	0.3648	0.3245	0.2679	0.2956	0.3370	0.3100	0.3450	0.2914	0.3184	0.2546	0.7291
18	GLCM Homogeneity (all dir.) Layer 3	0.1005	0.2073	0.2344	0.3478	0.2673	0.2472	0.3180	0.3052	0.2596	0.3378	0.1803	0.5991
19	GLCM Homogeneity (all dir.) Layer 4	0.1815	0.3585	0.3767	0.4907	0.4167	0.4065	0.4746	0.4548	0.4595	0.5407	0.3728	0.7902
20	GLCM Contrast (all dir.)	70.8090	20.1490	22.1430	11.5943	11.0403	11.8226	12.6997	11.1749	11.2349	5.9740	24.7120	3.5349
21	GLCM Contrast (all dir.) Layer 1	168.0340	39.4120	40.6620	20.3410	36.1820	22.9188	26.7096	27.8480	10.5014	5.8611	20.7260	4.4395
22	GLCM Contrast (all dir.) Layer 2	124.9140	25.1090	86.3860	239.7410	160.3160	72.4070	116.1380	29.3090	81.6290	45.2210	202.2950	26.3538
23	GLCM Contrast (all dir.) Layer 3	163.6500	49.3090	39.2940	9.3705	20.6314	29.6150	34.6352	29.2450	16.3907	8.2258	36.8400	5.6472
24	GLCM Contrast (all dir.) Layer 4	42.9020	10.1344	8.7847	3.3486	5.5086	7.3810	8.3476	7.8364	3.0779	1.8035	5.6095	0.8534
25	GLCM Dissimilarity (all dir.)	6.1720	3.1668	3.2601	2.4780	2.4074	2.3879	2.3003	2.1513	2.5581	1.8881	3.8123	0.9144

Table 4.7 (Continued).

No	Features	UR	PD1	PD2	CA1	CA2	MA	SU	PO	FO1	FO2	FO3	WA
26	GLCM Dissimilarity (all dir.) Layer 1	9.4565	4.4346	4.4989	3.0474	4.1695	3.1750	3.0912	3.0761	2.5611	1.9172	3.5861	1.188
27	GLCM Dissimilarity (all dir.) Layer 2	7.3220	3.1481	5.3652	9.7892	7.4848	4.8590	6.1254	3.4593	5.9352	4.4419	9.3823	1.175
28	GLCM Dissimilarity (all dir.) Layer 3	9.4263	4.8072	4.3369	2.2740	3.3108	3.7855	3.4648	3.3604	3.1484	2.2497	4.7425	1.253
29	GLCM Dissimilarity (all dir.) Layer 4	4.8539	2.2519	2.1274	1.3432	1.7418	1.8979	1.7285	1.7665	1.3939	1.0636	1.8795	0.474
30	GLCM Entropy (all dir.)	6.5429	5.6225	5.6513	5.2810	5.1552	5.0066	4.8263	4.3853	5.1139	4.5149	5.9715	2.454
31	GLCM Entropy (all dir.) Layer 1	7.3004	6.2242	6.3593	5.1608	6.0112	5.3935	5.1460	4.8734	4.6485	4.0815	5.4288	2.979
32	GLCM Entropy (all dir.) Layer 2	6.9366	5.8657	6.3329	7.1812	6.8625	6.0119	6.4216	5.7006	6.7957	6.2551	7.2123	2.543
33	GLCM Entropy (all dir.) Layer 3	7.2750	6.3225	6.1617	5.0761	5.8011	5.9669	5.3552	5.2205	5.4422	4.7954	6.3620	2.840
34	GLCM Entropy (all dir.) Layer 4	6.2275	4.7714	4.7849	3.7140	4.3506	4.5926	3.9644	3.9753	3.5480	3.0425	4.3738	1.353
35	GLCM Ang. 2nd moment (all dir.)	0.0021	0.0061	0.0063	0.0080	0.0093	0.0111	0.0158	0.0235	0.0095	0.0169	0.0037	0.154
36	GLCM Ang. 2nd moment (all dir.) Layer 1	0.0009	0.0032	0.0028	0.0097	0.0040	0.0081	0.0120	0.0176	0.0142	0.0252	0.0064	0.093
37	GLCM Ang. 2nd moment (all dir.) Layer 2	0.0016	0.0051	0.0037	0.0013	0.0021	0.0051	0.0030	0.0056	0.0022	0.0034	0.0013	0.148
38	GLCM Ang. 2nd moment (all dir.) Layer 3	0.0010	0.0030	0.0037	0.0094	0.0051	0.0042	0.0104	0.0114	0.0067	0.0129	0.0025	0.118
39	GLCM Ang. 2nd moment (all dir.) Layer 4	0.0029	0.0145	0.0149	0.0380	0.0199	0.0172	0.0393	0.0386	0.0426	0.0693	0.0179	0.401
40	GLCM Mean (all dir.)	61.911	90.5000	74.1320	71.7480	58.364	61.010	66.2010	53.4240	41.9110	49.6800	65.0000	11.52
41	GLCM Mean (all dir.)Layer 1	52.147	87.7980	65.4250	24.9310	42.529	43.640	33.1420	26.0700	9.3418	11.4413	13.5506	36.85
42	GLCM Mean (all dir.)Layer 2	99.152	115.554	133.282	162.787	95.307	83.715	162.845	119.717	110.765	132.907	165.004	7.465
43	GLCM Mean (all dir.)Layer 3	71.663	118.772	76.1120	80.3570	72.011	88.923	57.5860	56.3160	41.1340	46.9700	68.4630	2.788
44	GLCM Mean (all dir.)Layer 4	26.170	41.4360	23.2630	20.3790	25.160	29.266	13.0070	13.1580	7.8945	8.8387	14.4750	0.492
45	GLCM StdDev (all dir.)	8.5013	5.4692	5.8676	4.5629	4.2201	4.0304	4.4700	3.0688	3.6444	2.7552	5.9425	1.420
46	GLCM StdDev (all dir.) Layer 1	13.494	7.3875	8.4742	4.1887	6.2862	5.1704	5.5804	4.6380	2.6124	1.9640	3.9731	1.750
47	GLCM StdDev (all dir.) Layer 2	13.305	7.0029	10.9722	18.3090	14.319	9.7184	13.6010	6.1399	9.9956	7.6838	15.2430	3.256
48	GLCM StdDev (all dir.) Layer 3	12.969	8.2839	7.9904	4.1813	6.3328	7.1666	7.3333	5.1199	4.3147	3.2016	7.3508	1.793
49	GLCM StdDev (all dir.) Layer 4	7.0223	3.5140	3.5500	1.7980	2.5738	3.3174	3.2069	2.6643	1.5358	1.1831	2.4369	0.628
50	GLCM Correlation (all dir.)	0.7151	0.8123	0.8176	0.8480	0.8285	0.7992	0.8203	0.6436	0.7707	0.7646	0.8098	0.465
51	GLCM Correlation (all dir.) Layer 1	0.7386	0.7971	0.8475	0.6391	0.7427	0.7647	0.7894	0.5996	0.4780	0.4814	0.5936	0.557

Table 4.7 (Continued).

No	Features	UR	PD1	PD2	CA1	CA2	MA	SU	PO	FO1	FO2	FO3	WA
52	GLCM Correlation (all dir.) Layer 2	0.8001	0.8645	0.8008	0.8006	0.7879	0.7923	0.8393	0.7819	0.7859	0.7868	0.7583	0.595
53	GLCM Correlation (all dir.) Layer 3	0.7172	0.7993	0.8347	0.8516	0.8575	0.8441	0.8270	0.6715	0.7551	0.7687	0.8125	0.439
54	GLCM Correlation (all dir.) Layer 4	0.7536	0.7651	0.8101	0.6943	0.7695	0.8188	0.7818	0.6786	0.5768	0.5910	0.7288	0.285
55	GLCM Homogeneity (quick 8/11) (all dir.)	0.1469	0.2804	0.2874	0.3351	0.3342	0.3424	0.3843	0.3916	0.3096	0.3819	0.2204	0.667
56	GLCM Homogeneity (quick 8/11) (all dir.) Layer 1	0.1019	0.2148	0.2219	0.2978	0.2383	0.2929	0.3369	0.3314	0.2987	0.3741	0.2249	0.592
57	GLCM Homogeneity (quick 8/11) (all dir.) Layer 2	0.2343	0.3616	0.3211	0.2629	0.2888	0.3340	0.3081	0.3426	0.2893	0.3166	0.2504	0.728
58	GLCM Homogeneity (quick 8/11) (all dir.) Layer 3	0.1001	0.2064	0.2333	0.3467	0.2652	0.2463	0.3175	0.3036	0.2593	0.3371	0.1797	0.598
59	GLCM Homogeneity (quick 8/11) (all dir.) Layer 4	0.1808	0.3570	0.3750	0.4877	0.4149	0.4049	0.4735	0.4526	0.4591	0.5403	0.3728	0.789
60	GLCM Contrast (quick 8/11) (all dir.)	72.165	21.1430	23.2550	12.2213	12.168	12.365	14.5515	11.8662	11.3372	6.0763	25.2250	3.555
61	GLCM Contrast (quick 8/11) (all dir.) Layer 1	171.19	41.1430	42.2230	21.3960	38.279	24.085	29.5381	29.5720	10.5161	5.8744	20.7440	4.461
62	GLCM Contrast (quick 8/11) (all dir.) Layer 2	127.84	29.1440	91.8930	255.662	178.33	75.652	122.295	31.9130	82.7080	46.5750	208.459	26.71
63	GLCM Contrast (quick 8/11) (all dir.) Layer 3	166.49	52.6510	40.8830	9.6770	22.428	31.056	40.4465	30.8150	16.4841	8.2897	37.3490	5.663
64	GLCM Contrast (quick 8/11) (all dir.) Layer 4	43.860	10.7947	9.0458	3.4704	5.7258	7.7838	9.1753	8.1829	3.0855	1.8081	5.6210	0.854
65	GLCM Dissimilarity (quick 8/11) (all dir.)	6.2148	3.2112	3.3108	2.5257	2.4718	2.4245	2.3469	2.1959	2.5685	1.8980	3.8459	0.916
66	GLCM Dissimilarity (quick 8/11) (all dir.) Layer 1	9.5308	4.4901	4.5563	3.1126	4.2669	3.2261	3.1368	3.1304	2.5630	1.9197	3.5877	1.191
67	GLCM Dissimilarity (quick 8/11) (all dir.) Layer 2	7.4203	3.2703	5.5234	10.0932	7.8547	4.9704	6.2565	3.5383	5.9847	4.4923	9.5623	1.183
68	GLCM Dissimilarity (quick 8/11) (all dir.) Layer 3	9.4877	4.8987	4.3932	2.2970	3.3902	3.8404	3.5506	3.4268	3.1553	2.2564	4.7676	1.255
69	GLCM Dissimilarity (quick 8/11) (all dir.) Layer 4	4.8940	2.2911	2.1496	1.3640	1.7642	1.9272	1.7610	1.7965	1.3957	1.0651	1.8802	0.475
70	GLCM Entropy (quick 8/11) (all dir.)	6.5475	5.6388	5.6654	5.2999	5.1836	5.0150	4.8348	4.4092	5.1176	4.5215	5.9798	2.455
71	GLCM Entropy (quick 8/11) (all dir.) Layer 1	7.3074	6.2366	6.3659	5.1885	6.0319	5.4019	5.1502	4.8913	4.6467	4.0805	5.4277	2.981
72	GLCM Entropy (quick 8/11) (all dir.) Layer 2	6.9515	5.8900	6.3561	7.2067	6.8976	6.0326	6.4325	5.7157	6.8050	6.2663	7.2334	2.546
73	GLCM Entropy (quick 8/11) (all dir.) Layer 3	7.2791	6.3387	6.1746	5.0814	5.8195	5.9714	5.3617	5.2429	5.4435	4.7975	6.3629	2.842
74	GLCM Entropy (quick 8/11) (all dir.) Layer 4	6.2375	4.7909	4.7961	3.7351	4.3667	4.6021	3.9745	3.9965	3.5461	3.0409	4.3659	1.354
75	GLCM Ang. 2nd moment (quick 8/11) (all dir.)	0.0021	0.0060	0.0063	0.0079	0.0091	0.0110	0.0157	0.0232	0.0095	0.0168	0.0037	0.154
76	GLCM Ang.2nd moment (quick 8/11)(all dir.)Layer 1	0.0009	0.0032	0.0028	0.0095	0.0039	0.0080	0.0120	0.0174	0.0142	0.0253	0.0064	0.093
77	GLCM Ang.2ndmoment(quick 8/11)(all dir.)Layer 2	0.0016	0.0050	0.0036	0.0013	0.0020	0.0050	0.0029	0.0055	0.0022	0.0034	0.0013	0.145

Table 4.7 (Continued).

No	Features	UR	PD1	PD2	CA1	CA2	MA	SU	PO	FO1	FO2	FO3	WA
78	GLCM Ang2ndmoment(quick 8/11)(all dir.)Layer 3	0.0010	0.0030	0.0037	0.0094	0.0050	0.0042	0.0104	0.0113	0.0067	0.0129	0.0024	0.118
79	GLCM Ang2nd moment(quick 8/11)(all dir.)Layer 4	0.0029	0.0144	0.0148	0.0375	0.0197	0.0171	0.0392	0.0382	0.0427	0.0693	0.0181	0.401
80	GLCM Mean (quick 8/11) (all dir.)	61.915	90.4670	74.0860	71.7160	58.418	61.037	66.2090	53.4400	41.9100	49.6760	65.0130	11.53
81	GLCM Mean (quick 8/11) (all dir.) Layer 1	52.093	87.7550	65.411	25.0140	42.454	43.648	33.1990	26.1140	9.3392	11.4495	13.5796	36.84
82	GLCM Mean (quick 8/11) (all dir.) Layer 2	99.242	115.579	133.10	162.54	95.586	83.847	162.697	119.685	110.7640	132.8840	164.9790	7.4724
83	GLCM Mean (quick 8/11) (all dir.) Layer 3	71.6660	118.6940	76.1090	80.3600	72.0500	88.9070	57.6660	56.3500	41.1330	46.9690	68.4890	2.7893
84	GLCM Mean (quick 8/11) (all dir.) Layer 4	26.1500	41.4050	23.2720	20.4080	25.1400	29.2540	13.041	13.1780	7.8936	8.8407	14.4870	0.4927
85	GLCM StdDev (quick 8/11) (all dir.)	8.5163	5.5354	5.9182	4.5858	4.2922	4.0396	4.5851	3.1480	3.6462	2.7670	5.9491	1.4239
86	GLCM StdDev (quick 8/11) (all dir.) Layer 1	13.5360	7.4658	8.4881	4.2934	6.3815	5.2206	5.7458	4.7833	2.6078	1.9620	3.9701	1.7553
87	GLCM StdDev (quick 8/11) (all dir.) Layer 2	13.3800	7.1535	11.1476	18.5790	14.6790	9.8098	13.7376	6.2611	10.0225	7.7460	15.3950	3.2787
88	GLCM StdDev (quick 8/11) (all dir.) Layer 3	13.0030	8.4316	8.0455	4.1774	6.3778	7.1753	7.5125	5.2328	4.3107	3.2015	7.3297	1.7965
89	GLCM StdDev (quick 8/11) (all dir.) Layer 4	7.0586	3.5833	3.5647	1.8200	2.5948	3.3377	3.2710	2.7125	1.5332	1.1814	2.4207	0.6291
90	GLCM Correlation (quick 8/11) (all dir.)	0.7099	0.8081	0.8121	0.8409	0.8196	0.7925	0.8155	0.6374	0.7686	0.7625	0.8059	0.4676
91	GLCM Correlation (quick 8/11) (all dir.) Layer 1	0.7347	0.7929	0.8421	0.6406	0.7369	0.7576	0.7890	0.5971	0.4740	0.4783	0.5918	0.5577
92	GLCM Correlation (quick 8/11) (all dir.) Layer 2	0.7974	0.8548	0.7942	0.7924	0.7773	0.7872	0.8354	0.7741	0.7840	0.7839	0.7556	0.5971
93	GLCM Correlation (quick 8/11) (all dir.) Layer 3	0.7135	0.7944	0.8296	0.8462	0.8497	0.8364	0.8218	0.6667	0.7529	0.7669	0.8082	0.4383
94	GLCM Correlation (quick 8/11) (all dir.) Layer 4	0.7506	0.7609	0.8051	0.6907	0.7651	0.8114	0.7784	0.6738	0.5732	0.5879	0.7236	0.2878

Table 4.8 Average variance value from 10 training areas of 94 features for 12 LULC classes.

No	Features	UR	PD1	PD2	CA1	CA2	MA	SU	PO	FO1	FO2	FO3	WA
1	Brightness	5.93348	17.58349	20.97233	7.5738	25.5669	11.22168	9.63385	6.86714	7.21922	17.175	42.8048	40.3266
2	Layer 1	62.43398	29.60654	71.94327	8.0347	53.2467	10.30389	20.69960	15.19901	3.57645	2.8184	10.2752	548.103
3	Layer 2	136.8587	23.67758	43.41089	169.80	365.736	24.90628	56.36748	38.25249	46.3787	118.43	261.258	17.9641
4	Layer 3	16.89658	37.24673	19.99311	3.6439	49.1224	41.81855	17.72993	7.80069	10.8823	14.436	48.8931	2.50346
5	Layer 4	15.65544	6.68385	2.78607	1.2780	2.47834	5.89148	2.96235	1.46911	0.70991	0.5950	2.62894	0.19148
6	Max. diff.	0.06438	0.00026	0.00610	0.0164	0.06460	0.00055	0.01285	0.00914	0.00674	0.0014	0.00363	0.26531
7	Std Layer 1	2.12804	0.96065	4.49271	0.5216	0.74018	2.02160	4.96062	1.00387	0.13633	0.0469	0.22250	0.13577
8	Std Layer 2	5.25714	2.58424	7.11835	14.853	3.69962	7.97967	16.51873	1.04448	3.79713	1.9519	4.56083	4.60989
9	Std Layer 3	2.01667	1.42625	2.30525	0.4331	1.93005	1.35182	15.52165	0.77369	0.59839	0.1557	0.62594	0.27510
10	Std Layer 4	0.53583	0.20863	0.44331	0.0255	0.15290	0.51746	2.39000	0.25783	0.06102	0.0155	0.06806	0.03727
11	Pixel-based Layer 1	0.00081	0.00003	0.00031	0.0001	0.00186	0.00004	0.00019	0.00016	0.00009	0.0000	0.00009	0.01439
12	Pixel-based Layer 2	0.00243	0.00008	0.00031	0.0007	0.00274	0.00040	0.00056	0.00038	0.00031	0.0000	0.00011	0.00584
13	Pixel-based Layer 3	0.00008	0.00005	0.00004	0.0000	0.00003	0.00011	0.00010	0.00011	0.00007	0.0000	0.00007	0.00188
14	Pixel-based Layer 4	0.00020	0.00002	0.00001	0.0000	0.00013	0.00002	0.00003	0.00002	0.00001	0.0000	0.00000	0.00010
15	GLCM Homogeneity (all dir.)	0.00033	0.00092	0.00212	0.0013	0.00106	0.00176	0.00268	0.00288	0.00277	0.0007	0.00124	0.00454
16	GLCM Homogeneity (all dir.) Layer 1	0.00025	0.00056	0.00155	0.0002	0.00096	0.00198	0.00389	0.00421	0.00193	0.0008	0.00093	0.00382
17	GLCM Homogeneity (all dir.) Layer 2	0.00010	0.00071	0.00112	0.0001	0.00057	0.00245	0.00074	0.00050	0.00061	0.0002	0.00027	0.00751
18	GLCM Homogeneity (all dir.) Layer 3	0.00017	0.00067	0.00146	0.0004	0.00129	0.00086	0.00344	0.00333	0.00203	0.0011	0.00083	0.00549
19	GLCM Homogeneity (all dir.) Layer 4	0.00063	0.00117	0.00216	0.0003	0.00176	0.00258	0.00543	0.00432	0.00231	0.0007	0.00150	0.00910
20	GLCM Contrast (all dir.)	487.8361	17.15037	74.72642	22.531	11.9514	33.76514	77.26862	14.62262	22.8373	2.2602	56.9720	19.8753
21	GLCM Contrast (all dir.) Layer 1	3094.888	65.65415	334.5973	24.740	138.012	240.9644	665.32471	201.4225	11.7130	1.1276	30.3886	9.02350
22	GLCM Contrast (all dir.) Layer 2	619.9752	131.5033	1100.324	8434.6	2843.03	1661.435	4561.6113	83.96025	1389.75	229.59	4664.14	1890.38
23	GLCM Contrast (all dir.) Layer 3	2357.238	152.8144	255.32458	2.61026	35.68402	152.95307	1105.55233	126.75781	40.37211	3.45056	93.82309	40.60748
24	GLCM Contrast (all dir.) Layer 4	191.02533	5.33850	12.05526	0.36060	3.31448	14.94232	62.79196	13.43445	0.80229	0.08471	2.05089	0.66350
25	GLCM Dissimilarity (all dir.)	0.79732	0.13698	0.47210	0.21922	0.09633	0.22750	0.45758	0.12290	0.30299	0.04489	0.37991	0.16846

Table 4.8 (Continued).

No	Features	UR	PD1	PD2	CA1	CA2	MA	SU	PO	FO1	FO2	FO3	WA
26	GLCM Dissimilarity (all dir.) Layer 1	2.10807	0.21905	0.92785	0.06681	0.44346	0.70540	1.74800	0.51173	0.18782	0.03395	0.25515	0.10263
27	GLCM Dissimilarity (all dir.) Layer 2	0.39116	0.33269	1.58339	3.54737	1.71354	2.36823	3.04035	0.26978	2.05983	0.46468	2.88862	1.35380
28	GLCM Dissimilarity (all dir.) Layer 3	1.65501	0.42969	0.76906	0.03559	0.25826	0.46564	2.30689	0.39515	0.39111	0.06914	0.46428	0.24152
29	GLCM Dissimilarity (all dir.) Layer 4	0.49575	0.07510	0.15933	0.01019	0.07474	0.18086	0.50947	0.12188	0.04499	0.00829	0.06231	0.06385
30	GLCM Entropy (all dir.)	0.04861	0.08462	0.18778	0.18078	0.10590	0.11381	0.30192	0.12828	0.20954	0.10353	0.07250	0.30068
31	GLCM Entropy (all dir.) Layer 1	0.05484	0.05514	0.14697	0.03757	0.08418	0.21732	0.39772	0.25274	0.08795	0.04349	0.05146	0.23169
32	GLCM Entropy (all dir.) Layer 2	0.04959	0.08938	0.16951	0.07557	0.07896	0.31060	0.11629	0.05109	0.15765	0.08384	0.04406	0.61976
33	GLCM Entropy (all dir.) Layer 3	0.04612	0.08418	0.12995	0.04837	0.18540	0.09134	0.51153	0.20721	0.14488	0.05312	0.04757	0.29583
34	GLCM Entropy (all dir.) Layer 4	0.04517	0.07683	0.13390	0.02390	0.08445	0.17636	0.52239	0.20647	0.09030	0.03192	0.04689	0.37540
35	GLCM Ang. 2nd moment (all dir.)	0.00000	0.00000	0.00001	0.00001	0.00001	0.00001	0.00005	0.00009	0.00002	0.00003	0.00000	0.00723
36	GLCM Ang. 2nd moment (all dir.) Layer 1	0.00000	0.00000	0.00000	0.00000	0.00000	0.00001	0.00004	0.00012	0.00002	0.00003	0.00000	0.00152
37	GLCM Ang. 2nd moment (all dir.) Layer 2	0.00000	0.00000	0.00000	0.00000	0.00000	0.00001	0.00000	0.00000	0.00000	0.00000	0.00000	0.00683
38	GLCM Ang. 2nd moment (all dir.) Layer 3	0.00000	0.00000	0.00000	0.00000	0.00001	0.00000	0.00004	0.00004	0.00001	0.00001	0.00000	0.00393
39	GLCM Ang. 2nd moment (all dir.) Layer 4	0.00000	0.00001	0.00003	0.00003	0.00003	0.00004	0.00036	0.00038	0.00020	0.00016	0.00002	0.05335
40	GLCM Mean (all dir.)	5.22752	17.51433	20.72102	7.06260	24.06694	11.11307	10.48179	6.82398	7.15901	17.07893	40.73533	40.20319
41	GLCM Mean (all dir.)Layer 1	58.66942	29.62260	70.37683	7.85352	49.87785	10.51431	20.95391	14.97511	3.59307	2.85972	10.34689	545.92428
42	GLCM Mean (all dir.)Layer 2	132.48380	22.39092	41.45524	158.37045	341.16825	25.70772	58.20081	38.07693	45.64923	116.02007	244.70325	21.42905
43	GLCM Mean (all dir.)Layer 3	14.76618	38.09586	20.85402	3.52247	46.52045	41.93951	20.01072	7.28494	10.89156	14.43822	46.63693	3.24318
44	GLCM Mean (all dir.)Layer 4	14.52036	6.82614	2.94929	1.24657	2.30220	5.87212	3.52913	1.45457	0.71844	0.60682	2.56158	0.25097
45	GLCM StdDev (all dir.)	1.20321	0.67048	2.61593	1.41756	0.64146	0.65069	3.33830	0.32292	0.60642	0.28021	0.66570	0.98734
46	GLCM StdDev (all dir.) Layer 1	2.36152	1.06646	4.71306	0.59187	0.82266	2.90306	7.45281	1.15470	0.13280	0.04716	0.20599	0.42892
47	GLCM StdDev (all dir.) Layer 2	4.02667	2.89739	5.84911	15.95710	4.72952	8.55520	17.30435	1.00907	3.98526	2.23541	5.36725	12.00341
48	GLCM StdDev (all dir.) Layer 3	1.96650	1.68197	2.42611	0.41461	1.72931	1.67639	18.91460	0.97847	0.60783	0.16040	0.64830	1.09051
49	GLCM StdDev (all dir.) Layer 4	0.53252	0.25557	0.47151	0.03308	0.17513	0.69282	3.32477	0.37112	0.05856	0.01407	0.06617	0.10678
50	GLCM Correlation (all dir.)	0.00466	0.00071	0.00272	0.00090	0.00148	0.00430	0.00455	0.00421	0.00051	0.00552	0.00096	0.05004

Table 4.8 (Continued).

No	Features	UR	PD1	PD2	CA1	CA2	MA	SU	PO	FO1	FO2	FO3	WA
51	GLCM Correlation (all dir.) Layer 1	0.00264	0.00098	0.00099	0.00465	0.00230	0.00559	0.00344	0.01611	0.01432	0.00836	0.00262	0.01611
52	GLCM Correlation (all dir.) Layer 2	0.00152	0.00062	0.00285	0.00194	0.00058	0.00439	0.00094	0.00302	0.00105	0.00126	0.00162	0.03161
53	GLCM Correlation (all dir.) Layer 3	0.00406	0.00101	0.00096	0.00088	0.00135	0.00213	0.00421	0.00510	0.00238	0.00319	0.00142	0.03775
54	GLCM Correlation (all dir.) Layer 4	0.00335	0.00189	0.00114	0.00113	0.00092	0.00292	0.00553	0.00546	0.01185	0.00484	0.00207	0.03372
55	GLCM Homogeneity (quick 8/11) (all dir.)	0.00034	0.00093	0.00212	0.00135	0.00113	0.00180	0.00270	0.00288	0.00277	0.00073	0.00126	0.00455
56	GLCM Homogeneity (quick 8/11) (all dir.) Layer 1	0.00026	0.00057	0.00152	0.00026	0.00102	0.00201	0.00393	0.00418	0.00190	0.00089	0.00093	0.00382
57	GLCM Homogeneity (quick 8/11) (all dir.) Layer 2	0.00010	0.00082	0.00115	0.00016	0.00056	0.00253	0.00080	0.00050	0.00063	0.00023	0.00032	0.00750
58	GLCM Homogeneity (quick 8/11) (all dir.) Layer 3	0.00018	0.00068	0.00144	0.00049	0.00135	0.00087	0.00349	0.00331	0.00202	0.00113	0.00083	0.00549
59	GLCM Homogeneity (quick 8/11) (all dir.) Layer 4	0.00066	0.00123	0.00213	0.00037	0.00192	0.00261	0.00555	0.00430	0.00227	0.00075	0.00150	0.00911
60	GLCM Contrast (quick 8/11) (all dir.)	523.141	22.95009	84.16441	23.71750	20.03817	41.89930	147.94257	14.57495	23.26586	2.52704	60.28701	20.12300
61	GLCM Contrast (quick 8/11) (all dir.) Layer 1	3376.54	97.89169	358.22242	30.01798	184.77401	282.02716	1066.1033	187.8643	11.56239	1.15053	30.59147	9.12560
62	GLCM Contrast (quick 8/11) (all dir.) Layer 2	612.138	366.18538	1185.1384	8715.9064	4888.4368	1774.6276	5461.7540	159.5403	1422.1511	263.208	4942.3131	1960.3605
63	GLCM Contrast (quick 8/11) (all dir.) Layer 3	2536.16	237.37608	259.79158	2.97660	57.15860	165.17792	2042.6364	124.0346	40.64427	3.80055	98.38343	40.62012
64	GLCM Contrast (quick 8/11) (all dir.) Layer 4	217.314	8.61061	12.22333	0.44703	4.45072	17.36209	93.64939	12.95795	0.79053	0.08729	2.10856	0.66328
65	GLCM Dissimilarity (quick 8/11) (all dir.)	0.82860	0.14905	0.48815	0.22680	0.13065	0.25826	0.55636	0.12768	0.30663	0.04804	0.39607	0.16940
66	GLCM Dissimilarity (quick 8/11) (all dir.) Layer 1	2.23566	0.24501	0.93752	0.07062	0.53628	0.78644	1.98456	0.50439	0.18536	0.03443	0.25494	0.10325
67	GLCM Dissimilarity (quick 8/11) (all dir.) Layer 2	0.34644	0.53736	1.64459	3.63587	2.24991	2.52804	3.45692	0.31792	2.10383	0.50113	3.08352	1.37706
68	GLCM Dissimilarity (quick 8/11) (all dir.) Layer 3	1.72632	0.52116	0.77154	0.03700	0.32817	0.49338	2.74279	0.40656	0.39164	0.07316	0.47704	0.24155
69	GLCM Dissimilarity (quick 8/11) (all dir.) Layer 4	0.54081	0.09144	0.15874	0.01112	0.08970	0.19748	0.58119	0.12259	0.04438	0.00849	0.06278	0.06383
70	GLCM Entropy (quick 8/11) (all dir.)	0.04788	0.08650	0.18724	0.18297	0.11815	0.11758	0.30337	0.12890	0.21100	0.10630	0.07163	0.30171
71	GLCM Entropy (quick 8/11) (all dir.) Layer 1	0.05604	0.05614	0.14725	0.03611	0.09044	0.22627	0.40412	0.25153	0.08665	0.04317	0.05192	0.23189
72	GLCM Entropy (quick 8/11) (all dir.) Layer 2	0.04703	0.09843	0.16844	0.07801	0.07906	0.31911	0.12029	0.05344	0.16001	0.08554	0.04502	0.61981
73	GLCM Entropy (quick 8/11) (all dir.) Layer 3	0.04536	0.08873	0.12820	0.04859	0.19727	0.09502	0.52197	0.20694	0.14480	0.05582	0.04612	0.29597

Table 4.8 (Continued).

No	Features	UR	PD1	PD2	CA1	CA2	MA	SU	PO	FO1	FO2	FO3	WA
74	GLCM Entropy (quick 8/11) (all dir.) Layer 4	0.04760	0.08150	0.13301	0.02511	0.09426	0.18509	0.53696	0.20542	0.08917	0.03278	0.04591	0.37537
75	GLCM Ang. 2nd moment (quick 8/11) (all dir.)	0.00000	0.00000	0.00001	0.00001	0.00001	0.00001	0.00005	0.00008	0.00002	0.00003	0.00000	0.00721
76	GLCM Ang. 2nd moment (quick 8/11) (all dir.) Layer 1	0.00000	0.00000	0.00000	0.00000	0.00000	0.00001	0.00004	0.00011	0.00002	0.00003	0.00000	0.00151
77	GLCM Ang. 2nd moment (quick 8/11) (all dir.) Layer 2	0.00000	0.00000	0.00000	0.00000	0.00000	0.00001	0.00000	0.00000	0.00000	0.00000	0.00000	0.00681
78	GLCM Ang. 2nd moment (quick 8/11) (all dir.) Layer 3	0.00000	0.00000	0.00000	0.00000	0.00001	0.00000	0.00004	0.00004	0.00001	0.00001	0.00000	0.00391
79	GLCM Ang. 2nd moment (quick 8/11) (all dir.) Layer 4	0.00000	0.00002	0.00003	0.00003	0.00003	0.00004	0.00036	0.00037	0.00020	0.00017	0.00002	0.05332
80	GLCM Mean (quick 8/11) (all dir.)	4.96425	17.55540	20.67472	7.01140	23.84744	11.00556	10.69254	6.81124	7.14198	17.07552	40.44767	40.19324
81	GLCM Mean (quick 8/11) (all dir.) Layer 1	57.68396	29.73743	69.91859	7.80374	49.52143	10.48068	21.08648	14.82703	3.59205	2.85961	10.48729	545.98064
82	GLCM Mean (quick 8/11) (all dir.) Layer 2	131.43633	21.95892	41.84651	157.00108	336.81778	26.01149	58.70916	37.80767	45.28347	115.80469	239.13823	21.45433
83	GLCM Mean (quick 8/11) (all dir.) Layer 3	14.17027	38.68680	20.68559	3.53856	46.04187	42.08120	20.83883	7.40756	10.89631	14.43217	46.70061	3.24579
84	GLCM Mean (quick 8/11) (all dir.) Layer 4	14.13873	6.90425	2.90788	1.24357	2.30936	5.88698	3.66608	1.46491	0.71999	0.60701	2.61749	0.25091
85	GLCM StdDev (quick 8/11) (all dir.)	1.20992	0.71387	2.68923	1.39935	0.73767	0.70920	3.87822	0.31926	0.61151	0.28724	0.63199	0.99958
86	GLCM StdDev (quick 8/11) (all dir.) Layer 1	2.41869	1.20531	4.75504	0.59409	0.96633	3.19669	9.33982	1.01398	0.13068	0.04671	0.20978	0.43134
87	GLCM StdDev (quick 8/11) (all dir.) Layer 2	3.70758	3.47525	6.20902	15.70852	5.85794	8.41966	18.14851	1.28997	4.04060	2.32227	5.27396	12.22956
88	GLCM StdDev (quick 8/11) (all dir.) Layer 3	1.99656	1.85705	2.41913	0.40459	1.83632	1.74817	21.52678	0.95500	0.60718	0.16682	0.60168	1.09433
89	GLCM StdDev (quick 8/11) (all dir.) Layer 4	0.55826	0.28815	0.46830	0.03583	0.19699	0.74062	3.71934	0.36772	0.05802	0.01429	0.06290	0.10681
90	GLCM Correlation (quick 8/11) (all dir.)	0.00492	0.00065	0.00251	0.00094	0.00128	0.00394	0.00416	0.00445	0.00052	0.00567	0.00117	0.04765
91	GLCM Correlation (quick 8/11) (all dir.) Layer 1	0.00298	0.00101	0.00086	0.00448	0.00232	0.00549	0.00333	0.01612	0.01420	0.00841	0.00296	0.01643
92	GLCM Correlation (quick 8/11) (all dir.) Layer 2	0.00164	0.00109	0.00258	0.00219	0.00074	0.00438	0.00096	0.00305	0.00107	0.00140	0.00182	0.03133
93	GLCM Correlation (quick 8/11) (all dir.) Layer 3	0.00425	0.00093	0.00102	0.00094	0.00111	0.00220	0.00381	0.00484	0.00237	0.00326	0.00166	0.03806
94	GLCM Correlation (quick 8/11) (all dir.) Layer 4	0.00361	0.00178	0.00124	0.00114	0.00113	0.00290	0.00527	0.00530	0.01189	0.00489	0.00234	0.03293

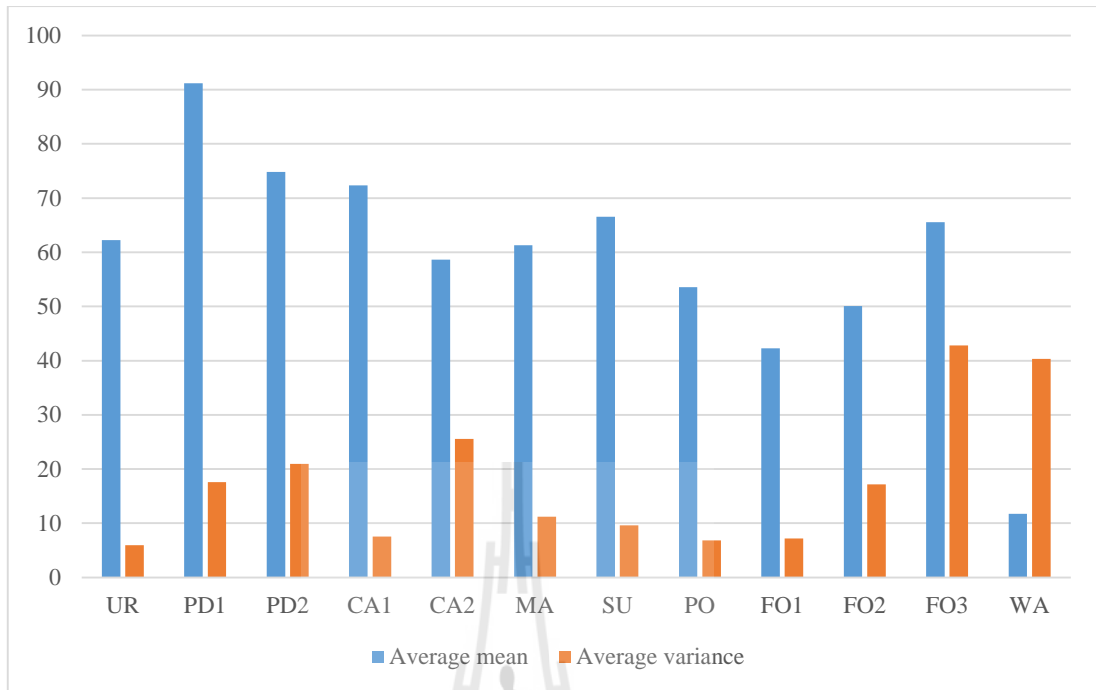


Figure 4.5 Average mean and standard deviation of brightness feature of LULC classes.

These statistical data of each feature of LULC class are then used to calculate separability using Jeffries-Matusita distance (Eq. 2.9) of all possibly pairwise between two LULC classes. In this study, the separability value of any pairwise LULC classes that provides separability value equal or greater than 1.3 are selected to calculate the threshold value (Eq. 2.13). The feature which has the calculated threshold value between mean values of two considered classes are here considered as candidate features for semantic modelling and classification. Table 4.9 shows an example of candidate features may be used to classify forest land type I (FO1) from others LULC classes. In general, the most dominate features with widely range threshold value are selected for semantic modelling and classification. In case of forest land type I (FO1), Brightness, Layer 3 and Layer 4 as top three dominant features, which were presented

in 10 of 11 pairwise are firstly selected for separating (classifying) forest land type I (FO1) from other classes. Then threshold values of 10 pairwise (forest land type I and others classes) are reconsidered to identify an optimum threshold value by comparison range between threshold value and mean of forest land type I. After that it may be required to add some more features to minimize fuzzy between forest land type I with others vegetation classes. (See final feature extraction for forest land type I (FO1) in Figure 4.6 and Table 4.10).

Table 4.9 Candidate features may be used to classify forest land type I (FO1) from others LULC classes.

LULC pairwise	J Distance	Member function	Average Mean	Threshold value
Forest type I and Urban and Built-up area				
Brightness	2.00	Descending	42.282	52.735
Layer 1	2.00	Descending	9.343	17.827
Layer 3	2.00	Descending	41.136	54.76
Layer 4	1.99	Descending	7.895	11.225
Max.diff.	1.99	Ascending	2.435	2.118
StdLayer 1	2.00	Descending	2.563	4.773
StdLayer 3	2.00	Descending	4.229	7.279
StdLayer 4	2.00	Descending	1.497	2.88
Pixel-based Layer 1	2.00	Descending	0.055	0.095
Pixel-based Layer 2	2.00	Ascending	0.655	0.586
Pixel-based Layer 3	1.92	Descending	0.243	0.264
Pixel-based Layer 4	1.98	Descending	0.047	0.058
GLCMHomogeneity (all dir.)	1.82	Ascending	0.31	0.192
GLCMHomogeneity (all dir.) Layer 1	1.98	Ascending	0.299	0.156
GLCMHomogeneity (all dir.) Layer 2	1.42	Ascending	0.291	0.254
GLCMHomogeneity (all dir.) Layer 3	1.92	Ascending	0.26	0.138
GLCMHomogeneity (all dir.) Layer 4	2.00	Ascending	0.46	0.278
GLCMContrast (all dir.)	1.77	Descending	11.235	22.962
GLCMContrast (all dir.) Layer 1	1.91	Descending	10.501	20.999
GLCMContrast (all dir.) Layer 3	1.89	Descending	16.391	35.202
GLCMContrast (all dir.) Layer 4	1.91	Descending	3.078	5.848
GLCMDissimilarity (all dir.)	1.90	Descending	2.558	3.965
GLCMDissimilarity (all dir.) Layer 1	1.99	Descending	2.561	4.194
GLCMDissimilarity (all dir.) Layer 3	1.99	Descending	3.148	5.242

Table 4.9 (Continued).

LULC pairwise	J Distance	Member function	Average Mean	Threshold value
GLCMDissimilarity (all dir.) Layer 4	1.99	Descending	1.394	2.217
GLCMEntropy (all dir.)	1.76	Descending	5.114	6.056
GLCMEntropy (all dir.) Layer 1	2.00	Descending	4.649	6.128
GLCMEntropy (all dir.) Layer 3	1.98	Descending	5.442	6.603
GLCMEntropy (all dir.) Layer 4	2.00	Descending	3.548	5.114
GLCMAng.2 nd moment (all dir.)	1.50	Ascending	0.01	0.003
GLCMAng.2 nd moment (all dir.) Layer 1	1.90	Ascending	0.014	0.002
GLCMAng.2 nd moment (all dir.) Layer 3	1.76	Ascending	0.007	0.001
GLCMAng.2 nd moment (all dir.) Layer 4	1.91	Ascending	0.043	0.005
GLCMMean (all dir.)	2.00	Descending	41.911	52.675
GLCMMean (all dir.) Layer 1	2.00	Descending	9.342	18.037
GLCMMean (all dir.) Layer 3	2.00	Descending	41.134	55.267
GLCMMean (all dir.) Layer 4	2.00	Descending	7.895	11.334
GLCMStdDev (all dir.)	1.93	Descending	3.644	5.687
GLCMStdDev (all dir.) Layer 1	2.00	Descending	2.612	4.73
GLCMStdDev (all dir.) Layer 3	2.00	Descending	4.315	7.439
GLCMStdDev (all dir.) Layer 4	2.00	Descending	1.536	2.917
GLCMCorrelation (all dir.) Layer 1	1.37	Descending	0.478	0.652
GLCMHomogeneity (quick8/11) (all dir.)	1.81	Ascending	0.31	0.192
GLCMHomogeneity (quick8/11) (all dir.) Layer 1	1.98	Ascending	0.299	0.156
GLCMHomogeneity (quick8/11) (all dir.) Layer 2	1.40	Ascending	0.289	0.252
GLCMHomogeneity (quick8/11) (all dir.) Layer 3	1.92	Ascending	0.259	0.138
GLCMHomogeneity (quick8/11) (all dir.) Layer 4	2.00	Ascending	0.459	0.279
GLCMContrast (quick8/11) (all dir.)	1.77	Descending	11.337	23.106
GLCMContrast (quick8/11) (all dir.) Layer 1	1.90	Descending	10.516	20.809
GLCMContrast (quick8/11) (all dir.) Layer 3	1.89	Descending	16.484	35.174
GLCMContrast (quick8/11) (all dir.) Layer 4	1.90	Descending	3.086	5.77
GLCMDissimilarity (quick8/11) (all dir.)	1.90	Descending	2.569	3.977
GLCMDissimilarity (quick8/11) (all dir.) Layer 1	1.99	Descending	2.563	4.17
GLCMDissimilarity (quick8/11) (all dir.) Layer 3	1.98	Descending	3.155	5.24
GLCMDissimilarity (quick8/11) (all dir.) Layer 4	1.99	Descending	1.396	2.198
GLCMEntropy (quick8/11) (all dir.)	1.76	Descending	5.118	6.064
GLCMEntropy (quick8/11) (all dir.) Layer 1	2.00	Descending	4.647	6.119
GLCMEntropy (quick8/11) (all dir.) Layer 3	1.98	Descending	5.444	6.609
GLCMEntropy (quick8/11) (all dir.) Layer 4	2.00	Descending	3.546	5.098
GLCMAng.2 nd moment (quick8/11) (all dir.)	1.50	Ascending	0.009	0.003

Table 4.9 (Continued).

LULC pairwise	J Distance	Member function	Average Mean	Threshold value
GLCMAng.2 nd moment (quick8/11) (all dir.) Layer 1	1.91	Ascending	0.014	0.002
GLCMAng.2 nd moment (quick8/11) (all dir.) Layer 3	1.76	Ascending	0.007	0.001
GLCMAng.2 nd moment (quick8/11) (all dir.) Layer 4	1.91	Ascending	0.043	0.005
GLCMMean (quick8/11) (all dir.)	2.00	Descending	41.91	52.796
GLCMMean (quick8/11) (all dir.) Layer 1	2.00	Descending	9.339	18.079
GLCMMean (quick8/11) (all dir.) Layer 3	2.00	Descending	41.133	55.421
GLCMMean (quick8/11) (all dir.) Layer 4	2.00	Descending	7.894	11.366
GLCMStdDev (quick8/11) (all dir.)	1.93	Descending	3.646	5.696
GLCMStdDev (quick8/11) (all dir.) Layer 1	2.00	Descending	2.608	4.701
GLCMStdDev (quick8/11) (all dir.) Layer 3	2.00	Descending	4.311	7.433
GLCMStdDev (quick8/11) (all dir.) Layer 4	2.00	Descending	1.533	2.896
GLCMCorrelation (quick8/11) (all dir.) Layer 1	1.35	Descending	0.474	0.645
Forest type I and Paddy Field type I				
Brightness	2.00	Descending	42.282	61.415
Layer 1	2.00	Descending	9.343	29.725
Layer 3	2.00	Descending	41.136	68.603
Layer 4	2.00	Descending	7.895	16.225
Max.diff.	2.00	Ascending	2.435	1.117
StdLayer 1	1.98	Descending	2.563	3.777
StdLayer 3	1.50	Descending	4.229	5.575
StdLayer 4	1.86	Descending	1.497	2.102
Pixel-based Layer 1	2.00	Descending	0.055	0.176
Pixel-based Layer 2	2.00	Ascending	0.655	0.432
Pixel-based Layer 3	2.00	Descending	0.243	0.289
Pixel-based Layer 4	2.00	Descending	0.047	0.077
GLCMContrast (all dir.) Layer 1	1.89	Descending	10.501	19.441
GLCMContrast (all dir.) Layer 3	1.56	Descending	16.391	28.246
GLCMContrast (all dir.) Layer 4	1.78	Descending	3.078	5.168
GLCMDissimilarity (all dir.) Layer 1	1.77	Descending	2.561	3.465
GLCMDissimilarity (all dir.) Layer 4	1.58	Descending	1.394	1.776
GLCMEntropy (all dir.) Layer 1	1.97	Descending	4.649	5.523
GLCMEntropy (all dir.) Layer 4	1.79	Descending	3.548	4.182
GLCMAng.2 nd moment (all dir.) Layer 1	1.67	Ascending	0.014	0.005
GLCMAng.2 nd moment (all dir.) Layer 4	1.43	Ascending	0.043	0.022
GLCMMean (all dir.)	2.00	Descending	41.911	60.905
GLCMMean (all dir.) Layer 1	2.00	Descending	9.342	29.668
GLCMMean (all dir.) Layer 3	2.00	Descending	41.134	68.255
GLCMMean (all dir.) Layer 4	2.00	Descending	7.895	16.143
GLCMStdDev (all dir.) Layer 1	1.99	Descending	2.612	3.893

Table 4.9 (Continued).

LULC pairwise	J Distance	Member function	Average Mean	Threshold value
GLCMStdDev (all dir.) Layer 3	1.66	Descending	4.315	5.861
GLCMStdDev (all dir.) Layer 4	1.92	Descending	1.536	2.196
GLCMCorrelation (all dir.) Layer 1	1.74	Descending	0.478	0.724
GLCMContrast (quick8/11) (all dir.) Layer 1	1.82	Descending	10.516	18.849
GLCMContrast (quick8/11) (all dir.) Layer 3	1.48	Descending	16.484	28.082
GLCMContrast (quick8/11) (all dir.) Layer 4	1.69	Descending	3.086	5.048
GLCMDissimilarity (quick8/11) (all dir.) Layer 1	1.77	Descending	2.563	3.466
GLCMDissimilarity (quick8/11) (all dir.) Layer 4	1.56	Descending	1.396	1.774
GLCMEntropy (quick8/11) (all dir.) Layer 1	1.98	Descending	4.647	5.523
GLCMEntropy (quick8/11) (all dir.) Layer 4	1.79	Descending	3.546	4.181
GLCMAng.2 nd moment (quick8/11) (all dir.) Layer 1	1.68	Ascending	0.014	0.005
GLCMAng.2 nd moment (quick8/11) (all dir.) Layer 4	1.43	Ascending	0.043	0.022
GLCMMean (quick8/11) (all dir.)	2.00	Descending	41.91	60.865
GLCMMean (quick8/11) (all dir.) Layer 1	2.00	Descending	9.339	29.624
GLCMMean (quick8/11) (all dir.) Layer 3	2.00	Descending	41.133	68.097
GLCMMean (quick8/11) (all dir.) Layer 4	2.00	Descending	7.894	16.106
GLCMStdDev (quick8/11) (all dir.) Layer 1	1.98	Descending	2.608	3.85
GLCMStdDev (quick8/11) (all dir.) Layer 3	1.67	Descending	4.311	5.872
GLCMStdDev (quick8/11) (all dir.) Layer 4	1.92	Descending	1.533	2.19
GLCMCorrelation (quick8/11) (all dir.) Layer 1	1.73	Descending	0.474	0.719
Forest type I and Paddy Field type II				
Brightness	2.00	Descending	42.282	54.401
Layer 1	2.00	Descending	9.343	19.795
Layer 2	1.56	Descending	110.757	122.571
Layer 3	2.00	Descending	41.136	56.108
Layer 4	2.00	Descending	7.895	13.087
Max.diff.	2.00	Ascending	2.435	1.947
StdLayer 1	1.79	Descending	2.563	3.497
StdLayer 4	1.69	Descending	1.497	2.03
Pixel-based Layer 1	2.00	Descending	0.055	0.113
Pixel-based Layer 2	2.00	Ascending	0.655	0.552
Pixel-based Layer 4	2.00	Descending	0.047	0.064
GLCMContrast (all dir.) Layer 1	1.38	Descending	10.501	16.609
GLCMEntropy (all dir.) Layer 1	1.91	Descending	4.649	5.402
GLCMEntropy (all dir.) Layer 4	1.64	Descending	3.548	4.113
GLCMAng.2 nd moment (all dir.) Layer 1	1.63	Ascending	0.014	0.005
GLCMAng.2 nd moment (all dir.) Layer 4	1.31	Ascending	0.043	0.023
GLCMMean (all dir.)	2.00	Descending	41.911	53.926
GLCMMean (all dir.) Layer 1	2.00	Descending	9.342	19.86

Table 4.9 (Continued).

LULC pairwise	J Distance	Member function	Average Mean	Threshold value
GLCMMean (all dir.) Layer 2	1.53	Descending	110.765	122.254
GLCMMean (all dir.) Layer 3	2.00	Descending	41.134	55.868
GLCMMean (all dir.) Layer 4	2.00	Descending	7.895	13.002
GLCMStdDev (all dir.) Layer 1	1.81	Descending	2.612	3.555
GLCMStdDev (all dir.) Layer 3	1.41	Descending	4.315	5.638
GLCMStdDev (all dir.) Layer 4	1.77	Descending	1.536	2.097
GLCMCorrelation (all dir.) Layer 1	1.85	Descending	0.478	0.765
GLCMCorrelation (all dir.) Layer 4	1.47	Descending	0.577	0.747
GLCMContrast (quick8/11) (all dir.) Layer 1	1.40	Descending	10.516	16.702
GLCMContrast (quick8/11) (all dir.) Layer 4	1.30	Descending	3.086	4.579
GLCMEntropy (quick8/11) (all dir.) Layer 1	1.92	Descending	4.647	5.401
GLCMEntropy (quick8/11) (all dir.) Layer 4	1.66	Descending	3.546	4.116
GLCMAng.2 nd moment (quick8/11) (all dir.) Layer 1	1.64	Ascending	0.014	0.005
GLCMAng.2 nd moment (quick8/11) (all dir.) Layer 4	1.33	Ascending	0.043	0.023
GLCMMean (quick8/11) (all dir.)	2.00	Descending	41.91	53.908
GLCMMean (quick8/11) (all dir.) Layer 1	2.00	Descending	9.339	19.881
GLCMMean (quick8/11) (all dir.) Layer 2	1.52	Descending	110.764	122.123
GLCMMean (quick8/11) (all dir.) Layer 3	2.00	Descending	41.133	55.902
GLCMMean (quick8/11) (all dir.) Layer 4	2.00	Descending	7.894	13.032
GLCMStdDev (quick8/11) (all dir.) Layer 1	1.81	Descending	2.608	3.544
GLCMStdDev (quick8/11) (all dir.) Layer 3	1.44	Descending	4.311	5.653
GLCMStdDev (quick8/11) (all dir.) Layer 4	1.78	Descending	1.533	2.098
GLCMCorrelation (quick8/11) (all dir.) Layer 1	1.86	Descending	0.474	0.764
GLCMCorrelation (quick8/11) (all dir.) Layer 4	1.45	Descending	0.573	0.741
Forest type I and Cassava type I				
Brightness	2.00	Descending	42.282	57.124
Layer 1	1.99	Descending	9.343	15.51
Layer 2	1.93	Descending	110.757	129.462
Layer 3	2.00	Descending	41.136	66.032
Layer 4	2.00	Descending	7.895	13.197
Max.diff.	1.79	Ascending	2.435	2.254
Pixel-based Layer 2	1.73	Ascending	0.655	0.619
Pixel-based Layer 3	1.73	Descending	0.243	0.26
Pixel-based Layer 4	1.93	Descending	0.047	0.055
GLCMMean (all dir.)	2.00	Descending	41.911	56.879
GLCMMean (all dir.) Layer 1	1.99	Descending	9.342	15.69
GLCMMean (all dir.) Layer 2	1.93	Descending	110.765	129.377
GLCMMean (all dir.) Layer 3	2.00	Descending	41.134	66.099
GLCMMean (all dir.) Layer 4	2.00	Descending	7.895	13.291
GLCMCorrelation (all dir.)	1.32	Descending	0.771	0.805

Table 4.9 (Continued).

LULC pairwise	J Distance	Member function	Average Mean	Threshold value
GLCMMean (quick8/11) (all dir.)	2.00	Descending	41.91	56.881
GLCMMean (quick8/11) (all dir.) Layer 1	1.99	Descending	9.339	15.732
GLCMMean (quick8/11) (all dir.) Layer 2	1.93	Descending	110.764	129.293
GLCMMean (quick8/11) (all dir.) Layer 3	2.00	Descending	41.133	66.082
GLCMMean (quick8/11) (all dir.) Layer 4	2.00	Descending	7.894	13.31
GLCMStdDev (quick8/11) (all dir.) Layer 1	1.34	Descending	2.608	3.199
Forest type I and Cassava type II				
Brightness	1.77	Descending	42.282	48.192
Layer 1	1.99	Descending	9.343	16.462
Layer 3	1.97	Descending	41.136	51.259
Layer 4	2.00	Descending	7.895	13.967
Max.diff.	2.00	Ascending	2.435	2.117
StdLayer 1	1.92	Descending	2.563	3.576
StdLayer 4	1.31	Descending	1.497	1.878
Pixel-based Layer 1	1.85	Descending	0.055	0.081
Pixel-based Layer 2	1.99	Ascending	0.655	0.589
Pixel-based Layer 3	2.00	Descending	0.243	0.282
Pixel-based Layer 4	2.00	Descending	0.047	0.061
GLCMContrast (all dir.) Layer 1	1.51	Descending	10.501	17.094
GLCMDissimilarity (all dir.) Layer 1	1.31	Descending	2.561	3.228
GLCMEntropy (all dir.) Layer 1	1.87	Descending	4.649	5.337
GLCMAng.2 nd moment (all dir.) Layer 1	1.52	Ascending	0.014	0.006
GLCMMean (all dir.)	1.79	Descending	41.911	47.926
GLCMMean (all dir.) Layer 1	1.99	Descending	9.342	16.592
GLCMMean (all dir.) Layer 3	1.97	Descending	41.134	51.431
GLCMMean (all dir.) Layer 4	2.00	Descending	7.895	14.101
GLCMStdDev (all dir.) Layer 1	1.95	Descending	2.612	3.701
GLCMStdDev (all dir.) Layer 4	1.41	Descending	1.536	1.939
GLCMCorrelation (all dir.) Layer 1	1.42	Descending	0.478	0.659
GLCMCorrelation (all dir.) Layer 4	1.31	Descending	0.577	0.719
GLCMContrast (quick8/11) (all dir.) Layer 1	1.49	Descending	10.516	17.013
GLCMDissimilarity (quick8/11) (all dir.) Layer 1	1.32	Descending	2.563	3.236
GLCMEntropy (quick8/11) (all dir.) Layer 1	1.87	Descending	4.647	5.332
GLCMAng.2 nd moment (quick8/11) (all dir.) Layer 1	1.53	Ascending	0.014	0.006
GLCMMean (quick8/11) (all dir.)	1.80	Descending	41.91	47.954
GLCMMean (quick8/11) (all dir.) Layer 1	1.99	Descending	9.339	16.592
GLCMMean (quick8/11) (all dir.) Layer 3	1.97	Descending	41.133	51.477
GLCMMean (quick8/11) (all dir.) Layer 4	2.00	Descending	7.894	14.092
GLCMStdDev (quick8/11) (all dir.) Layer 1	1.94	Descending	2.608	3.663
GLCMStdDev (quick8/11) (all dir.) Layer 4	1.39	Descending	1.533	1.933

Table 4.9 (Continued).

LULC pairwise	J Distance	Member function	Average Mean	Threshold value
GLCMCorrelation (quick8/11) (all dir.) Layer 1	1.41	Descending	0.474	0.653
Forest type I and Maize				
Brightness	1.99	Descending	42.282	50.784
Layer 1	2.00	Descending	9.343	22.111
Layer 2	1.87	Ascending	110.757	94.914
Layer 3	2.00	Descending	41.136	57.455
Layer 4	2.00	Descending	7.895	13.473
Max.diff.	2.00	Ascending	2.435	1.309
StdLayer 4	1.45	Descending	1.497	1.947
Pixel-based Layer 1	2.00	Descending	0.055	0.13
Pixel-based Layer 2	2.00	Ascending	0.655	0.507
Pixel-based Layer 3	2.00	Descending	0.243	0.296
Pixel-based Layer 4	2.00	Descending	0.047	0.076
GLCMEntropy (all dir.) Layer 4	1.30	Descending	3.548	4.001
GLCMMean (all dir.)	1.99	Descending	41.911	50.459
GLCMMean (all dir.) Layer 1	2.00	Descending	9.342	22.037
GLCMMean (all dir.) Layer 2	1.85	Ascending	110.765	95.469
GLCMMean (all dir.) Layer 3	2.00	Descending	41.134	57.397
GLCMMean (all dir.) Layer 4	2.00	Descending	7.895	13.476
GLCMStdDev (all dir.) Layer 4	1.49	Descending	1.536	1.995
GLCMCorrelation (all dir.) Layer 1	1.33	Descending	0.478	0.648
GLCMCorrelation (all dir.) Layer 4	1.34	Descending	0.577	0.731
GLCMMean (quick8/11) (all dir.)	1.99	Descending	41.91	50.487
GLCMMean (quick8/11) (all dir.) Layer 1	2.00	Descending	9.339	22.05
GLCMMean (quick8/11) (all dir.) Layer 2	1.85	Ascending	110.764	95.605
GLCMMean (quick8/11) (all dir.) Layer 3	2.00	Descending	41.133	57.376
GLCMMean (quick8/11) (all dir.) Layer 4	2.00	Descending	7.894	13.472
GLCMStdDev (quick8/11) (all dir.) Layer 4	1.48	Descending	1.533	1.988
GLCMCorrelation (quick8/11) (all dir.) Layer 1	1.32	Descending	0.474	0.642
GLCMCorrelation (quick8/11) (all dir.) Layer 4	1.32	Descending	0.573	0.725
Forest type I and Sugarcane				
Brightness	2.00	Descending	42.282	53.566
Layer 1	1.99	Descending	9.343	16.387
Layer 2	2.00	Descending	110.757	135.933
Layer 3	1.79	Descending	41.136	48.223
Layer 4	1.63	Descending	7.895	9.567
Pixel-basedLayer 1	1.97	Descending	0.055	0.083
Pixel-basedLayer 3	1.41	Ascending	0.243	0.23
GLCM Mean (all dir.)	2.00	Descending	41.911	52.931
GLCM Mean (all dir.) Layer 1	2.00	Descending	9.342	16.45
GLCM Mean (all dir.) Layer 2	2.00	Descending	110.765	135.278
GLCM Mean (all dir.) Layer 3	1.78	Descending	41.134	48.237

Table 4.9 (Continued).

LULC pairwise	J Distance	Member function	Average Mean	Threshold value
GLCM Mean (all dir.) Layer 4	1.63	Descending	7.895	9.59
GLCM Correlation (all dir.) Layer 1	1.55	Descending	0.478	0.68
GLCM Mean (quick8/11) (all dir.)	2.00	Descending	41.91	52.869
GLCM Mean (quick8/11) (all dir.) Layer 1	2.00	Descending	9.339	16.449
GLCM Mean (quick8/11) (all dir.) Layer 2	2.00	Descending	110.764	135.103
GLCM Mean (quick8/11) (all dir.) Layer 3	1.77	Descending	41.133	48.199
GLCM Mean (quick8/11) (all dir.) Layer 4	1.62	Descending	7.894	9.584
GLCM Correlation (quick8/11) (all dir.) Layer 1	1.57	Descending	0.474	0.68
Forest type I and Perennial trees and Or char d				
Brightness	1.79	Descending	42.282	47.987
Layer 1	1.95	Descending	9.343	14.815
Layer 3	1.89	Descending	41.136	49.09
Layer 4	1.89	Descending	7.895	9.979
Max.diff.	1.90	Ascending	2.435	2.231
Pixel-basedLayer 1	1.97	Descending	0.055	0.083
Pixel-basedLayer 2	1.93	Ascending	0.655	0.609
Pixel-basedLayer 4	1.49	Descending	0.047	0.052
GLCMEntropy (all dir.) Layer 2	1.56	Ascending	6.796	6.118
GLCMAng.2ndmoment (all dir.) Layer 2	1.45	Descending	0.002	0.004
GLCMMean (all dir.)	1.81	Descending	41.911	47.73
GLCMMean (all dir.) Layer 1	1.96	Descending	9.342	14.977
GLCMMean (all dir.) Layer 3	1.92	Descending	41.134	49.434
GLCMMean (all dir.) Layer 4	1.92	Descending	7.895	10.097
GLCMCorrelation (all dir.)	1.33	Ascending	0.771	0.733
GLCMEntropy (quick8/11) (all dir.) Layer 2	1.54	Ascending	6.805	6.135
GLCMAng.2ndmoment (quick8/11) (all dir.) Layer 2	1.42	Descending	0.002	0.004
GLCMMean (quick8/11) (all dir.)	1.82	Descending	41.91	47.737
GLCMMean (quick8/11) (all dir.) Layer 1	1.96	Descending	9.339	15.005
GLCMMean (quick8/11) (all dir.) Layer 3	1.92	Descending	41.133	49.424
GLCMMean (quick8/11) (all dir.) Layer 4	1.92	Descending	7.894	10.101
GLCMStdDev (quick8/11) (all dir.) Layer 1	1.43	Descending	2.608	3.254
GLCMCorrelation (quick8/11) (all dir.)	1.34	Ascending	0.769	0.73
Forest type I and Forest type II				
Layer 2	1.11	Descending	110.757	120.018
GLCMContrast (all dir.) Layer 1	1.01	Ascending	10.501	7.318
GLCMContrast (all dir.) Layer 4	1.03	Ascending	3.078	2.207
GLCMMean (all dir.) Layer 2	1.11	Descending	110.765	119.956
GLCMContrast (quick8/11) (all dir.) Layer 1	1.01	Ascending	10.516	7.342
GLCMContrast (quick8/11) (all dir.) Layer 4	1.03	Ascending	3.086	2.217
GLCMMean (quick8/11) (all dir.) Layer 2	1.11	Descending	110.764	119.932
Forest type I and Forest type III				
Brightness	1.89	Descending	42.282	49.349
Layer 2	1.85	Descending	110.757	127.749
Layer 3	1.93	Descending	41.136	50.228
Layer 4	1.93	Descending	7.895	10.216
StdLayer 1	1.46	Descending	2.563	3.174
StdLayer 3	1.61	Descending	4.229	5.631

Table 4.9 (Continued).

LULC pairwise	J Distance	Member function	Average Mean	Threshold value
StdLayer 4	1.57	Descending	1.497	1.932
Pixel-basedLayer 4	1.45	Descending	0.047	0.052
GLCMEntropy (all dir.) Layer 1	1.34	Descending	4.649	5.081
GLCMEntropy (all dir.) Layer 3	1.38	Descending	5.442	6.005
GLCMEntropy (all dir.) Layer 4	1.44	Descending	3.548	4.017
GLCMMean (all dir.)	1.90	Descending	41.911	49.007
GLCMMean (all dir.) Layer 2	1.86	Descending	110.765	127.827
GLCMMean (all dir.) Layer 3	1.93	Descending	41.134	50.297
GLCMMean (all dir.) Layer 4	1.93	Descending	7.895	10.229
GLCMStdDev (all dir.) Layer 1	1.50	Descending	2.612	3.23
GLCMStdDev (all dir.) Layer 3	1.68	Descending	4.315	5.811
GLCMStdDev (all dir.) Layer 4	1.61	Descending	1.536	1.974
GLCMEntropy (quick8/11) (all dir.) Layer 1	1.35	Descending	4.647	5.077
GLCMEntropy (quick8/11) (all dir.) Layer 3	1.39	Descending	5.444	6.009
GLCMEntropy (quick8/11) (all dir.) Layer 4	1.44	Descending	3.546	4.012
GLCMMean (quick8/11) (all dir.)	1.90	Descending	41.91	49.019
GLCMMean (quick8/11) (all dir.) Layer 2	1.87	Descending	110.764	127.888
GLCMMean (quick8/11) (all dir.) Layer 3	1.93	Descending	41.133	50.302
GLCMMean (quick8/11) (all dir.) Layer 4	1.93	Descending	7.894	10.22
GLCMStdDev (quick8/11) (all dir.)	1.31	Descending	3.646	4.79
GLCMStdDev (quick8/11) (all dir.) Layer 1	1.50	Descending	2.608	3.221
GLCMStdDev (quick8/11) (all dir.) Layer 3	1.70	Descending	4.311	5.823
GLCMStdDev (quick8/11) (all dir.) Layer 4	1.61	Descending	1.533	1.969
Forest type I and Water Body				
Brightness	1.99	Ascending	42.282	32.992
Layer 1	1.43	Descending	9.343	12.749
Layer 2	2.00	Ascending	110.757	46.922
Layer 3	2.00	Ascending	41.136	15.128
Layer 4	2.00	Ascending	7.895	2.979
StdLayer 1	1.41	Ascending	2.563	1.986
StdLayer 2	1.69	Ascending	9.73	5.952
StdLayer 3	1.84	Ascending	4.229	2.492
StdLayer 4	1.87	Ascending	1.497	0.925
Pixel-basedLayer 1	2.00	Descending	0.055	0.11
Pixel-basedLayer 2	2.00	Ascending	0.655	0.559
Pixel-basedLayer 3	1.98	Ascending	0.243	0.213
Pixel-basedLayer 4	1.93	Ascending	0.047	0.037
GLCMHomogeneity (all dir.)	1.98	Descending	0.31	0.468
GLCMHomogeneity (all dir.) Layer 1	1.96	Descending	0.299	0.422
GLCMHomogeneity (all dir.) Layer 2	2.00	Descending	0.291	0.391
GLCMHomogeneity (all dir.) Layer 3	1.96	Descending	0.26	0.39
GLCMHomogeneity (all dir.) Layer 4	1.84	Descending	0.46	0.574

Table 4.9 (Continued).

LULC pairwise	J Distance	Member function	Average Mean	Threshold value
GLCMDissimilarity (all dir.)	1.53	Ascending	2.558	1.634
GLCMDissimilarity (all dir.) Layer 1	1.61	Ascending	2.561	1.785
GLCMDissimilarity (all dir.) Layer 2	1.62	Ascending	5.935	3.339
GLCMDissimilarity (all dir.) Layer 3	1.52	Ascending	3.148	2.104
GLCMDissimilarity (all dir.) Layer 4	1.72	Ascending	1.394	0.97
GLCMEntropy (all dir.)	1.94	Ascending	5.114	3.896
GLCMEntropy (all dir.) Layer 1	1.79	Ascending	4.649	3.994
GLCMEntropy (all dir.) Layer 2	2.00	Ascending	6.796	5.348
GLCMEntropy (all dir.) Layer 3	1.96	Ascending	5.442	4.359
GLCMEntropy (all dir.) Layer 4	1.87	Ascending	3.548	2.8
GLCMAng.2ndmoment (all dir.)	1.68	Descending	0.01	0.02
GLCMAng.2ndmoment (all dir.) Layer 1	1.65	Descending	0.014	0.025
GLCMAng.2ndmoment (all dir.) Layer 2	1.87	Descending	0.002	0.004
GLCMAng.2ndmoment (all dir.) Layer 3	1.74	Descending	0.007	0.013
GLCMAng.2ndmoment (all dir.) Layer 4	1.62	Descending	0.043	0.073
GLCMMean (all dir.)	1.99	Ascending	41.911	32.687
GLCMMean (all dir.) Layer 1	1.43	Descending	9.342	12.756
GLCMMean (all dir.) Layer 2	2.00	Ascending	110.765	49.515
GLCMMean (all dir.) Layer 3	2.00	Ascending	41.134	16.366
GLCMMean (all dir.) Layer 4	2.00	Ascending	7.895	3.255
GLCMStdDev (all dir.) Layer 4	1.44	Ascending	1.536	1.138
GLCMCorrelation (all dir.)	1.44	Ascending	0.771	0.729
GLCMHomogeneity (quick8/11) (all dir.)	1.98	Descending	0.31	0.467
GLCMHomogeneity (quick8/11) (all dir.) Layer 1	1.96	Descending	0.299	0.422
GLCMHomogeneity (quick8/11) (all dir.) Layer 2	2.00	Descending	0.289	0.391
GLCMHomogeneity (quick8/11) (all dir.) Layer 3	1.96	Descending	0.259	0.39
GLCMHomogeneity (quick8/11) (all dir.) Layer 4	1.84	Descending	0.459	0.573
GLCMDissimilarity (quick8/11) (all dir.)	1.53	Ascending	2.569	1.638
GLCMDissimilarity (quick8/11) (all dir.) Layer 1	1.62	Ascending	2.563	1.79
GLCMDissimilarity (quick8/11) (all dir.) Layer 2	1.62	Ascending	5.985	3.363
GLCMDissimilarity (quick8/11) (all dir.) Layer 3	1.53	Ascending	3.155	2.108
GLCMDissimilarity (quick8/11) (all dir.) Layer 4	1.72	Ascending	1.396	0.973
GLCMEntropy (quick8/11) (all dir.)	1.94	Ascending	5.118	3.898
GLCMEntropy (quick8/11) (all dir.) Layer 1	1.79	Ascending	4.647	3.997
GLCMEntropy (quick8/11) (all dir.) Layer 2	2.00	Ascending	6.805	5.348
GLCMEntropy (quick8/11) (all dir.) Layer 3	1.96	Ascending	5.444	4.36
GLCMEntropy (quick8/11) (all dir.) Layer 4	1.87	Ascending	3.546	2.802

Table 4.9 (Continued).

LULC pairwise	J Distance	Member function	Average Mean	Threshold value
GLCMAng.2ndmoment (quick8/11) (all dir.)	1.68	Descending	0.009	0.02
GLCMAng.2ndmoment (quick8/11) (all dir.) Layer 1	1.65	Descending	0.014	0.025
GLCMAng.2ndmoment (quick8/11) (all dir.) Layer 2	1.87	Descending	0.002	0.004
GLCMAng.2ndmoment (quick8/11) (all dir.) Layer 3	1.74	Descending	0.007	0.013
GLCMAng.2ndmoment (quick8/11) (all dir.) Layer 4	1.62	Descending	0.043	0.073
GLCMMean (quick8/11) (all dir.)	1.99	Ascending	41.91	32.694
GLCMMean (quick8/11) (all dir.) Layer 1	1.43	Descending	9.339	12.753
GLCMMean (quick8/11) (all dir.) Layer 2	2.00	Ascending	110.764	49.633
GLCMMean (quick8/11) (all dir.) Layer 3	2.00	Ascending	41.133	16.368
GLCMMean (quick8/11) (all dir.) Layer 4	2.00	Ascending	7.894	3.253
GLCMStdDev (quick8/11) (all dir.) Layer 4	1.43	Ascending	1.533	1.138
GLCMCorrelation (quick8/11) (all dir.)	1.43	Ascending	0.769	0.727

4.2.3 Semantic modelling

Semantic modelling, which is constructed as a rule-based semantic network was here created for representing spatial semantics associated with image databases by selecting the most dominant features with wider range. The developed semantic model for LULC extraction in reference area with pan-sharpened Landsat 8 data of 2013 for Layer 1 (Band 4), Layer 2 (Band 5), Layer 3 (Band 6) and Layer 4 (Band 3) is presented in Figure 4.6 and Table 4.10. The rule-based semantic model was directly migrated to eCognition software for LULC classification.

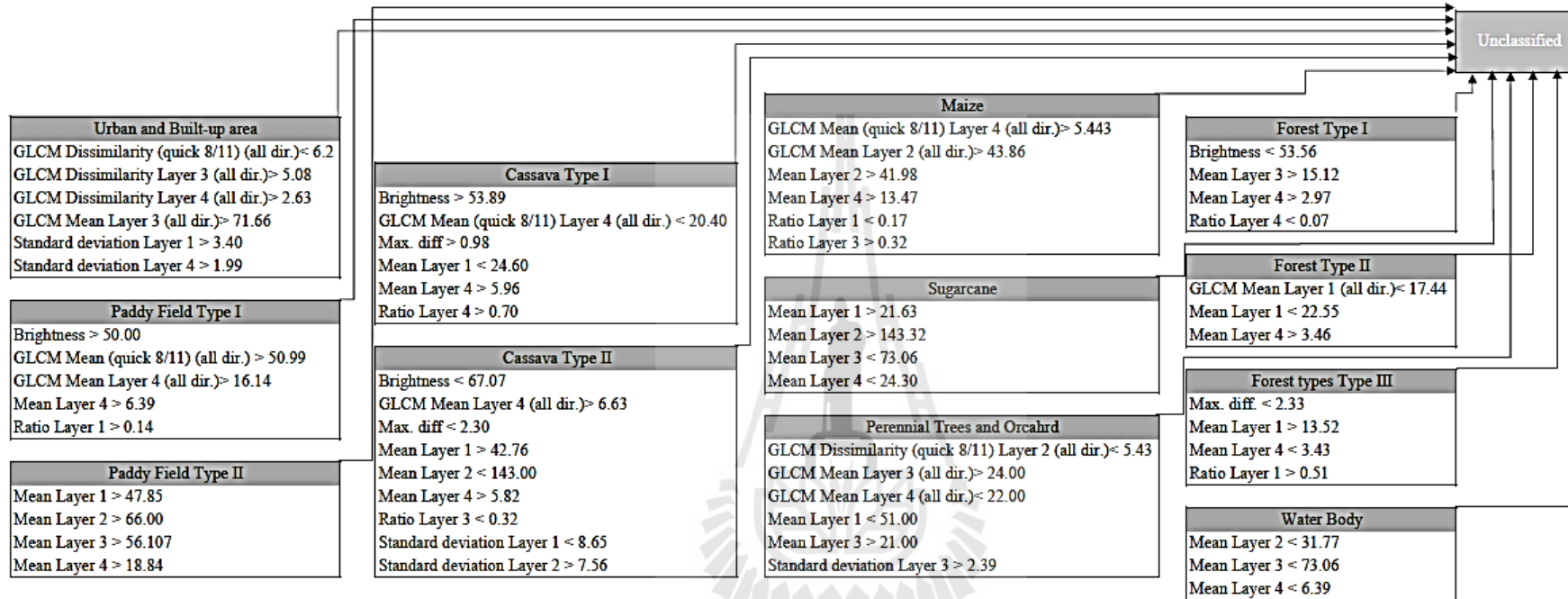


Figure 4.6 Graphical semantic model for LULC extraction in reference area with Landsat 8 data of 2013.

Table 4.10 Semantic model for LULC extraction in reference area with Landsat 8 data of 2013 in table form.

LULC classes	Membership function and threshold value		
	Membership function	Left border	Right border
Urban and built-up area			
GLCM Dissimilarity (quick 8/11) (all dir.)	Descending	2.5	6.2
GLCM Dissimilarity Layer 3 (all dir.)	Ascending	5.08	9.42
GLCM Dissimilarity Layer 4 (all dir.)	Ascending	2.63	4.85
GLCM Mean Layer 3 (all dir.)	Ascending	71.662	77.25
Standard deviation Layer 1	Ascending	3.4	13.36
Standard deviation Layer 4	Ascending	1.99	6.914
Paddy field Type I			
Brightness	Ascending	50	91.16
GLCM Mean (quick 8/11) (all dir.)	Ascending	50.996	90.467
GLCM Mean Layer 4 (all dir.)	Ascending	16.143	41.436
Mean Layer 4	Ascending	6.396	41.655
Ratio Layer 1	Ascending	0.14	0.242
Paddy field Type II			
Mean Layer 1	Ascending	47.85	65
Mean Layer 2	Ascending	66	134.05
Mean Layer 3	Ascending	56.107	76.27
Mean Layer 4	Ascending	18.841	23.29
Cassava Type I			
Brightness	Ascending	53.897	72.32
GLCM Mean (quick 8/11) Layer 4 (all dir.)	Descending	6.67	20.408
Max. diff	Ascending	0.985	3.29
Mean Layer 1	Descending	24.6	46.43
Mean Layer 4	Ascending	5.963	20.288
Ratio Layer 4	Ascending	0.07	0.097
Cassava Type II			
Brightness	Descending	58.663	67.079
GLCM Mean Layer 4 (all dir.)	Ascending	6.63	25.16
Max. diff	Descending	1.665	2.306
Mean Layer 1	Ascending	16.462	42.769
Mean Layer 2	Descending	94	143
Mean Layer 4	Ascending	5.823	25.251
Ratio Layer 3	Descending	0.307	0.325
Standard deviation Layer 1	Descending	5.82	8.655
Standard deviation Layer 2	Ascending	7.56	12.738
Maize			
GLCM Mean (quick 8/11) Layer 4 (all dir.)	Ascending	5.443	29.254
GLCM Mean Layer 2 (all dir.)	Ascending	43.868	83.715

Table 4.10 (Continued).

LULC classes	Membership function and threshold value		
	Membership function	Left border	Right border
Mean Layer 2	Ascending	41.985	83.018
Mean Layer 4	Ascending	13.473	29.372
Ratio Layer 1	Descending	0.178	0.212
Ratio Layer 3	Ascending	0.326	0.363
Sugarcane			
Mean Layer 1	Ascending	21.634	32.86
Mean Layer 2	Ascending	143.32	163.6
Mean Layer 3	Descending	57.058	73.06
Mean Layer 4	Descending	12.702	24.3
Perennial trees and orchard			
GLCM Dissimilarity (quick 8/11) Layer 2 (all dir.)	Descending	3.5	5.439
GLCM Mean Layer 3 (all dir.)	Ascending	24	56
GLCM Mean Layer 4 (all dir.)	Descending	13	22
Mean Layer 1	Descending	25	51
Mean Layer 3	Ascending	21	55
Standard deviation Layer 3	Ascending	2.39	4.17
Forest land type I			
Brightness	Descending	42.282	53.566
Mean Layer 3	Ascending	15.128	41.136
Mean Layer 4	Ascending	2.97	7.895
Ratio Layer 4	Descending	0.047	0.0758
Forest land type II			
GLCM Mean Layer 1 (all dir.)	Descending	11.441	17.44
Mean Layer 1	Descending	11.436	22.553
Mean Layer 4	Ascending	3.468	8.843
Forest land types III			
Max. diff.	Descending	2.21	2.33
Mean Layer 1	Ascending	13.529	22.73
Mean Layer 4	Descending	3.431	14.511
Ratio Layer 1	Ascending	0.051	0.1747
Water Body			
Mean Layer 2	Descending	7.09	31.77
Mean Layer 3	Descending	2.59	37.9
Mean Layer 4	Descending	0.404	6.39

As results, it can be observed that the required number of features among LULC classes varies between 3 and 9. Herewith, cassava type II (CA2) requires the

highest number of features while forest land type 2 (FO2) and water body (WA) requires the lowest number of features.

4.2.4 Semantic classification of LULC in 2013 in reference area

The semantic classification, which determines whether or not an object belongs to a certain object class on the basis of its significance, was here performed under eCognition software. The original LULC classification without LULC reclassification is shown in Figure 4.7 while the final LULC classification with LULC reclassification for 8 LULC classes: urban and built-up area, paddy field, cassava, maize, sugarcane, perennial trees and orchard, forest land, and water body is shown in Figure 4.8. Additionally field photographs of 8 LULC type is displayed in Figure 4.9. Meanwhile area and percentage of final LULC classification in 2013 in reference area is summarized in Table 4.11.

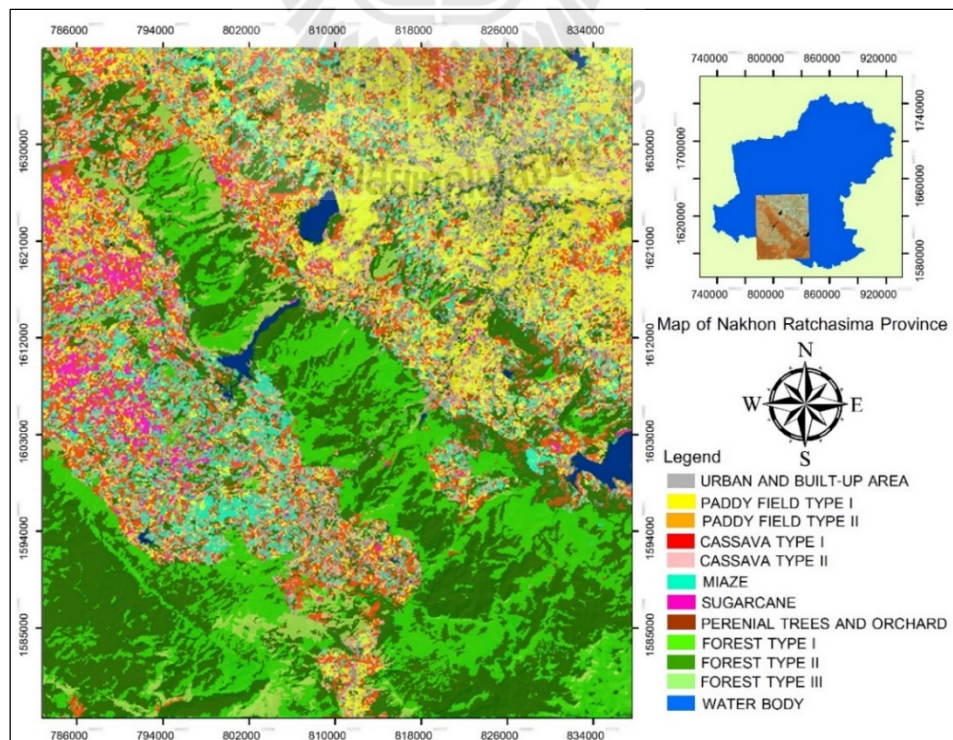


Figure 4.7 Distribution of original LULC classification for year 2013 in reference area.

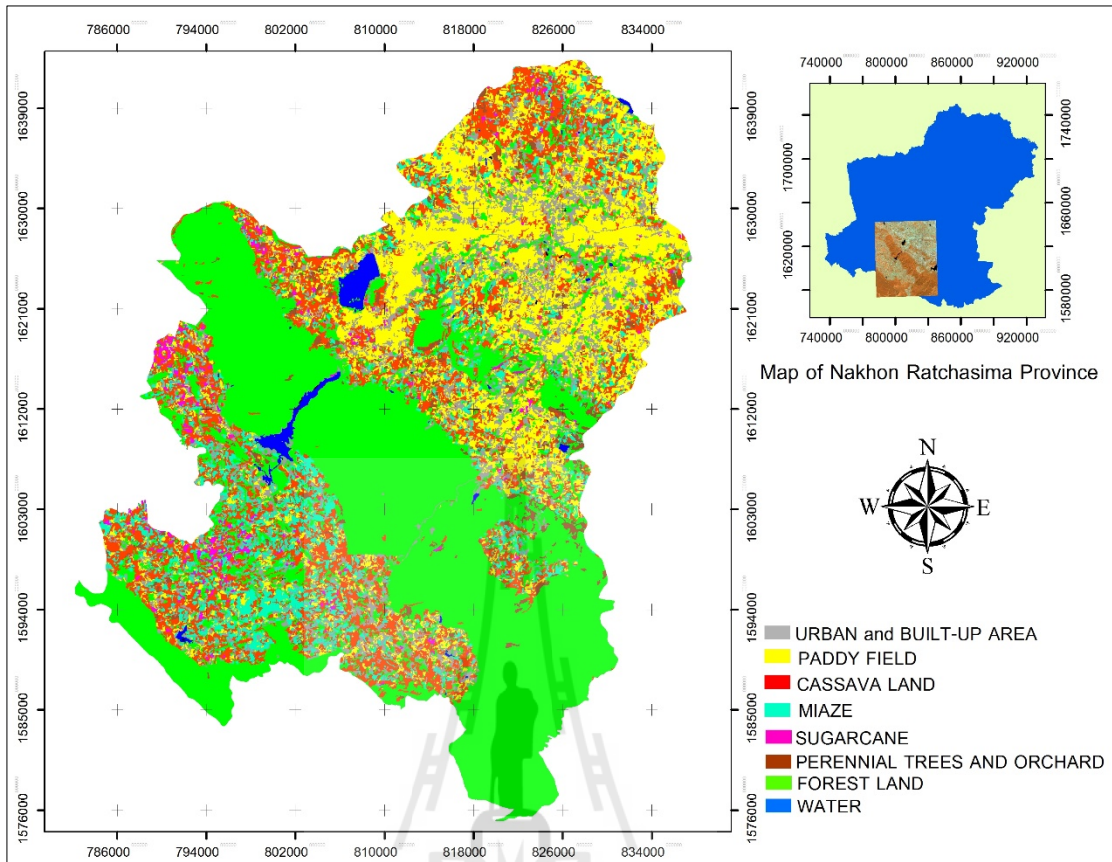


Figure 4.8 Distribution of final LULC classification for year 2013 in reference area.

มหาวิทยาลัยเทคโนโลยีสุรนารี



Urban and built-up area



Paddy field



Cassava



Maize



Sugarcane



Perennial tree and orchard



Forest land



Water body

Figure 4.9 Ground photograph of 8 LULC type.

Table 4.11 Area and percentage of LULC classification for year 2013 in reference area.

No.	LULC class	Area in sq.km	Percent
1	Urban and built-up area (UR)	223.27	10.77
2	Paddy field (PD)	329.46	15.89
3	Cassava (CA)	309.77	14.94
4	Maize (MA)	324.18	15.64
5	Sugarcane (SU)	112.47	5.42
6	Perennial trees and orchard (PO)	22.84	1.10
7	Forest land (FO)	733.56	35.39
8	Water body (WA)	16.37	0.78
9	Unclassified (UC)	0.57	0.03
Total		2,072.49	100.00

As results, the dominant LULC class was forest land, which covered area of 733.56 sq. km or 35.39%. Meanwhile the dominant agricultural classes were paddy field, maize, and cassava which covered area of 329.46, 324.18, and 309.77 sq. km or 15.89%, 15.64% and 14.94%, respectively.

Additionally, the final LULC classes in 2013 of reference area is reclassified into 5 major land use classes of LDD, namely urban and built-up area, agricultural land, forest land, water body and miscellaneous land for comparison with the existing land use data in 2011 of LDD as result shown in Table 4.12 and Figure 4.10. As results, it was found that areas of both land use class are somewhat different due to different methods for extraction land use and LULC data but land use and LULC pattern of both data are similar.

Consequently, there are some observations to address about area and its change. Herein, area of urban and built-up area by OBIA is higher than visual interpreted land use data of LDD because urban and built-up area by OBIA includes

farmhouse, landfill, active or abandoned soil/sand pits that are assigned as miscellaneous land by LDD. Likewise, area of agricultural land by OBIA is higher than land use data of LDD because rangeland and scrub as miscellaneous land by LDD is included in agricultural land by OBIA. In contrast, area of the classified forest land by OBIA is lower than land use data of LDD because forest land of LDD includes disturbed forest that is not classified by OBIA. Similarly, area of water body by OBIA is lower than land use data of LDD because it does not include farm ponds of LDD.

Table 4.12 Comparison of LDD's land use data in 2011 and LULC data in 2013 by OBIA in reference area.

Land use class	Area in sq. km		
	Land use data in 2011 by LDD	LULC data in 2013 by OBIA	Difference
Urban and built-up area	115.32	223.27	107.95
Agricultural land	982.44	1108.71	126.27
Forest land	841.06	733.56	-107.50
Water body	43.18	16.37	-36.81
Miscellaneous land	90.49	0.57	-89.92
Total	2,072.49	2,072.49	0.00

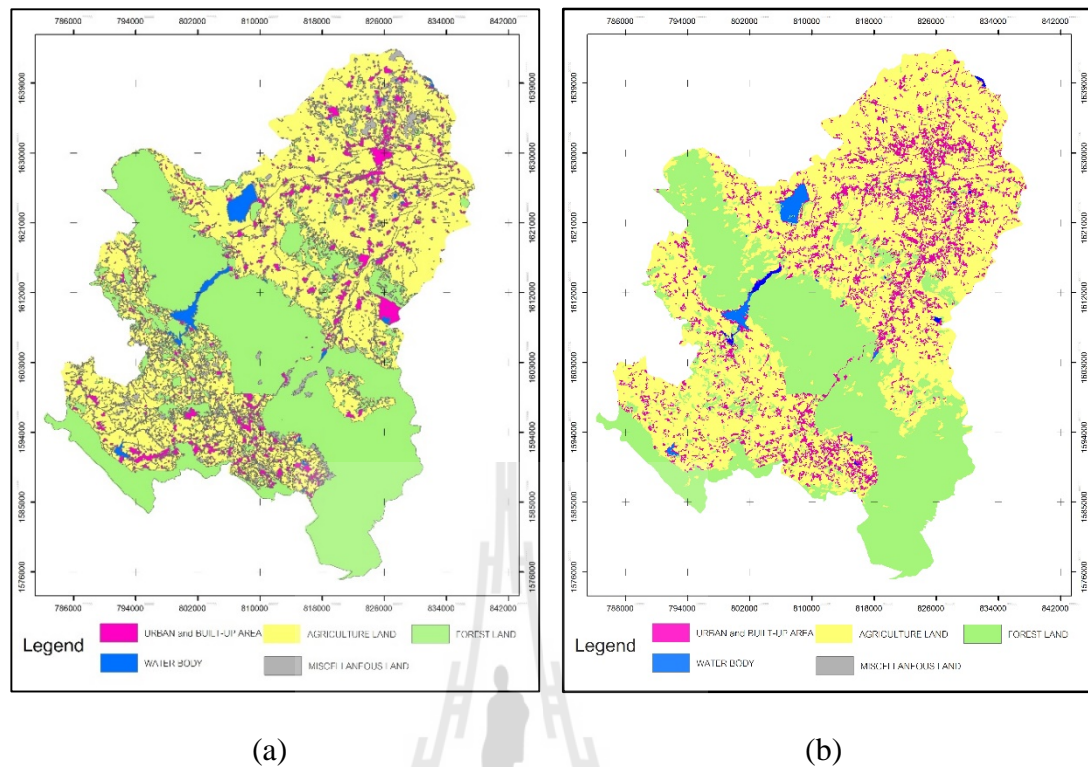


Figure 4.10 Land use and LULC pattern comparison: (a) land use data in 2011 by LDD
(b) LULC data in 2013 by OBIA.

4.2.5 Accuracy assessment of thematic LULC map of 2013 in reference area

Thematic LULC data of 2013 in reference area which are derived from semantic classification was assessed accuracy based on the existing high spatial resolution images in 2013 and 2014 from Google Earth of Google Inc. and ground survey in 2015. Number of sample points, which was calculated based on the binomial probability distribution theory with the expected accuracy of 85% at the allowable error of 5%, was 203 points. The distribution of sample point with stratified random sampling is presented in Figure 4.11. Detail of sampling point for accuracy assessment in reference area is presented in Table 1 of Appendix A. Herewith, overall accuracy and Kappa hat coefficient of thematic LULC map in 2013 in reference area are around

84.24% and 80.37%, respectively. In the meantime, producer's accuracy (PA), which infers about omission error, varied between the lowest value of 57.89% for sugarcane and the highest value of 100% for water body. Meanwhile, user's accuracy (UA), which infers about commission error, varied between the lowest value of 64.29% for cassava and the highest value of 100% for water body. Detail of accuracy assessment as error matrix with PA and UA is presented in Table 4.13.

As results, it was found that both accuracy values are higher than the defined accuracy for acceptance semantic modelling and classification, overall accuracy and Kappa hat coefficient are equal or higher than 80%. According to Fitzpatrick-Lins (1981), Kappa hat coefficient more than 80% represents strong agreement or accuracy between the classification map and the ground reference information.

In addition, the derived accuracy obtained in this study with overall accuracy at 84.24% and Kappa hat coefficient at 80.37% proved to be acceptable when it was compared with other studies that applied rule-based classifier under OBIA as summary below.

Campbell and Congalton (2012), who applied OBIA for LULC classification with Landsat-5 image, obtained an overall accuracy at 80%.

Myint et al. (2011), who applied OBIA for urban land cover extraction with QuikBird data, achieved an overall accuracy at 90%.

Khamphilung et al. (2013), who applied OBIA for village forms classification with QuikBird pan-sharpened image, obtained an overall accuracy and Kappa hat coefficient at 70% and 64%, respectively.

Wu et al. (2013), who applied OBIA for building seismic vulnerability assessment with WorldView-2 imagery, achieved an overall accuracy at 80%

Zhou et al. (2013), who applied OBIA for land cover classification of shaded areas with color-infrared digital aerial image data from Emerge, attained an overall accuracy at 88%.

Ceccarelli et al. (2013), who applied OBIA for LULC classification with Landsat 7 image, obtained an overall accuracy and Kappa hat coefficient at 86% and 75%, respectively.

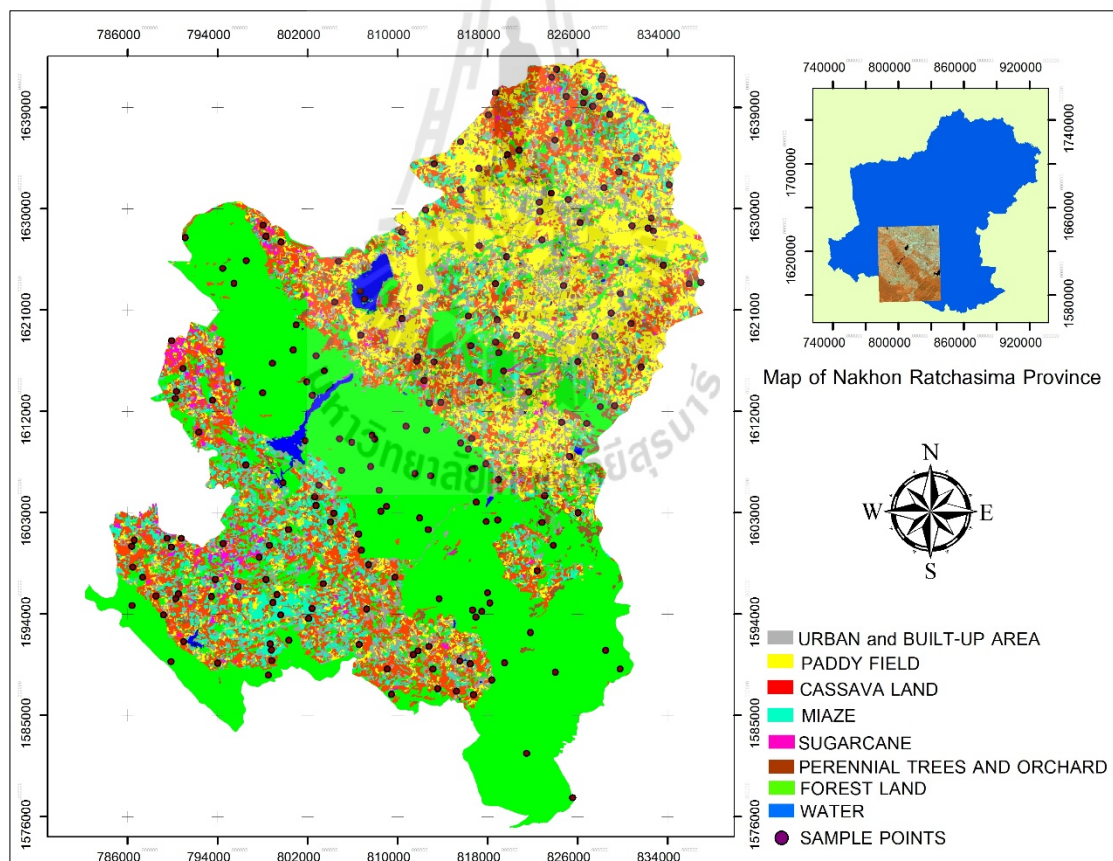


Figure 4.11 Distribution of sample points for accuracy assessment of thematic LULC map in 2013.

Table 4.13 Error matrix and accuracy assessment of LULC of 2013 in reference area.

Classified LULC class	Reference data								Row Total	PA	UA
	UR	PD	CA	MA	SU	PO	FO	WA			
Urban and built-up area	17	3	0	0	0	0	0	0	20	89.47%	85.00%
Paddy field	1	26	0	3	0	0	0	0	30	65.00%	86.67%
Cassava	0	2	18	0	8	0	0	0	28	90.00%	64.29%
Maize	1	8	1	19	0	1	0	0	29	86.36%	65.52%
Sugarcane	0	1	1	0	11	0	0	0	13	57.89%	84.62%
Perennial trees and orchard	0	0	0	0	0	7	2	0	9	87.50%	77.78%
Forest land	0	1	0	0	0	0	69	0	70	97.18%	98.57%
Water body	0	0	0	0	0	0	0	4	4	100.00%	100.00%
Column Total	19	40	20	22	19	8	71	4	203		
Overall accuracy	84.24%										
Kappa hat coefficient	80.37%										

4.3 Spatial transferability analysis

The result and finding of spatial transferability analysis, which is applied to determine whether the developed semantic model and classification can be transferred to testing area in the same year, is here described and discussed.

4.3.1 Semantic classification of LULC in 2013 in testing area

A semantic model for LULC extraction which was developed in Pak Thong Chai and Wang Nam Khieo districts, Nakhon Ratchasima province is directly applied for spatial transferability analysis in Khon Buri district of Nakhon Ratchasima province. The result of original LULC classification without LULC reclassification for spatial transferability analysis is shown in Figure 4.12 while the final LULC classification with reclassification for 8 LULC classes: urban and built-up area, paddy field, cassava, maize, sugarcane, perennial trees and orchard, forest land, and water body is summarized as area and percent of LULC classes in Table 4.14 and displayed in Figure 4.13.

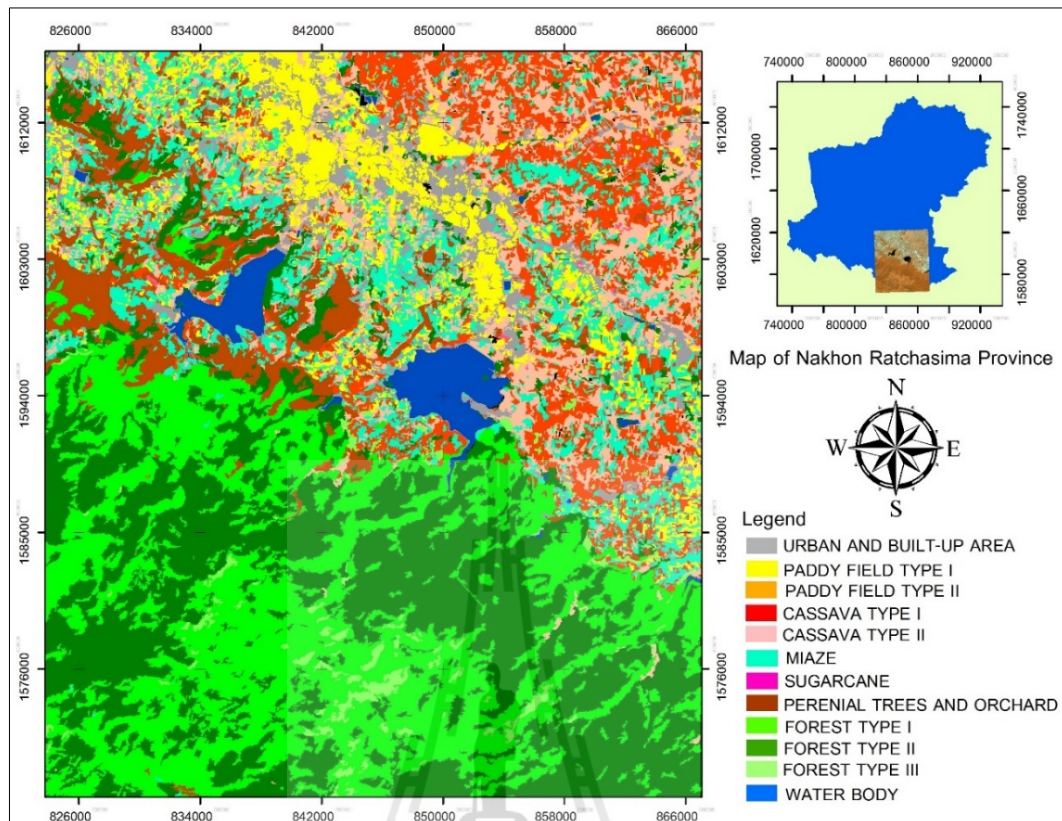


Figure 4.12 Original LULC classification of 2013 of spatial transferability analysis.

Table 4.14 Area and percentage of final LULC classification of 2013 for spatial transferability analysis.

No.	LULC class	Area in sq.km	Percent
1	Urban and built-up area	106.11	5.67
2	Paddy field	159.82	8.54
3	Cassava	372.40	19.91
4	Maize	152.42	8.15
5	Sugarcane	2.28	0.12
6	Perennial trees and orchard	50.75	2.71
7	Forest land	936.97	50.09
8	Water body	87.93	4.70
9	Unclassified	1.88	0.10
Total		1,870.55	100

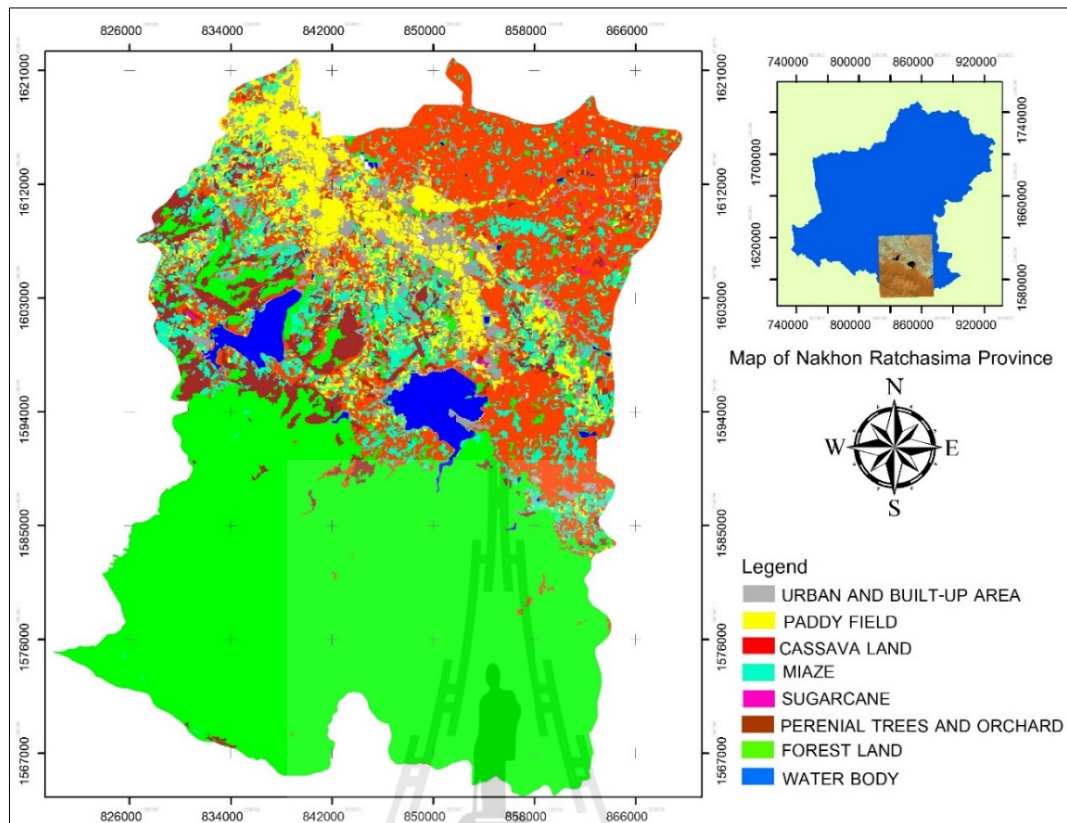


Figure 4.13 Final LULC classification of 2013 of spatial transferability analysis.

As results, the most dominant LULC type was forest land, which covers area of 936.97 sq. km or 50.09%. Meanwhile the dominant agricultural classes were cassava which covered area of 372.40 sq. km or 19.91%. Also, final LULC classes in 2013 of testing area is reclassified into 5 major land use classes of LDD: urban and built-up area, agricultural land, forest land, water body and miscellaneous land for comparison with land use data in 2011 of LDD as result shown in Table 4.15 and Figure 4.14. Herewith, areas of land use classes are slightly different according to different methods for extraction land use and LULC data with explanation as mentioned in the previous section. In addition, land use and LULC pattern from LDD and OBIA in

testing area was similar. The area of water surface over reservoirs and dams in 2011 and 2013 is rather different due to the temporal change.

Table 4.15 Comparison of LDD's land use data in 2011 and LULC data in 2013 by OBIA

Land use class	Area in sq. km		
	Land use data in 2011 by LDD	LULC data in 2013 by OBIA	Difference
Urban and built-up area	50.22	106.11	55.89
Agricultural land	726.44	737.67	11.23
Forest land	1,023.52	936.97	-86.55
Water body	53.82	87.38	33.56
Miscellaneous land	16.55	1.88	-14.67
Total	1,870.55	1,870.55	0.00

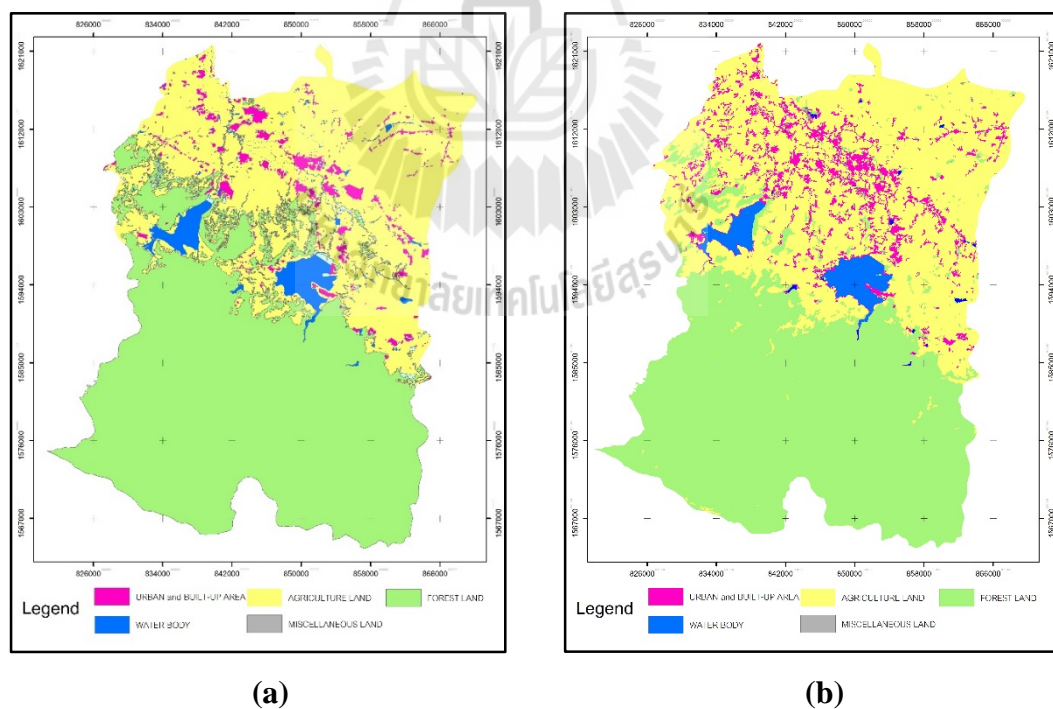


Figure 4.14 Comparison of land use data 2011 by LDD and LULC in 2013 by OBIA:

(a) by LDD (b) by OBIA.

4.3.2 Accuracy assessment of thematic LULC map in 2013 in testing area

Similarly to accuracy assessment of LULC data in reference area, 203 sample points based on binomial probability distribution theory with the expected accuracy of 85% at the allowable error of 5% and stratified random sampling as shown in Figure 4.15 was applied to assess accuracy of thematic LULC data in testing area based on the existing high spatial resolution images in 2013 and 2014 from Google earth of Google Inc. and ground survey in 2015. Detail of sampling point for accuracy assessment in testing area is presented in Table 2 of Appendix A. It was found that overall accuracy and Kappa hat coefficient of thematic LULC in 2013 of testing area in Khon Buri district for spatial transferability analysis was around 83.25% and 79.17%, respectively. In the meantime, PA varied between the lowest value of 58.33% for sugarcane and the highest value of 95.83% for forest land and UA varied between the lowest value of 47.06% for urban and built-up area and the highest value of 100% for water body.

The result revealed that both accuracy values showed a strong agreement between the classification map and the ground reference information according to Fitzpatrick-Lins, (1981) and it can be comparable with accuracy assessment of thematic LULC map deriving from semantic model in reference area. Detail of accuracy assessment as error matrix with PA and UA is presented in Table 4.16

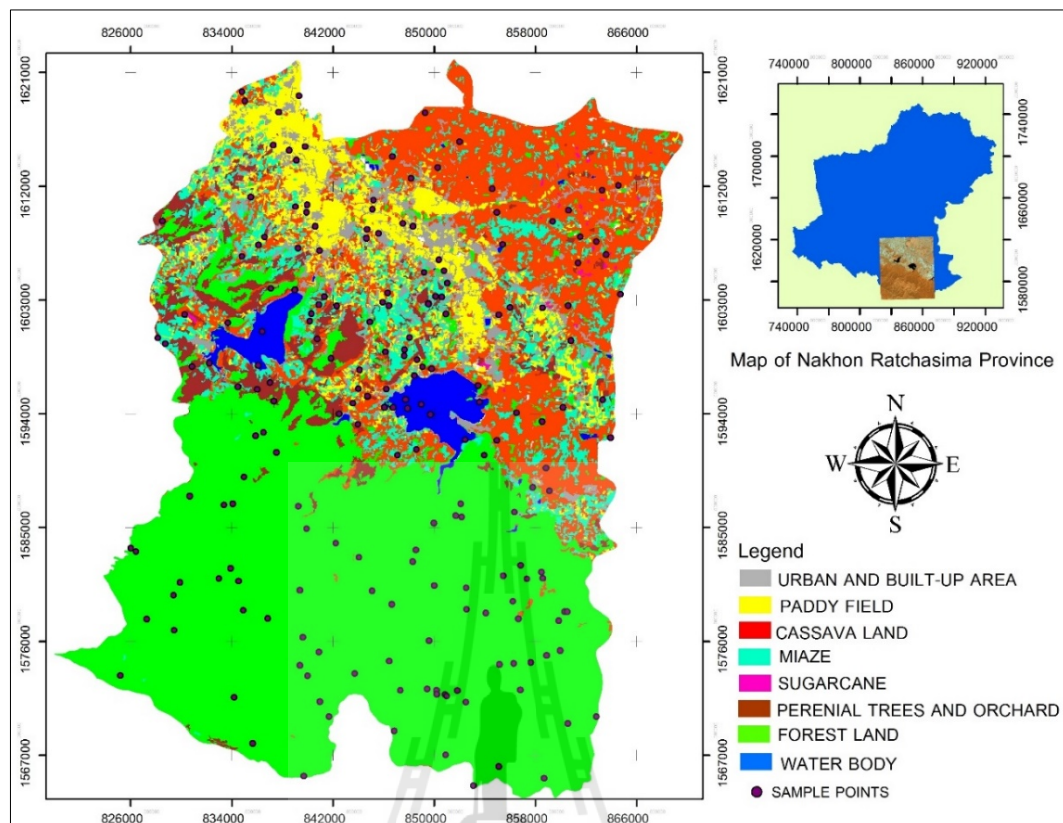


Figure 4.15 Sample points distribution for LULC data of 2013 accuracy assessment under spatial transferability analysis.

Table 4.16 Error matrix and accuracy assessment of LULC of 2013 of spatial transferability analysis in testing area.

Classified LULC class	Reference data								Row Total	PA	UAs
	UR	PD	CA	MA	SU	PO	FO	WA			
Urban and built-up area	8	0	3	3	0	0	0	3	17	72.73%	47.06%
Paddy field	1	15	1	1	3	0	2	1	24	68.18%	62.50%
Cassava	2	0	31	1	1	0	0	0	35	83.78%	88.57%
Maize	0	6	0	14	0	0	0	0	20	73.68%	70.00%
Sugarcane	0	1	1	0	7	0	0	0	9	58.33%	77.78%
Perennial trees and orchard	0	0	0	0	0	12	1	0	13	92.31%	92.31%
Forest land	0	0	1	0	1	1	69	0	72	95.83%	95.83%
Water body	0	0	0	0	0	0	0	13	13	76.47%	100.00%
Column Total	11	22	37	19	12	13	72	17	203		
Overall accuracy	83.32%										
Kappa hat coefficient	79.17%										

In addition, result of pairwise Z test between Kappa hat coefficient of reference area and testing area showed that accuracy of LULC extraction in both areas are not significantly different for the 100% two side confidence level (see Table 4.17). This finding infers that the developed semantic model and classification for LULC extraction in reference area can be transferred to testing area for LULC classification and it can provide indifferent accuracy.

Table 4.17 Pairwise Z test of Kappa hat coefficient value for LULC extraction by semantic model and classification between reference area and testing area.

Pairwise Z test	Kappa hat	Variance	Z-Statistic	Two-side confidential level of critical value		
				90%	95%	100%
LULC data in reference area	0.803717	0.00096	0.101257	1.65	1.96	2.58
LULC data in testing area	0.799232	0.00100				

4.4 Temporal transferability analysis

Likewise spatial transferability analysis, result and finding of temporal transferability analysis, which is examined to verify the consistency of the developed semantic model and classification can be applied in the same area at different points of time, is here described and discussion.

4.4.1 Semantic classification of LULC in 2014 in reference area

A developed semantic model for LULC extraction, which derived from Landsat 8 data of 2013 in Pak Thong Chai and Wang Nam Khieo districts, was directly adopted to classify LULC classes from another Landsat 8 data of 2014. The result of original LULC classification without semantic model modification and reclassification

for temporal transferability analysis is shown in Figure 4.16 and the final LULC classification with reclassification for 8 LULC classes: urban and built-up area, paddy field, cassava, maize, sugarcane, perennial trees and orchard, forest land, and water body is presented in Table 4.18 and Figure 4.17. As results, it revealed that semantic model and classification can extract small amount of water body, which is generally easy to classify by few features. The most dominant LULC class was forest land, which covers area of 638.43 sq. km or 30.80%. Meanwhile the dominant agricultural class was paddy field which covered area of 340.45 sq. km or 16.43%. Also, area of unclassified was 16.11 sq. km or 0.78%.

In addition, accuracy assessment for the final LULC map of 2014 without semantic model modification using 203 ground reference data in 2013 of reference area is summarized in Table 4.19. It was found that overall accuracy and Kappa hat coefficient for temporal transferability analysis without semantic model modification was only 46.30% and 34.48%, respectively. The Kappa hat coefficient less 40% represents poor agreement or accuracy between the classification map and the ground reference information as suggestion by Fitzpatrick-Lins (1981).

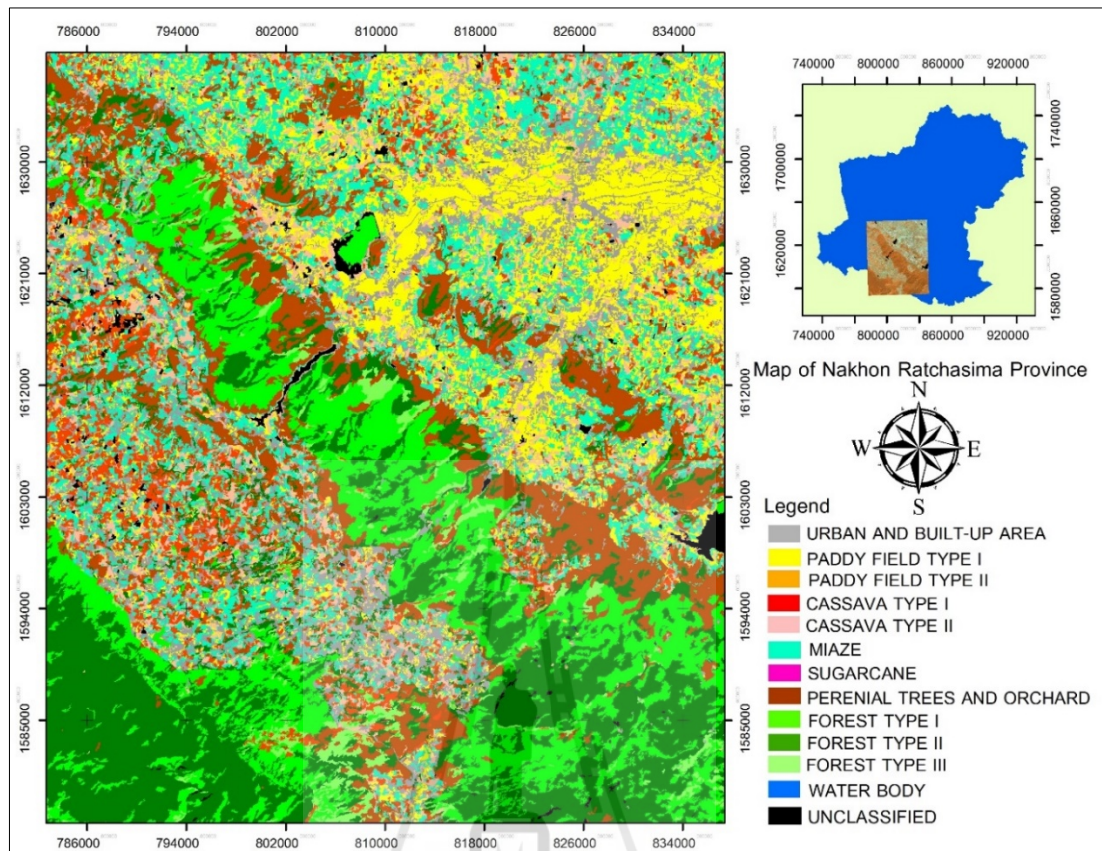


Figure 4.16 Original LULC classification of 2014 of temporal transferability analysis without semantic model modification.

Table 4.18 Area and percentage of LULC classification of year 2014 of temporal transferability analysis without semantic model modification.

No.	LULC class	Area in sq.km	Percent
1	Urban and built-up area	298.83	14.42
2	Paddy field	340.45	16.43
3	Cassava	273.90	13.22
4	Maize	273.59	13.20
5	Sugarcane	0.08	0.00
6	Perennial trees and orchard	231.00	11.15
7	Forest land	638.43	30.80
8	Water body	0.10	0.00
9	Unclassified	16.11	0.78
Total		2,072.49	100.00

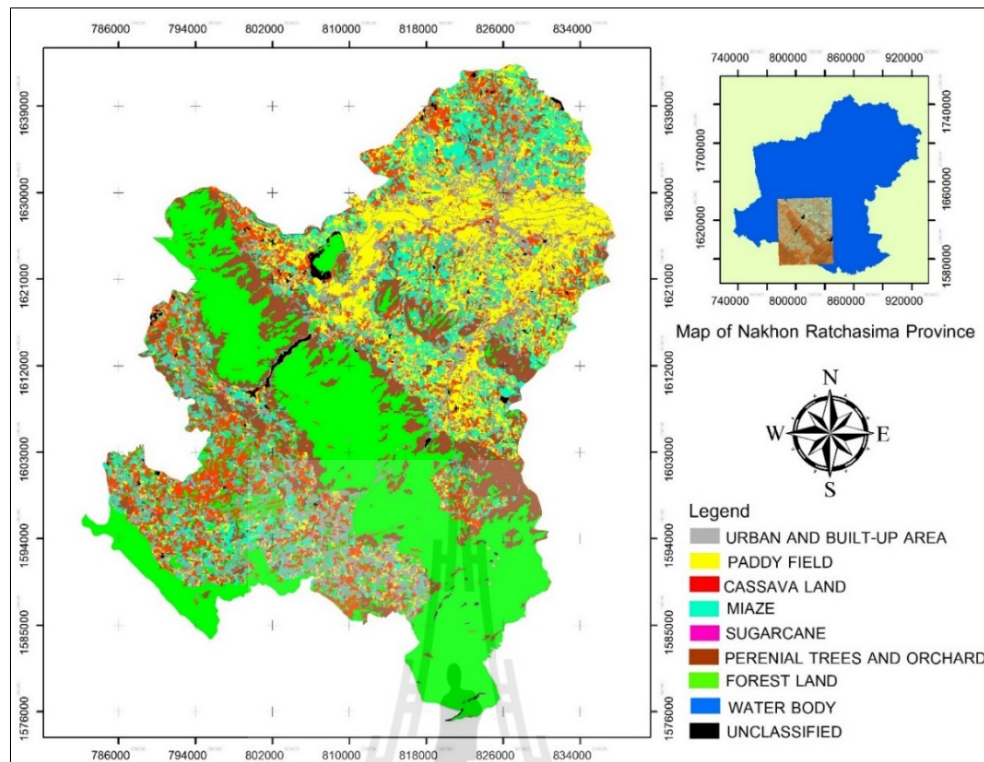


Figure 4.17 Final LULC classification of 2014 of temporal transferability analysis without semantic model modification.

Table 4.19 Error matrix and accuracy assessment of LULC of 2014 of temporal transferability analysis without semantic modification.

Classified LULC class	Reference data								Row Total	PA	UA
	UR	PD	CA	MA	SU	PO	FO	UC			
Urban and built-up area	7	4	1	7	1	1	3	0	24	31.58%	17.65%
Paddy field	4	12	0	3	2	0	7	0	28	31.58%	30.77%
Cassava	4	12	14	2	7	0	3	0	42	10.00%	7.41%
Maize	4	6	4	8	1	1	0	0	24	46.15%	36.36%
Sugarcane	0	0	0	0	0	0	0	0	0	n.a.	n.a.
Perennial trees and orchard	0	2	0	1	1	5	9	2	20	20.00%	11.11%
Forest land	0	4	1	1	3	1	48	2	61	57.75%	87.23%
Unclassified	0	0	0	0	4	0	1	0	5	n.a.	n.a.
Column Total	19	40	20	22	19	8	71	4	203		
Overall accuracy	46.30%										
Kappa hat coefficient	34.48%										

Herewith, the major problems of temporal transferability analysis is the change of spectral data of LULC classes between 2013 and 2014. In this study spectral data of major LULC classes of 2013 and 2014 was quite different due to phenological change of biological and physical features. Figure 4.18 demonstrates an example of phenological change of biological features of various LULC classes between 2013 and 2014. Herein, color composite image of Band 5 (NIR), 6 (SNIR), and 3 (Green) as RGB of paddy field appears as white and light orange color in 2013 looks as light blue and light magenta in 2014. Likewise, orange color of sugarcane in 2013 appears as magenta in 2014 while maize field in 2013 with blue color looks as light green in 2014. Meanwhile Figure to 4.19 shows the temporal change of physical features over water body. Area of water surface over reservoirs and dams in 2013 and 2014 are quite different and water body with dark blue color in 2013 appears as light blue in 2014. Nussbaum and Menz (2008), who applied temporal transferability analysis for building detection based on the derived semantic model and classification of reference area in 2002 for year 2003 and 2004 at Nuclear Fuel Research and Production Centre (NFRPC), Esfahan of Iran, suggested that thresholding values of spectral features, such as spectral data or NDVI, that changes over period of times, should be modified in the reference model.

Consequently, modification of Landsat 8 data and semantic model for LULC extraction of 2014 is required under temporal transferability analysis. In this study, histogram matching was firstly applied to fit histogram of Landsat data in 2014 with Landsat data in 2013 as result shown in Figure 4.20. Then the some selected spectral features of semantic model were modified by trial and error for LULC extraction under temporal transferability analysis.

The modified semantic model for LULC extraction of temporal transferability analysis for Landsat 8 data of 2014 with histogram matching is presented in Table 4.20.

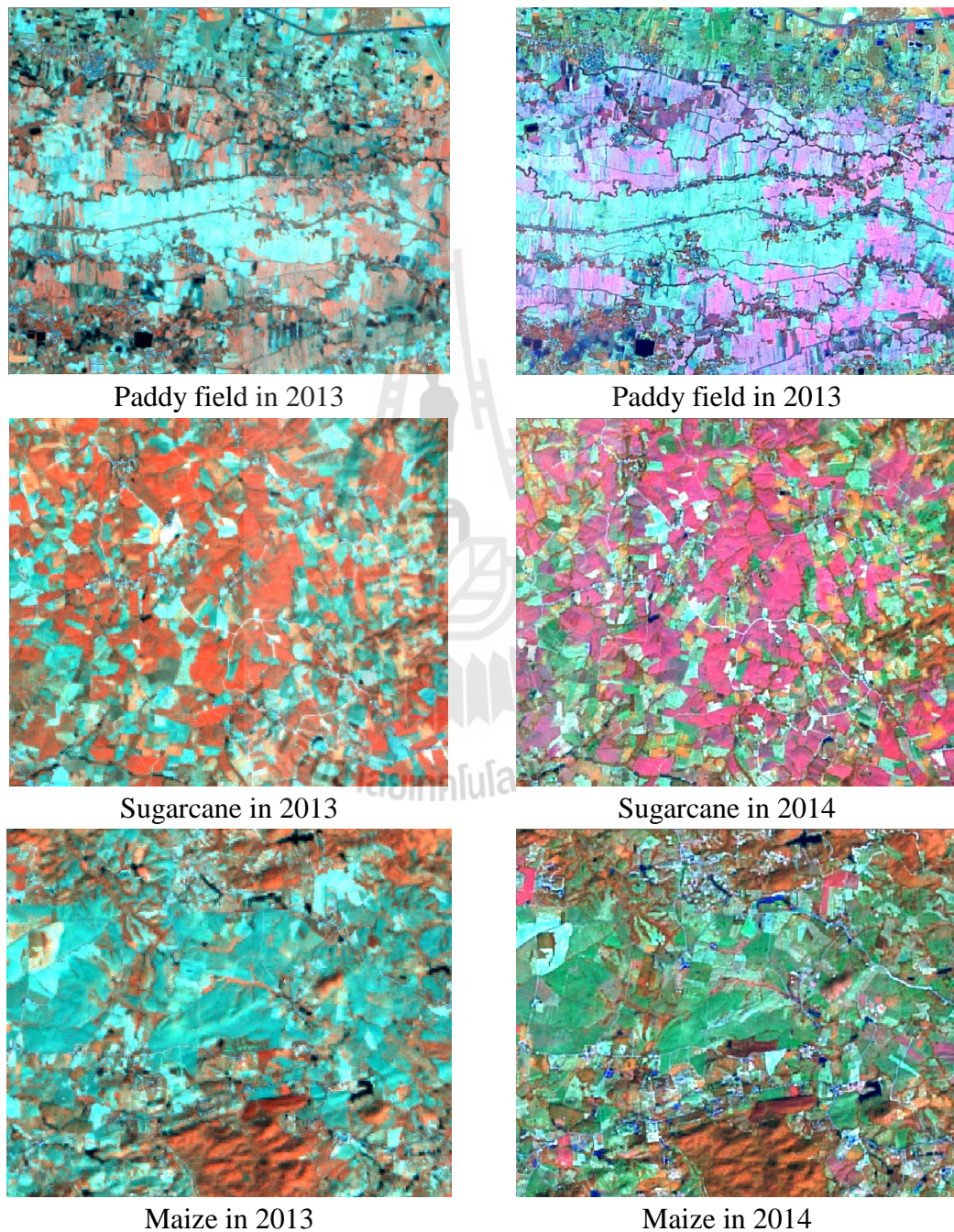
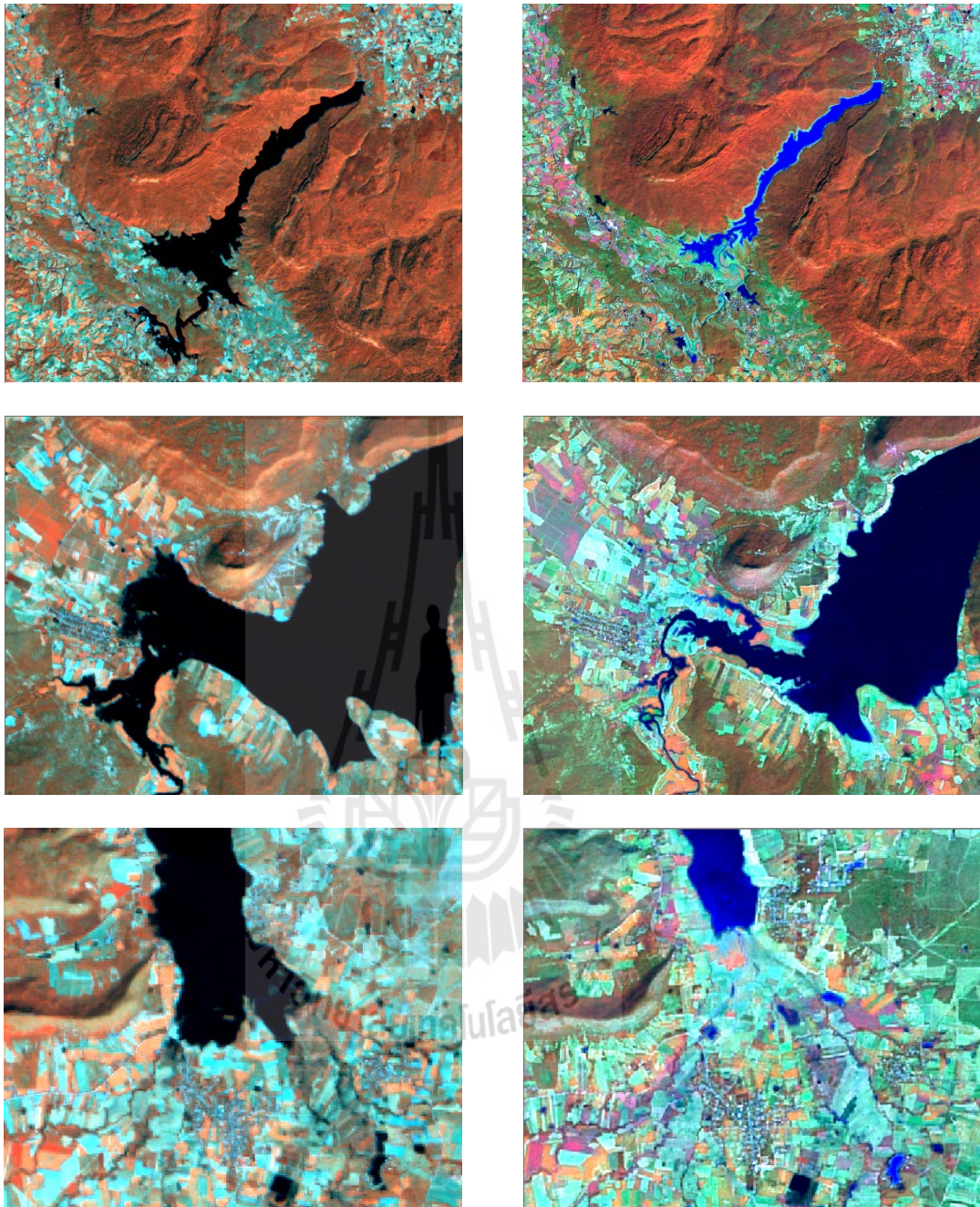


Figure 4.18 Landsat 8 color composite image comparison between 2013 and 2014 due to phenological change of biological features of various LULC classes.



Water body in 2013

Water body in 2014

Figure 4.19 Landsat 8 color composite image comparison between 2013 and 2014 due to phenological change of physical features of reservoirs and dams

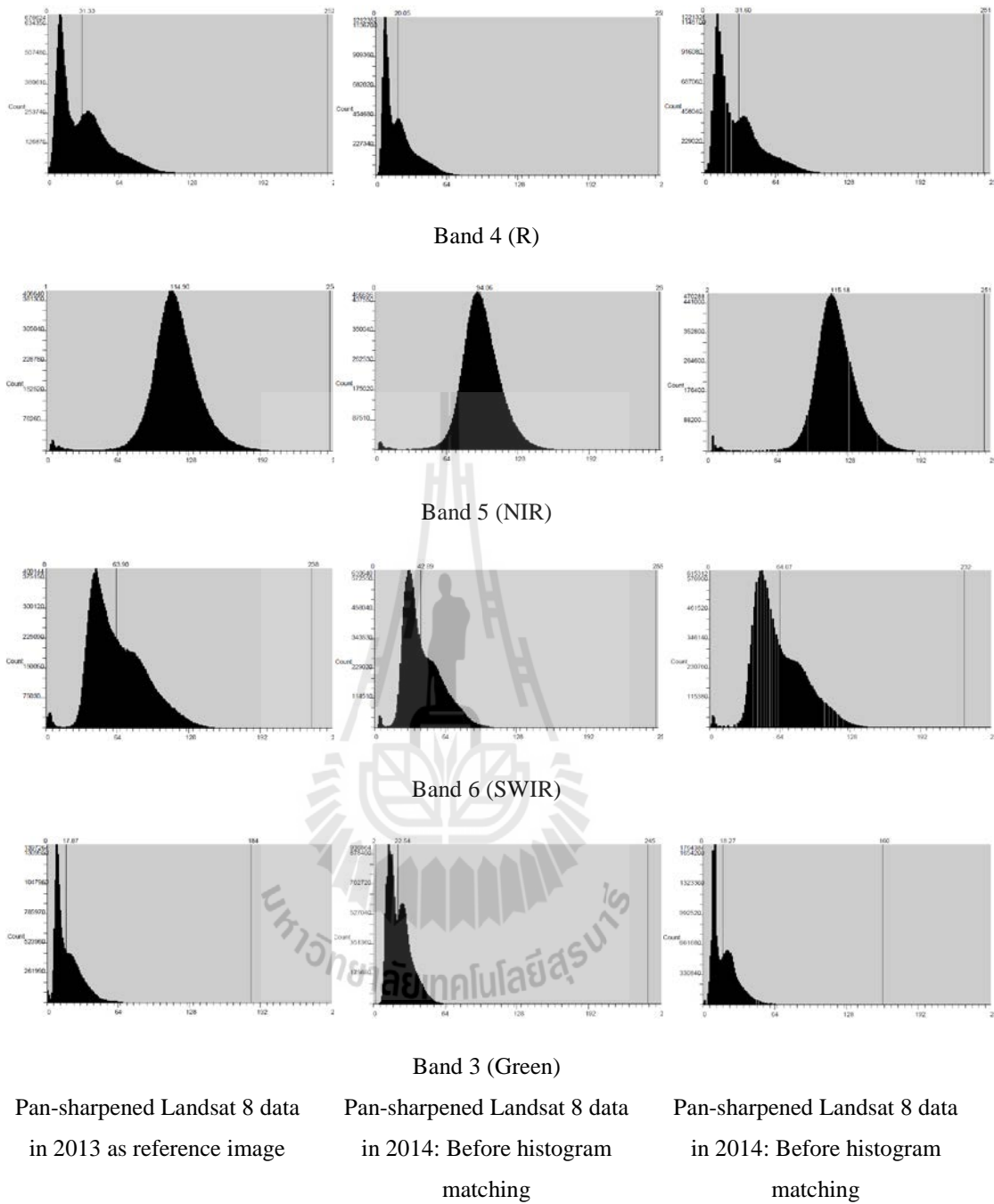


Figure 4.20 Comparison of histogram data of Landsat 8 data in 2014 before and after histogram matching with Landsat 8 data in 2013 as reference data.

Table 4.20 Modified semantic model for LULC extraction of temporal transferability analysis with Landsat 8 data in 2014.

LULC classes	Membership function and threshold value		
	Membership function	Left border	Right border
Urban and built-up area			
GLCM Dissimilarity (quick 8/11) (all dir.)	Ascending	2.5	6.2
GLCM Dissimilarity Layer 3 (all dir.)	Ascending	7.4*	9.42
GLCM Dissimilarity Layer 4 (all dir.)	Ascending	2.63	4.85
GLCM Mean Layer 3 (all dir.)	Descending	71.662	75*
Standard deviation Layer 1	Ascending	3.4	13.36
Standard deviation Layer 4	Ascending	1.99	6.9144
Paddy field Type I			
Brightness	Ascending	50	91.16
GLCM Mean (quick 8/11) (all dir.)	Ascending	40*	90.467
GLCM Mean Layer 4 (all dir.)	Ascending	10*	41.436
Mean Layer 4	Ascending	6.396	41.655
Ratio Layer 1	Ascending	0.14	0.2415
Paddy field Type II			
Mean Layer 1	Ascending	47.85	65
Mean Layer 2	Ascending	110	134.05
Mean Layer 3	Ascending	56.107	76.27
Mean Layer 4	Ascending	18.841	23.29
Cassava Type 1			
Brightness	Ascending	45*	72.32
GLCM Mean (quick 8/11) Layer 4 (all dir.)	Ascending	6.67	20.408
Max. diff	Descending	0.985	3*
Mean Layer 1	Descending	24.6	42*
Mean Layer 4	Ascending	5.963	20.288
Ratio Layer 4	Descending	0.07	1*
Cassava Type II			
Brightness	Descending	58.663	67.079
GLCM Mean Layer 4 (all dir.)	Ascending	6.63	25.16
Max. diff	Descending	1.665	2.306
Mean Layer 1	Ascending	16.462	42.769
Mean Layer 2	Descending	94	143
Mean Layer 4	Ascending	5.823	25.251
Ratio Layer 3	Descending	0.307	0.315*
Standard deviation Layer 1	Descending	5.82	10*
Standard deviation Layer 2	Ascending	5*	12.738
Maize			
GLCM Mean (quick 8/11) Layer 4 (all dir.)	Ascending	5.443	29.254

Table 4.20 (Continued).

LULC classes	Membership function and threshold value		
	Membership function	Left border	Right border
GLCM Mean Layer 2 (all dir.)	Ascending	43.868	83.715
Mean Layer 2	Ascending	41.985	83.018
Mean Layer 4	Ascending	9*	20*
Ratio Layer 1	Ascending	0.111	0.178
Ratio Layer 3	Ascending	0.326	0.3631
Sugarcane			
Mean Layer 1	Ascending	18*	32.86
Mean Layer 2	Ascending	110*	163.6
Mean Layer 3	Descending	57.058	73.06
Mean Layer 4	Descending	12.702	24.3
Perennial trees and orchard			
GLCM Dissimilarity (quick 8/11) Layer 2 (all dir.)	Descending	3.5	5.439
GLCM Mean Layer 3 (all dir.)	Ascending	49*	56
GLCM Mean Layer 4 (all dir.)	Descending	13	19*
Mean Layer 1	Descending	25	51
Mean Layer 3	Ascending	21	55
Standard deviation Layer 3	Ascending	3*	4.1699
Forest land type I			
Brightness	Descending	42.282	53.565
Mean Layer 3	Ascending	15.128	41.136
Mean Layer 4	Ascending	2.97	7.8954
Ratio Layer 4	Descending	0.047	0.0758
Forest land type II			
GLCM Mean Layer 1 (all dir.)	Descending	11.441	25*
Mean Layer 1	Descending	11.436	22.553
Mean Layer 4	Ascending	3.468	8.8432
Forest land types III			
Max. diff.	Descending	2.21	2.33
Mean Layer 1	Ascending	13.529	22.73
Mean Layer 4	Descending	3.431	14.511
Ratio Layer 1	Ascending	0.051	0.1747
Water Body			
Mean Layer 2	Descending	7.09	31.77
Mean Layer 3	Descending	2.59	37.9
Mean Layer 4	Descending	0.404	60

Note: * Modified thresholding value.

The result of original LULC classification with the modified semantic model and without reclassification for temporal transferability analysis is shown in Figure 4.21 and the final LULC classification with reclassification for 8 LULC classes: urban and built-up area, paddy field, cassava, maize, sugarcane, perennial trees and orchard, forest land, and water body is shown in Figure 4.22 and Table 4.21. As results, all assigned classes under semantic model with modification were here classified. The most dominant LULC class was forest land, which covers area of 730.39 sq. km or 35.24%. Meanwhile the dominant agricultural class was cassava which covered area of 383.63 sq. km or 18.51 percent. Additionally, unclassified area was decreased to be 1.83 sq. km or 0.09%.

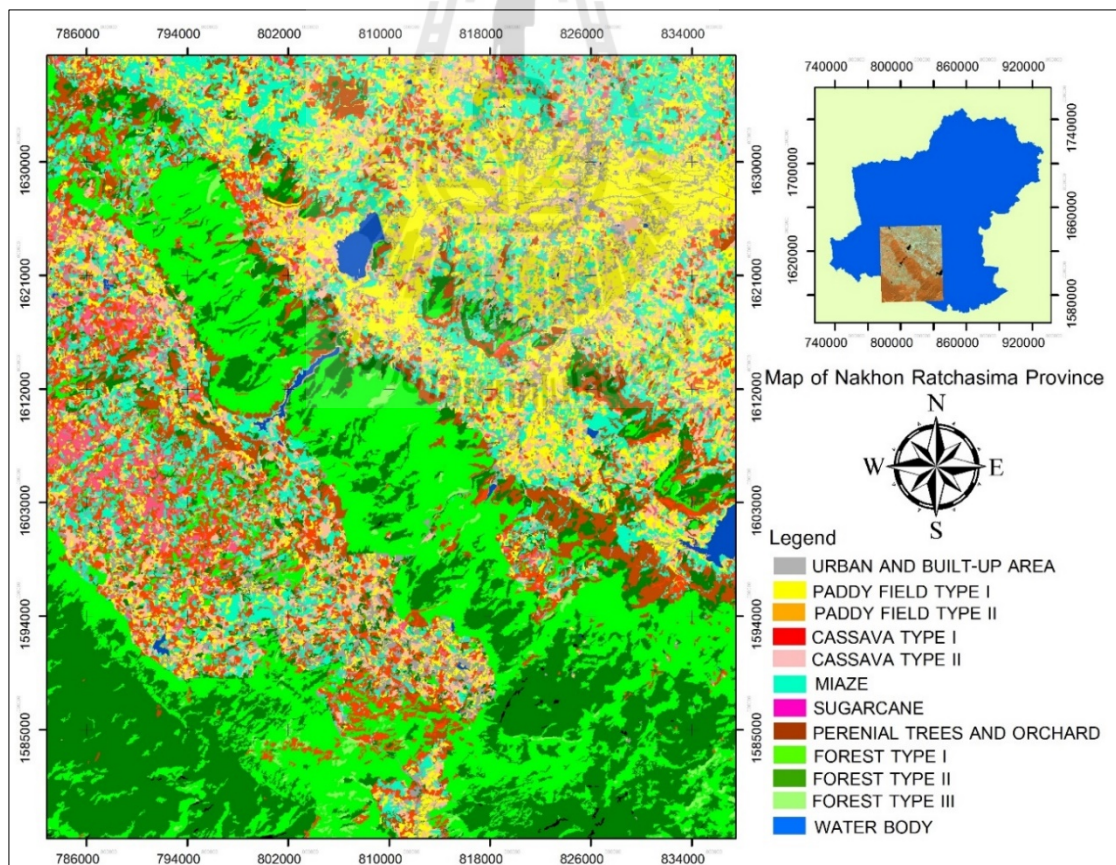


Figure 4.21 Original LULC classification of 2014 of temporal transferability analysis with the modified semantic model of reference area in 2013.

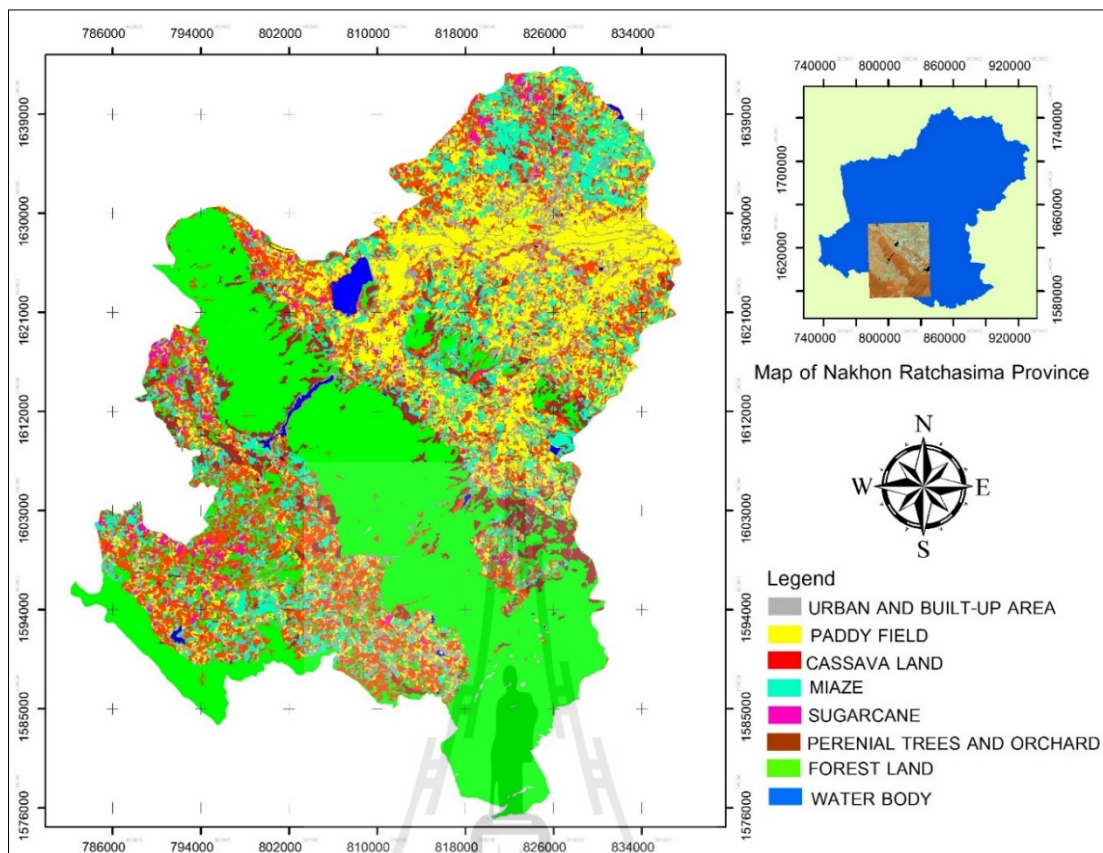


Figure 4.22 Final LULC classification of 2014 of temporal transferability analysis with modified semantic model of reference area in 2013.

Table 4.21 Area and percentage of LULC classification of year 2014 of temporal transferability analysis with semantic model modification.

No.	LULC class	Area in sq.km	Percent
1	Urban and built-up area	173.94	8.39
2	Paddy field	379.90	18.33
3	Cassava	383.63	18.51
4	Maize	253.71	13.24
5	Sugarcane	32.31	1.56
6	Perennial trees and orchard	98.06	4.73
7	Forest land	730.39	35.24
8	Water body	18.71	0.9
9	Unclassified	1.83	0.09
Total		2,072.49	100

In addition, accuracy assessment of the final LULC map of 2014 with semantic model modification based on 203 ground reference of 2013 in reference area is summarized in Table 4.22. It was found that accuracy of thematic LULC map of temporal transferability analysis with the modified semantic model had been improved with overall accuracy and Kappa hat coefficient of 66.00% and 57.83%, respectively. Additionally, PA varied between the lowest value of 26.32% for urban and built-up area and the highest value of 100% for water body and UA varied between the lowest value of 35.71% for urban and built-up area and the highest value of 100% for water body. According to Fitzpatrick-Lins (1981), Kappa hat coefficient values between 40 to 80% represents moderate agreement or accuracy between the classification map and the ground reference information.

Table 4.22 Error matrix and accuracy assessment of LULC of 2014 for temporal transferability analysis with semantic model modification.

Classified LULC class	Reference data								Row Total	PA	UA
	UR	PD	CA	MA	SU	PO	FO	WA			
Urban and built-up area	5	5	0	2	0	0	2	0	14	26.32%	35.71%
Paddy field	7	23	1	5	1	0	0	0	37	57.50%	62.16%
Cassava	3	2	17	5	9	2	3	0	41	85.00%	41.46%
Maize	4	10	0	9	0	0	0	0	23	40.91%	39.13%
Sugarcane	0	0	2	1	9	0	0	0	12	47.37%	75.00%
Perennial trees and orchard	0	0	0	0	0	4	3	0	7	50.00%	57.14%
Forest land	0	0	0	0	0	2	63	0	65	88.73%	96.92%
Water body	0	0	0	0	0	0	0	4	4	100.00%	100.00%
Column Total	19	40	20	22	19	8	71	4	203		
Overall accuracy	66.00%										
Kappa hat coefficient	57.83%										

Furthermore, result of pairwise Z test between Kappa hat coefficient of thematic LULC map of 2013 and 2014 in reference area showed that accuracy of LULC extraction of temporal transferability analysis are significantly different for the 90% two side confidence level (see Table 4.23). This finding infers that the developed semantic model for LULC of 2013 extraction cannot be directly transferred for LULC in 2014 classification although they are the same area. Herein, the developed semantic model required to modify by mean of trial and error for increasing the thematic accuracy. The modification of semantic model is time consumption and tiresome works.

Table 4.23 Pairwise Z test of Kappa hat coefficient value for LULC extraction by modified semantic model and classification in the same area in different years.

Pairwise Z test	Kappa hat	Variance	Z-Statistic	Confidential level of critical value		
				90%	95%	100%
LULC data of 2013	0.803717	0.00096	4.523715	1.65	1.96	2.58
LULC data of 2014	0.578300	0.001522				

CHAPTER V

CONCLUSION AND RECOMMENDATION

Under this chapter, image pre-processing products and three main results which were reported according to objectives in the study included (1) to develop semantic model and classification with SEaTH and expert's knowledge for LULC extraction in reference area; (2) to apply the developed semantic model and classification of reference area for spatial transferability analysis; and (3) to modify the developed semantic model and classification of reference area for temporal transferability analysis are here separately concluded and recommended for future research and development.

5.1 Conclusion

5.1.1 Optimum pan-sharpening method of Landsat 8

The Q average method is used to evaluate pan-sharpening methods for Landsat 8 image include EF, GS, HPF, MIHST, and WT. The most appropriate method for Landsat 8 data pan-sharpening processing is WT and the possibly appropriate methods include HPF, EF, and GS. This possibility is useful when software availability is considered. On contrary, the least appropriate method for pan-sharpening producing from Landsat 8 data is MIHST.

5.1.2 Optimum four band combination dataset of Landsat 8

OIF and SI are used to identify an optimum four band selection of the derived pan-sharpened Landsat 8 image. The most optimum four band combination of Landsat 8 data for bands reduction with low correlation is band 3 (G), 4 (R), 5 (NIR) and 6 (SWIR) and the least optimum four band combination is band 2 (B), 3 (G), 4 (R) and 7 (SWIR).

5.1.3 Development of semantic model and classification for LULC extraction.

Semantic modelling and classification with SEaTH analysis is successfully developed for LULC extraction in Pak Thong Chai and Wang Nam Khieo districts, Nakhon Ratchasima province as reference area. The extracted LULC in 2013 from the pan-sharpened Landsat 8 image include urban and built-up area, paddy field, cassava, maize, sugarcane, perennial trees and orchard, forest land, and water body. The obtained overall accuracy and Kappa hat coefficient of thematic LULC map are 84.24% and 80.37%, respectively and PA ranges between 57.89% and 100% and UA varies between 64.29% and 100%. Kappa hat coefficient more than 80% represents strong agreement or accuracy between the classification map and the ground reference information. Finally, the achieved accuracy proved to be acceptable when it was compared with other studies that applied rule-based classifier under OBIA.

5.1.4 Application of semantic model and classification for spatial transferability analysis.

Overall accuracy and Kappa hat coefficient of thematic LULC of 2013 in Khon Buri district as testing area based on the developed semantic model in reference area are 83.25% and 79.17%, respectively with PA between 58.33% and 95.83% and

UA between 47.06% and 100%. The result demonstrates strong accuracy between the classification map and the ground reference information. Additionally, result of pairwise Z test between Kappa hat coefficients of reference and testing areas shows accuracy of thematic LULC data from both areas are not significantly different at the 100% confidence level. This finding concludes that the developed semantic model and classification for LULC extraction in reference area can be transferred to testing area for LULC classification and it can provide indifferent accuracy.

5.1.5 Application of semantic model and classification for temporal transferability analysis.

Overall accuracy and Kappa hat coefficient of the final LULC map of 2014 with the modified semantic model of the reference area in 2013 are 66.00% and 57.83%, respectively while PA varies between 26.32% and 100% and UA varies between 35.71% and 100%. Based on Kappa hat coefficient value it represents moderate accuracy between the classification map and the ground reference information. Result of pairwise Z test between Kappa hat coefficient of thematic LULC map of 2013 and 2014 in same area shows that accuracy of LULC classification under temporal transferability analysis are significantly different for the 90% two side confidence level. This finding infers that the developed semantic model for LULC classification in 2013 in reference area cannot directly be transferred for LULC classification in 2014 in the same area. Herewith, the developed semantic model required to modify by mean of trial and error for increasing the thematic accuracy. The modification of semantic model is time consumption and tiresome works.

In conclusion, it appears that semantic modelling and classification with SEaTH analysis can be efficiently used as new tools for LULC extraction under OBIA. In order

to obtain initial information from recent remotely sensed data, spatial and temporal transferability analysis can be made available in a fast and simple manner.

5.2 Recommendation

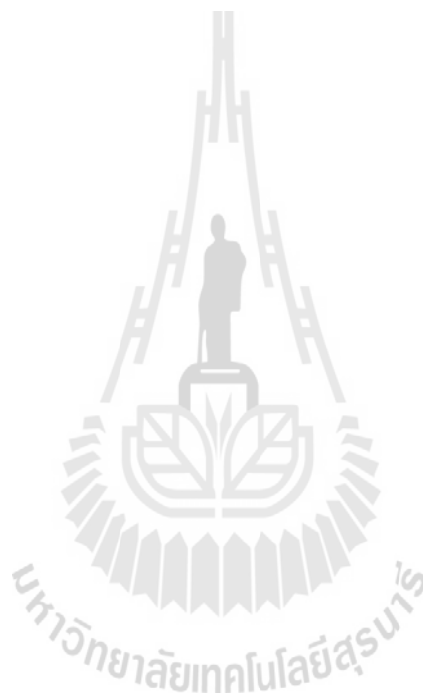
In this study, semantic modelling and classification with SEaTH analysis under OBIA was applied to extract LULC. The possibly expected recommendations could be made for further studies as follows:

(1) In the study, LULC classification system was modified from the existing land use classification system and land use data in 2011 of LDD. It was found that many LULC classes had been changed in 2013. Therefore, the preliminary field survey should be conducted as soon as possible after remotely sensed data is available for LULC classification.

(2) Basic object features, which include spectral response, shape, size, texture, and the customized features such as vegetation indices, should be carefully selected for feature extraction under SEaTH analysis. Because many features can be transferable over a long periods of time and places such as buildings and infrastructure but some features may be change over a short periods of time or many places such as vegetation. These characteristics are directly related with spatial and temporal transferability analysis.

(3) Number of training samples should be increased according to the proportional area of LULC classes, instead of equally number of samples as in this study. Additionally, variance among training samples of any LULC class should be minimal. Because if there is an overlap between two classes, it can assign wrong class due to commission or omission errors.

(4) Semantic modelling and classification with SEaTH analysis and spatial and temporal transferability analysis should be examined in another reference and testing areas for verification accuracy. Because the developed semantic model and classification can be prepared available in a fast and simple manner for updating LULC data that are, in general, required by various government agencies and private sectors.





REFERENCES

REFERENCES

- Al-Khatib, Wasfi, Francis Day, Y., Ghafoor, A., and Berra, B. (1999). Semantic modeling and knowledge representation in multimedia databases. **IEEE transactions on knowledge and data engineering**. (11): 64-80.
- Baatz, M., and Schäpe, A. (2000). **Multiresolution segmentation: An optimization approach for high quality multi-scale image segmentation**. In angewandte geographische informations-verarbeitung (12thed.). Quoted in Gao, J. (2009). **Digital analysis of remotely sensed imagery**. New York: McGraw-Hill.
- Benz, C., Hofmann, P., Willhauck, G., Lingenfelder, I., and Heynen, M. (2004). Multi-resolution, object-oriented fuzzy analysis of remote sensing data for GIS-ready information. **ISPRS Journal of Photogrammetry and Remote Sensing**. 58(3–4): 239 – 258.
- Blaschke, T., and G., Hay J. (2001). Object oriented image analysis and scale-space: Theory and methods for modeling and evaluating multiscale landscape structure. **International Archives of Photogrammetry and Remote Sensing**. 58:239–258
- Blaschke, T. (2010). Object based image analysis for remote sensing. **ISPRS journal of photogrammetry and remote Sensing**. (65): 2-16.

- Blaschke, T., Lang, S., and Hay, G. (2008). **Object-based image analysis: Spatial concepts for knowledge-driven remote sensing applications**. Berlin: Springer.
- Blaschke, T., and Strobl, J. (2001). **What's wrong with pixels? Some recent developments interfacing remote sensing and GIS** [On-line]. Available: <http://www.igp.ethz.ch/photogrammetry/education/lehrveranstaltungen/RSGISFS2011/coursematerial/gis2001.pdf>.
- Burnett, C., and Blaschke, T. (2003). A multi-scale segmentation/object relationship modeling methodology for landscape analysis. **Ecological Modeling**. 168(3):233–249.
- Campbell Michael J., and Congalton Russell G. (2012). Landsat-based land cover change analysis in Northerastern Oregon's Timeber-resource-dependent communities. **Proceedings of ASPRS Annual Conference**. [On-line]. Available: <http://www.asprs.org/a/publications/proceedings/Sacramento2012/files/Campbell.pdf>.
- Ceccarelli, T., Smiraglia, D., Bajocco, S., Rinaldo, S., De Angelis, A., Salvati, L., and Perini, L. (2013). Land cover data from Landsat single-date imagery: an approach integrating pixel-based and object-based classifiers. **European Journal of Remote Sensing**. 46: 699-717.
- Congalton, Russell G., and Green, Kass. (2009). **Assessing the Accuracy of Remotely Sensed Data: Principles and Practices**. (2nd ed.). Boca Raton: CRC Press.

- Debdip, B, and Girls, C. (2013). Optimum index factor (OIF) for LANDSAT data: A case study on Barasat town, west Bengal, India, **International Journal of Remote Sensing & Geoscience (IJRSG)**. 2(5): 11-16.
- Eddy, R., Smith, M., Hill, D., Peddle, R., Coburn, A., and Blackshaw, E. (2008). Hybrid segmentation–artificial neural network classification of high resolution hyperspectral imagery for site-specific herbicide management in Agriculture. **Photogrammetric engineering & remote sensing**. 74 (10): 1249-1257.
- Fitzpatrick-Lins, K., (1981). Comparison of sampling procedures and data analysis for a land-use and land cover map. **Photogrammetric Engineering and Remote Sensing** 47(3): 343 – 351.
- Gao, J. (2009). **Digital analysis of remotely sensed imagery**. New York: McGraw-Hill.
- Horning, N., Robinson, .A., Sterling, E.J, Turner, W., and Spector, S. (2010). **Remote sensing for ecology and conservation: A handbook of techniques**. New York: Oxford.
- Hu, X., Tao, V., and Prenzel B. (2005). Automatic segmentation of high-resolution satellite imagery by integrating texture, intensity, and color features. **Photogrammetric Engineering and Remote Sensing**. 71(12): 1399 – 1408.
- Jensen, John. R. (2007). **Remote sensing of the environment: An earth resource perspective** (2nd ed.). London: Pearson Education.
- Karnjanasin, Natthira. (2003). **Economic change of Nakhon Ratchasima, A.D. 1957-1997**. M.S. thesis, Silapakorn University, Thailand.

- Khamphilung, S., Strobl, J. and Tiede, D. (2013). Village forms classification by object-based image analysis. **International journal of Geoinformatics**. 9 (3): 59-68.
- Laiberte, S., Browning, M., and Rango, A. (2012). A comparison of three feature selection methods for object-based classification of sub-decimeter resolution UltraCam-L imagery. **International journal of applied earth observation and geoinformation**. (15): 70-78
- Lang, S. (2008). Object-based image analysis for remote sensing applications: modeling reality—dealing with complexity. **Object-based image analysis: Spatial concepts for knowledge-driven remote sensing applications**. (pp 3-18). Berlin: Springer.
- Liu, J., Pattey, E., and Nolin, M.C. (2008). Object-based Classification of High Resolution SAR Images for Within Field Homogeneous Zone Delineation. **Photogrammetric engineering & remote sensing**. (9): 1159-1168.
- Myint, W., Gober, P., Brazel, A., Grossman-Clarke, S., and Weng, Q. (2011). Per-pixel vs. object-based classification of urban land cover extraction using high spatial resolution imagery. **Remote sensing of environment**. (115): 1145-1161.
- Navulur, K. (2007). **Multispectral image analysis using the object-oriented paradigm**. Florida: CRC Press.
- Nussbaum, S., and Menz, G. (2008). **Object-based image analysis and treaty verification: New approaches in remote sensing—applied to nuclear facilities in Iran**. Berlin: Springer.

Richards, A., and Jia, X. (2013). **Remote sensing digital image analysis: An introduction.** (5th ed.). New York: Springer-Verlag.

Ryherd, S., and Woodcock, Curtls. (1996). Combining spectral and texture data in the segmentation of remotely sensed images. **Photogrammetric Engineering and Remote Sensing.** 62(2): 181 – 194.

Shruthi, R., Kerle, N., and Jetten, V. (2011). Object-based gully feature extraction using high spatial resolution imagery. **Geomorphology** 2011 (134): 260-268.

Sun, K., Chen, Y., and Li, D. (2006). Multiscale image segmentation and its application in image information extraction. **Proceedings of SPIE The International Society for Optical Engineering.** 6419:64191I. Quoted in Gao, J. (2009). **Digital analysis of remotely sensed imagery.** New York: McGraw-Hill.

Timble Germany GmbH. (2011). **eCognition developer 8.7 reference book.** München: Wikipublisher.

Tizhoosh, H.R. (1998). **Fuzzy-bildverarbeitung, einföhrung in theorie und praxis.** Berlin: Springer. Quoted in Nussbaum, S. and Menz, G. (2008). **Object-based image analysis and treaty verification: New approaches in remote sensing applied to nuclear facilities in Iran.** Berlin: Springer.

U.S. Geological Service, (2014). **Landsat 8** [On-line]. Available:

<http://landsat.usgs.gov/landsat8.php>.

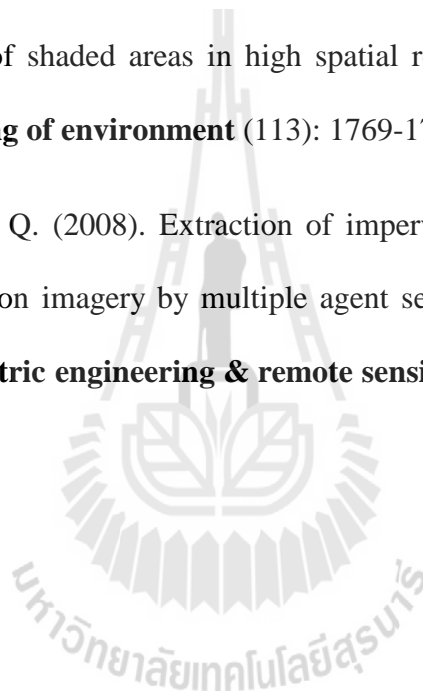
Wilkinson, G. (1999). **Recent developments in remote sensing technology and the importance of computer vision analysis techniques.** Quoted in Nussbaum, S. and Menz, G. (2008). **Object-based image analysis and treaty**

verification: New approaches in remote sensing–applied to nuclear facilities in Iran. Berlin: Springer.

Wu, H., Cheng, Z., Shi, W., Miao, Z., and Xu, C. (2013). An object-based image analysis for building seismic vulnerability assessment using high-resolution remote sensing imagery. **Nat hazard** (71): 151-174.

Zhou, W., Huang, G., Troy, A., and Cadenasso, M.L. (2009). Object-based land cover classification of shaded areas in high spatial resolution a comparison study. **Remote sensing of environment** (113): 1769-1777.

Zhou, Y., and Wang, Q. (2008). Extraction of impervious surface areas from high spatial resolution imagery by multiple agent segmentation and classification. **Photogrammetric engineering & remote sensing**. (7) 74: 857 - 868.



APPENDIX

Table 1 Detail of sampling point for accuracy assessment in reference area.

No.	X	Y	Ground reference class
1	156386.5	1597192	Cassava
2	157481.5	1603447	Cassava
3	139676.5	1601512	Cassava
4	152111.5	1628212	Cassava
5	146816.5	1590412	Cassava
6	142601.5	1601587	Cassava
7	174161.5	1618807	Cassava
8	143831.5	1592377	Cassava
9	164246.5	1590697	Cassava
10	158051.5	1622212	Cassava
11	177956.5	1610992	Cassava
12	183641.5	1625047	Cassava
13	165821.5	1615042	Cassava
14	182696.5	1612342	Cassava
15	187346.5	1624702	Cassava
16	178046.5	1636072	Cassava
17	172181.5	1638472	Cassava
18	179126.5	1639927	Cassava
19	167966.5	1587337	Cassava
20	143756.5	1614637	Cassava
21	172376.5	1623457	Urban and Built-up area
22	171206.5	1633747	Urban and Built-up area
23	164651.5	1591012	Urban and Built-up area
24	160301.5	1619227	Urban and Built-up area
25	173456.5	1625842	Urban and Built-up area
26	151691.5	1600747	Urban and Built-up area
27	170051.5	1618012	Urban and Built-up area
28	141461.5	1596517	Urban and Built-up area
29	169916.5	1620622	Urban and Built-up area
30	182606.5	1620592	Urban and Built-up area
31	179066.5	1630762	Urban and Built-up area
32	165626.5	1591387	Urban and Built-up area
33	160196.5	1594852	Urban and Built-up area
34	178436.5	1623112	Urban and Built-up area

Table 1 (Continued).

No.	X	Y	Ground reference class
35	168371.5	1590022	Urban and Built-up area
36	151511.5	1591972	Urban and Built-up area
37	172211.5	1606042	Urban and Built-up area
38	182606.5	1620592	Urban and Built-up area
39	179066.5	1630762	Urban and Built-up area
40	155336.5	1595017	Maize
41	142961.5	1600807	Maize
42	169541.5	1631902	Maize
43	160466.5	1598797	Maize
44	155006.5	1594147	Maize
45	143651.5	1613992	Maize
46	151631.5	1590487	Maize
47	166331.5	1587622	Maize
48	171161.5	1588282	Maize
49	183641.5	1633087	Maize
50	143471.5	1596652	Maize
51	182276.5	1631707	Maize
52	157166.5	1602682	Maize
53	188081.5	1631842	Maize
54	151871.5	1595632	Maize
55	181481.5	1638997	Maize
56	146966.5	1613782	Maize
57	151601.5	1591432	Maize
58	139466.5	1599097	Maize
59	167246.5	1634242	Maize
60	186116.5	1628017	Maize
61	171041.5	1626877	Maize
62	159656.5	1601542	Forest
63	162191.5	1603912	Forest
64	165911.5	1610617	Forest
65	176831.5	1588822	Forest
66	155936.5	1604167	Forest
67	171176.5	1595122	Forest
68	148181.5	1625467	Forest
69	159851.5	1600087	Forest
70	149246.5	1615282	Forest
71	182591.5	1588942	Forest
72	155861.5	1613977	Forest
73	171116.5	1607497	Forest
74	172031.5	1602457	Forest
75	158171.5	1610032	Forest
76	156281.5	1617457	Forest
77	142661.5	1590637	Forest

Table 1 (Continued).

No.	X	Y	Ground reference class
78	155396.5	1615192	Forest
79	156986.5	1616107	Forest
80	166661.5	1595602	Forest
81	154256.5	1618072	Forest
82	161561.5	1605382	Forest
83	151451.5	1614307	Forest
84	166211.5	1613017	Forest
85	150281.5	1626082	Forest
86	172271.5	1618282	Forest
87	139316.5	1595707	Forest
88	161681.5	1603522	Forest
89	165116.5	1602832	Forest
90	164801.5	1606777	Forest
91	166181.5	1606537	Forest
92	169901.5	1609747	Forest
93	166346.5	1630177	Forest
94	159266.5	1609717	Forest
95	176951.5	1600072	Forest
96	161081.5	1610302	Forest
97	180776.5	1640287	Forest
98	168926.5	1609387	Forest
99	162191.5	1587232	Forest
100	169586.5	1594522	Forest
101	190676.5	1623097	Forest
102	171026.5	1602337	Forest
103	164111.5	1611022	Forest
104	170981.5	1596007	Forest
105	170126.5	1607092	Forest
106	154586.5	1620262	Forest
107	169886.5	1607047	Forest
108	140351.5	1598197	Forest
109	170171.5	1604092	Forest
110	172916.5	1615687	Forest
111	151286.5	1589197	Forest
112	170441.5	1594372	Forest
113	160871.5	1607512	Forest
114	169601.5	1608832	Forest
115	139436.5	1600957	Forest
116	149771.5	1607947	Forest
117	165836.5	1601752	Forest
118	169886.5	1593877	Forest
119	174701.5	1592392	Forest
120	174071.5	1581667	Forest

Table 1 (Continued).

No.	X	Y	Ground reference class
121	179291.5	1637527	Forest
122	149141.5	1624102	Forest
123	158276.5	1607212	Forest
124	172331.5	1589767	Forest
125	162761.5	1597597	Forest
126	172511.5	1617322	Forest
127	152381.5	1616902	Forest
128	181361.5	1590637	Forest
129	161291.5	1609912	Forest
130	153191.5	1592257	Forest
131	180191.5	1610842	Forest
132	175121.5	1613737	Forest
133	146801.5	1597852	Paddy Filed
134	185141.5	1615717	Paddy Filed
135	186416.5	1628917	Paddy Filed
136	178586.5	1607932	Paddy Filed
137	153431.5	1627687	Paddy Filed
138	156221.5	1605967	Paddy Filed
139	182396.5	1641652	Paddy Filed
140	182306.5	1641322	Paddy Filed
141	169271.5	1589752	Paddy Filed
142	182096.5	1639867	Paddy Filed
143	151286.5	1597717	Paddy Filed
144	175451.5	1597882	Paddy Filed
145	178046.5	1577602	Paddy Filed
146	165356.5	1617142	Paddy Filed
147	176636.5	1627237	Paddy Filed
148	177581.5	1631362	Paddy Filed
149	184346.5	1619587	Paddy Filed
150	176276.5	1604497	Paddy Filed
151	158486.5	1625812	Paddy Filed
152	185231.5	1634302	Paddy Filed
153	172451.5	1620262	Paddy Filed
154	170741.5	1614712	Paddy Filed
155	182966.5	1638247	Paddy Filed
156	167276.5	1613062	Paddy Filed
157	165686.5	1623277	Paddy Filed
158	179216.5	1602907	Paddy Filed
159	163991.5	1620592	Paddy Filed
160	179561.5	1616332	Paddy Filed
161	176486.5	1630582	Paddy Filed
162	181091.5	1618582	Paddy Filed
163	178346.5	1642357	Paddy Filed

Table 1 (Continued).

No.	X	Y	Ground reference class
164	186566.5	1627792	Paddy Filed
165	174836.5	1635277	Paddy Filed
166	143231.5	1596187	Paddy Filed
167	180086.5	1628662	Paddy Filed
168	176516.5	1629772	Paddy Filed
169	166736.5	1616647	Paddy Filed
170	169646.5	1636147	Paddy Filed
171	183491.5	1622272	Paddy Filed
172	142121.5	1594807	Paddy Filed
173	184676.5	1628272	Sugarcane
174	189611.5	1622977	Sugarcane
175	153416.5	1602097	Sugarcane
176	159431.5	1591702	Sugarcane
177	151856.5	1629202	Sugarcane
178	144941.5	1628287	Sugarcane
179	165941.5	1589362	Sugarcane
180	161861.5	1589467	Sugarcane
181	143876.5	1601572	Sugarcane
182	148811.5	1597147	Sugarcane
183	147566.5	1601032	Sugarcane
184	180626.5	1639282	Sugarcane
185	150761.5	1599697	Sugarcane
186	143456.5	1619167	Sugarcane
187	146411.5	1596337	Sugarcane
188	145676.5	1610977	Sugarcane
189	147686.5	1618057	Sugarcane
190	144401.5	1616632	Sugarcane
191	177896.5	1641667	Sugarcane
192	155126.5	1609957	Water Body
193	160361.5	1623097	Water Body
194	160706.5	1622407	Water Body
195	153056.5	1606252	Water Body
196	152531.5	1594522	Perennial trees and Orchard
197	181451.5	1612282	Perennial trees and Orchard
198	175991.5	1602127	Perennial trees and Orchard
199	173756.5	1634902	Perennial trees and Orchard
200	164171.5	1628257	Perennial trees and Orchard
201	165221.5	1616752	Perennial trees and Orchard
202	172841.5	1640422	Perennial trees and Orchard
203	155816.5	1604962	Perennial trees and Orchard

Table 2 Detail of sampling point for accuracy assessment in testing area.

No.	X	Y	Ground reference class
1	208223.0	1601000	Cassava
2	198995.0	1593950	Cassava
3	208668.6	1606550	Cassava
4	202083.6	1597055	Cassava
5	216798.6	1591085	Cassava
6	203688.6	1612775	Cassava
7	201573.6	1611980	Cassava
8	208278.6	1609115	Cassava
9	196878.6	1592630	Cassava
10	193263.6	1600910	Cassava
11	201453.6	1590545	Cassava
12	211878.6	1586990	Cassava
13	216078.6	1606595	Cassava
14	197913.6	1607345	Cassava
15	201123.6	1599395	Cassava
16	213093.6	1593560	Cassava
17	196968.6	1595450	Cassava
18	196518.6	1594310	Cassava
19	213948.6	1609130	Cassava
20	202833.6	1617125	Cassava
21	188853.6	1610840	Cassava
22	211638.6	1588790	Cassava
23	217878.6	1602365	Cassava
24	207963.6	1611005	Cassava
25	212688.6	1608275	Cassava
26	217953.6	1610975	Cassava
27	214833.6	1607000	Cassava
28	188598.6	1618430	Cassava
29	209118.6	1601570	Cassava
30	199473.6	1602965	Cassava
31	200148.6	1613735	Cassava
32	192378.6	1620635	Cassava
33	195033.6	1605590	Cassava
34	184248.6	1612175	Cassava
35	211413.6	1592495	Cassava
36	189378.6	1607045	Cassava
37	213198.6	1612580	Cassava
38	206419.0	1595450	Urban and Built-up area
39	206445.0	1595460	Urban and Built-up area
40	209523.6	1603250	Urban and Built-up area
41	198899.0	1607710	Urban and Built-up area
42	192170.0	1603420	Urban and Built-up area
43	192003.6	1614455	Urban and Built-up area

Table 2 (Continued).

No.	X	Y	Reference
44	193248.6	1609505	Urban and Built-up area
45	209343.6	1587800	Urban and Built-up area
46	205323.6	1609265	Urban and Built-up area
47	199743.6	1606340	Urban and Built-up area
48	201633.6	1608200	Urban and Built-up area
49	199175.0	1595370	Maize
50	192543.6	1613660	Maize
51	182418.6	1605215	Maize
52	191748.6	1607660	Maize
53	195438.6	1602050	Maize
54	181803.6	1599395	Maize
55	203763.6	1602545	Maize
56	216273.6	1594085	Maize
57	181218.6	1599890	Maize
58	199563.6	1601960	Maize
59	207813.6	1591070	Maize
60	211683.6	1601465	Maize
61	194013.6	1602185	Maize
62	204048.6	1601180	Maize
63	202683.6	1602065	Maize
64	189873.6	1607645	Maize
65	202683.6	1602020	Maize
66	198031.0	1600710	Maize
67	195558.6	1596335	Maize
68	192033.6	1584485	Forest
69	202518.6	1571450	Forest
70	182478.6	1580510	Forest
71	181938.6	1579490	Forest
72	204843.6	1586150	Forest
73	199173.6	1578350	Forest
74	205083.6	1577780	Forest
75	215103.6	1569035	Forest
76	189378.6	1592195	Forest
77	186813.6	1586615	Forest
78	187893.6	1567625	Forest
79	187758.6	1588715	Forest
80	193998.6	1569590	Forest
81	200898.6	1581680	Forest
82	191943.6	1579640	Forest
83	187428.6	1578155	Forest
84	209133.6	1576940	Forest
85	189333.6	1577480	Forest
86	209043.6	1585385	Forest

Table 2 (Continued).

No.	X	Y	Reference
87	204843.6	1570460	Forest
88	201783.6	1571570	Forest
89	204168.6	1571390	Forest
90	212388.6	1574345	Forest
91	203118.6	1566320	Forest
92	207303.6	1565300	Forest
93	202038.6	1575410	Forest
94	202668.6	1584695	Forest
95	191868.6	1564940	Forest
96	185568.6	1580720	Forest
97	199668.6	1571525	Forest
98	207543.6	1573370	Forest
99	202563.6	1579730	Forest
100	205098.6	1579490	Forest
101	193278.6	1570790	Forest
102	208038.6	1580390	Forest
103	186513.6	1571300	Forest
104	202533.6	1571150	Forest
105	192363.6	1572845	Forest
106	179073.6	1583045	Forest
107	178653.6	1583315	Forest
108	177558.6	1573250	Forest
109	203193.6	1571105	Forest
110	209913.6	1580075	Forest
111	198858.6	1573850	Forest
112	194868.6	1583285	Forest
113	192078.6	1575905	Forest
114	211158.6	1580105	Forest
115	190353.6	1590605	Forest
116	209433.6	1581155	Forest
117	209148.6	1571315	Forest
118	187113.6	1580480	Forest
119	197658.6	1579460	Forest
120	212343.6	1576700	Forest
121	193308.6	1574705	Forest
122	205248.6	1563845	Forest
123	196113.6	1572935	Forest
124	211293.6	1573985	Forest
125	204393.6	1585235	Forest
126	212838.6	1568570	Forest
127	179763.6	1577675	Forest
128	181923.6	1576745	Forest
129	199113.6	1568330	Forest

Table 2 (Continued).

No.	X	Y	Reference
130	212823.6	1577420	Forest
131	211053.6	1580585	Forest
132	208743.6	1578335	Forest
133	213018.6	1577405	Forest
134	208698.6	1573430	Forest
135	201183.6	1582595	Forest
136	206778.6	1589930	Forest
137	205788.6	1600730	Forest
138	192993.6	1616120	Forest
139	193833.6	1599485	Forest
140	216813.6	1605560	Paddy Field
141	213873.6	1598810	Paddy Field
142	200658.6	1597970	Paddy Field
143	201663.6	1597610	Paddy Field
144	192363.6	1609970	Paddy Field
145	198981.0	1593920	Paddy Field
146	203343.6	1609970	Paddy Field
147	191043.6	1613375	Paddy Field
148	204588.6	1598420	Paddy Field
149	206898.6	1605680	Paddy Field
150	187323.6	1616615	Paddy Field
151	199069.0	1602230	Paddy Field
152	197992.0	1608030	Paddy Field
153	200853.6	1608425	Paddy Field
154	190758.6	1614905	Paddy Field
155	198543.6	1610315	Paddy Field
156	198453.6	1609610	Paddy Field
157	200703.6	1598450	Paddy Field
158	193248.6	1614710	Paddy Field
159	191253.6	1617485	Paddy Field
160	188058.6	1606160	Paddy Field
161	207093.6	1597070	Paddy Field
162	216648.6	1610630	Sugarcane
163	209403.6	1593230	Sugarcane
164	192888.6	1618745	Sugarcane
165	203613.6	1605485	Sugarcane
166	194178.6	1606445	Sugarcane
167	194478.6	1602800	Sugarcane
168	183468.6	1601315	Sugarcane
169	216768.6	1604660	Sugarcane
170	214758.6	1613585	Sugarcane
171	183813.6	1601390	Sugarcane
172	211953.6	1606460	Sugarcane

Table 2 (Continued).

No.	X	Y	Reference
173	219543.6	1609730	Sugarcane
174	201406.0	1596390	Water Body
175	192156.0	1603410	Water Body
176	188928.6	1600925	Water Body
177	200478.6	1593185	Water Body
178	186978.6	1599695	Water Body
179	202998.6	1592405	Water Body
180	199678.0	1593900	Water Body
181	205323.6	1591190	Water Body
182	200688.6	1594520	Water Body
183	200808.6	1593815	Water Body
184	206510.0	1594140	Water Body
185	189093.6	1597520	Water Body
186	202593.6	1593275	Water Body
187	189483.6	1600175	Water Body
188	201918.6	1594085	Water Body
189	202278.6	1594985	Water Body
190	207183.6	1600640	Water Body
191	190263.6	1603565	Perennial trees and Orchard
192	199188.6	1598315	Perennial trees and Orchard
193	188973.6	1595600	Perennial trees and Orchard
194	193413.6	1601480	Perennial trees and Orchard
195	195393.6	1593500	Perennial trees and Orchard
196	181818.6	1609115	Perennial trees and Orchard
197	203253.6	1602605	Perennial trees and Orchard
198	190263.6	1594655	Perennial trees and Orchard
199	190008.6	1596125	Perennial trees and Orchard
200	186798.6	1600925	Perennial trees and Orchard
201	183378.6	1601690	Perennial trees and Orchard
202	183858.6	1597550	Perennial trees and Orchard
203	202788.6	1596875	Perennial trees and Orchard

CURRICULUM VITAE

Name Miss PHAWINEE POOJARIT

Date of Birth October 4, 1988

Place of Birth Kalasin, Thailand

Education 2007 - 2011 Bachelor of Science (Geo-informatics), Khon Kaen University, Khon Kaen, Thailand.

Publications

Ongsomwang, S., and Poojarit, P. (2015). An optimum pan-sharpening method and band combination selection from Landsat 8 data for land use data extraction under object-based image analysis. **Remote sensing and GIS association of Thailand.** (2) 16. 11-21.

Poojarit, P. and Ongsomwang, S. (2015). **Optimum scale of multiresolution segmentation of landsat-8 for land use and land cover extraction using object-based image analysis.** The 41st Congress on Science and Technology of Thailand (STT41). 6-8 November, 12p.

Grants and Fellowships Potential scholarship, Suranaree University of Technology
Teaching assistants and research assistant scholarship,
Suranaree University of Technology